

STABILITY STUDIES OF ROOPEROL AND ANALOGUES  
BY *IN VITRO* METABOLISM WITH HPLC/MS DETECTION

by

Amanda Bohanon, B.S.

A thesis submitted to the Graduate Council of  
Texas State University in partial fulfillment  
of the requirements for the degree of  
Master of Science  
with a Major in Biochemistry  
May 2019

Committee Members:

Sean M. Kerwin, Chair

Wendi David

Liqin Du

**COPYRIGHT**

by

Amanda Bohanon

2019

## **FAIR USE AND AUTHOR'S PERMISSION STATEMENT**

### **Fair Use**

This work is protected by the Copyright Laws of the United States (Public Law 94-553, section 107). Consistent with fair use as defined in the Copyright Laws, brief quotations from this material are allowed with proper acknowledgement. Use of this material for financial gain without the author's express written permission is not allowed.

### **Duplication Permission**

As the copyright holder of this work I, Amanda Bohanon, authorize duplication of this work, in whole or in part, for educational or scholarly purposes only.

## **ACKNOWLEDGEMENTS**

I would like to thank my research advisor, Dr. Sean M. Kerwin, for his unwavering support, advice, and mentorship throughout the cultivation of this research project. I would also like to thank Dr. Wendi David and Dr. Liqin Du for serving on my committee and offering their guidance and expertise for the completion of this project. I would like to express my gratitude to Jake Hermanson, who has dedicated so much of his time to this project and will undoubtedly be successful in continuing and expanding on the work done in this thesis. I would like to thank my fellow lab members for creating a supportive and enjoyable lab environment. Lastly, I would like to thank Brandie Taylor, for her never-ending loyalty, encouragement, and friendship.

## TABLE OF CONTENTS

	<b>Page</b>
ACKNOWLEDGEMENTS.....	iv
LIST OF TABLES.....	vii
LIST OF FIGURES.....	viii
LIST OF ABBREVIATIONS.....	ix
ABSTRACT.....	x
CHAPTER	
I. BACKGROUND.....	1
1. Natural Product Anticancer Drugs.....	1
2. African Potato.....	1
3. Anticancer Agent Rooperol.....	3
4. Rooperol Analogues.....	5
5. Drug Metabolism.....	7
6. Glucuronidation & UDP-Glucuronosyltransferase.....	9
7. UGT Isoforms & Species Differences.....	11
8. Drug Metabolism Studies <i>In Vitro</i> .....	11
9. Research Aims.....	13
II. EXPERIMENTAL.....	15
1. Materials & Instruments.....	15
2. Preparation of Stock Solutions.....	16
3. Standard Curves.....	16
4. Original <i>In Vitro</i> Assay with Hydroxytyrosol.....	18
5. Optimized <i>In Vitro</i> Assay with Hydroxytyrosol and Rooperol.....	19
6. Negative Controls for the <i>In Vitro</i> Assays.....	20
7. Half-life and Intrinsic Clearance Determination by HPLC.....	21
8. Identification of Metabolites by HPLC/MS.....	22

III. RESULTS .....	24
1. Standard Curves .....	24
2. <i>In Vitro</i> Assays with Hydroxytyrosol .....	27
3. <i>In Vitro</i> Assays with Rooperol.....	33
4. HPLC/MS of Glucuronide Metabolites .....	40
IV. DISCUSSION.....	44
V. CONCLUSION.....	50
APPENDIX SECTION.....	51
LITERATURE CITED .....	85

## LIST OF TABLES

<b>Table</b>	<b>Page</b>
1. Summary of Results from <i>In Vitro</i> Assays with Hydroxytyrosol.....	33
2. Summary of Results from <i>In Vitro</i> Assays with Rooperol .....	40
3. Molecular Weights of Hydroxytyrosol, Rooperol, and Glucuronides .....	41

## LIST OF FIGURES

Figure	Page
1. The Pharmacologically Relevant Compounds in African Potato .....	2
2. The Phase II Metabolism of Rooperol .....	5
3. Rooperol Analogues.....	7
4. Phase I and II Drug Metabolism .....	8
5. Glucuronidation Catalyzed by UGT .....	10
6. The Catechol-Containing Compounds 3-Hydroxytyrosol and Rooperol .....	14
7. HPLC Mobile Phase Gradient .....	17
8. Standard Curve for Hydroxytyrosol.....	25
9. Standard Curve for Rooperol .....	26
10. Results for the <i>In Vitro</i> Assay with 100 $\mu$ M Hydroxytyrosol.....	28
11. The Percent of Hydroxytyrosol Remaining Over Time.....	30
12. Results for the <i>In Vitro</i> Assay with 10 $\mu$ M Hydroxytyrosol.....	31
13. The Disappearance of Rooperol Over 60 Minutes .....	34
14. Results for the <i>In Vitro</i> Assay with 100 $\mu$ M Rooperol .....	37
15. The Percent of Rooperol Remaining Over Time .....	38
16. Results for the <i>In Vitro</i> Assay with 10 $\mu$ M Rooperol .....	39
17. HPLC/MS of Hydroxytyrosol Metabolites.....	41
18. HPLC/MS of Rooperol Metabolites .....	43

## LIST OF ABBREVIATIONS

<b>Abbreviation</b>	<b>Description</b>
MAPK	Mitogen-activated protein kinase
UGT	Uridine 5'-diphospho-glucuronosyltransferase
ER	Endoplasmic reticulum
UDPGA	Uridine 5'-diphospho-glucuronic acid
DTT	Dithiothreitol
HPLC	High-performance liquid chromatography
MS	Mass spectrometry
APCI	Atmospheric-pressure chemical ionization
PAR	Peak area ratio
$t_{1/2}$	Half-life
$CL'_{int}$	Intrinsic clearance
RT	Retention Time
DMSO	Dimethylsulfoxide
ACN	Acetonitrile

## ABSTRACT

African Potato, *Hypoxis hemerocallidea*, has a long history of use by the indigenous people of South Africa to treat cancer and a variety of other diseases. Extracts from the corm contain the norlignan bisglycoside hypoxoside, which is hydrolyzed in the body to yield the anticancer agent rooperol (1,5-bis(3',4'-dihydroxyphenyl)pent-1-en-4-yne). Studies have shown that rooperol selectively inhibits the growth of several cancer cell lines. Phase I clinical trials of rooperol in lung cancer patients suggested promising activity with no dose-limiting toxicity. However, rooperol is rapidly converted to biologically inactive sulfate and glucuronide metabolites. Thus, a relatively small amount of the drug reaches the tumor site. Bioisosteric analogues of rooperol have been synthesized with the aim of increasing metabolic stability while preserving the anticancer properties of the parent drug. The goal of this research is to investigate the metabolic stability of rooperol and analogues. As part of this study, we employ an *in vitro* metabolism assay with porcine liver microsomes. Microsomes are supplemented with the cofactor UDP-glucuronic acid and the pore-forming peptide alamethicin. The suitability of this assay to characterize the Phase II metabolism of phenolic compounds was established with the plant phytochemical 3-hydroxytyrosol. The time-dependent metabolism of this compound was determined by HPLC assay, and the formation of the glucuronide Phase II metabolite was confirmed by HPLC/MS. The time course for disappearance of 3-hydroxytyrosol followed first-order kinetics with an apparent half-life

of around 61 minutes. We have recently employed this assay to quantify the metabolic lability of rooperol. The disappearance of rooperol monitored by HPLC revealed an exceptionally short half-life of about 3 minutes. The identities of monoglucuronide and diglucuronide metabolites of rooperol were verified by HPLC/MS. The extreme metabolic lability of rooperol demonstrates the need to identify more metabolically stable analogues. We will discuss the integration of this *in vitro* metabolism assay in a workflow designed to identify rooperol analogues exhibiting increased metabolic stability while retaining the cytotoxic activity of rooperol.

## I. BACKGROUND

### 1. Natural Product Anticancer Drugs

Natural products have been important in traditional medicine for thousands of years. Plants are an abundant resource for these natural compounds and have been particularly valuable in the advancement of chemotherapeutics.<sup>1</sup> Plant secondary metabolism produces a wide variety of molecules that are not involved in growth but increase the ability of plants to survive and respond to their environment.<sup>2</sup> The multitude of plant species that exist in a variety of environments results in a collection of diverse and complex organic compounds. These compounds have unique properties that have led to the development of anticancer drugs.<sup>3</sup> Many chemotherapeutics in use today were developed from plant-derived compounds. Podophyllotoxins, derived from *Podophyllum peltatum*, have natural antimitotic activity. The chemotherapy drug, Etoposide, is a synthetic derivative of these podophyllotoxins.<sup>4</sup> The drug Vincristine, which blocks microtubule polymerization, is a vinca alkaloid from the periwinkle, *Catharanthus roseus*.<sup>5,6</sup> Paclitaxel was first isolated from the Pacific yew, *Taxus brevifolia*, and also effects the assembly of the mitotic spindle.<sup>7</sup> These are just a few examples of the plant-derived drugs that have led to major advances in cancer treatment. Due to the diversity of plants, there is likely a wide selection of undiscovered natural compounds with promising anticancer potential.

### 2. African Potato

African plants have been an important area of research due to the large variety of native plant species and the rich history of traditional medicine.<sup>8</sup> *Hypoxis*, a widespread genus of plants in South Africa, has played a central role in African traditional medicine.<sup>8</sup>

*Hypoxis hemerocallidea*, more commonly known as African Potato, was recognized early on by indigenous South Africans for its medicinal properties and is still relevant to modern African healthcare. African Potato is known for its immune boosting properties and has been used to treat cancers, urinary infections, prostate hyperplasia, HIV/AIDS, inflammation, and many other conditions.<sup>8-10</sup> The component of the plant generally used for medicinal purposes is the corm, an underground rootstock. Extracts from the corm contain norlignan glycosides, which have a common diphenylpentane structure.<sup>11</sup> The major constituent of these glycosides is hypoxoside, which consists of a diphenyl-1-en-4-yne-pentane backbone flanked by two  $\beta$ -D-glucopyranosyl groups.<sup>12, 13</sup> Hydrolysis of hypoxoside yields its biologically active aglycone, rooperol (1,5-bis(3',4'-dihydroxyphenyl)pent-1-en-4-yne) (Figure 1).<sup>14-16</sup>

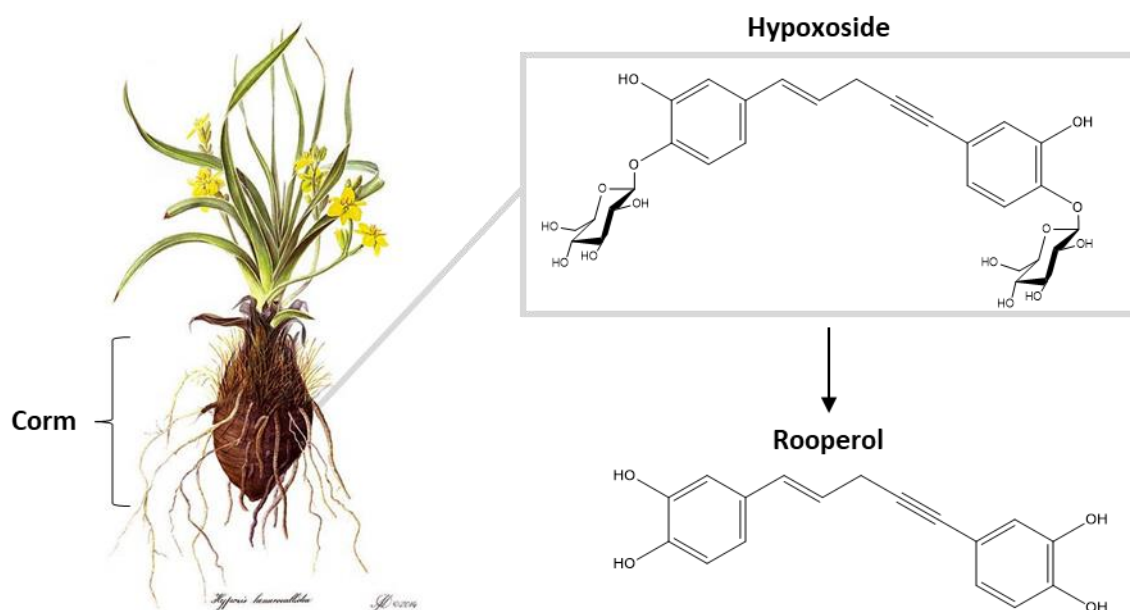


**Figure 1:** The Pharmacologically Relevant Compounds in African Potato. The corm of African Potato (*Hypoxis hemerocallidea*) contains the major glycoside hypoxoside (1,5-Bis[4-(beta-D-glucopyranosyloxy)-3-hydroxyphenyl]-1-pentene-4-yne). The hydrolysis product of hypoxoside is the biologically active rooperol.

### 3. Anticancer Agent Rooperol

Rooperol has been reported to exhibit antioxidant, anti-inflammatory, and cytotoxic activity.<sup>17</sup> *In vitro* studies have shown that the parent compound, hypoxoside, is not biologically active, but hydrolysis of hypoxoside yields rooperol which is active.<sup>18</sup> From *in vivo* experiments with mice, hypoxoside was converted to rooperol in the gut via bacterial  $\beta$ -glucosidases, which catalyze the cleavage of the  $\beta$ -D-glucopyranosyl groups in hypoxoside (Figure 2).<sup>18</sup> Studies on the anticancer properties of rooperol showed that it selectively inhibits the growth of several cancer cell lines, including B16, HeLa, HT-29, and MCF-7.<sup>19, 20</sup> Additionally, rooperol has been observed to selectively target stem-like cancer cells.<sup>21</sup> These cell types have proven to be more resistant to chemotherapy and radiation treatments and may be an important target for relapse prevention.<sup>22</sup> The exact mechanism by which rooperol inhibits the growth of cancer cells is not fully understood. Studies with HeLa, H-29, and MCF-7 cancer cells lines showed that rooperol acts by arresting the cell cycle at late G1 or early S phase, which causes the cells to become apoptotic in response.<sup>20</sup> A more recent study demonstrated that rooperol inhibits p38 $\alpha$ , a mitogen-activated protein kinase (MAPK).<sup>23</sup> MAPKs phosphorylate and activate proteins that are involved in many cellular activities including cell division, gene expression, movement, and apoptosis.<sup>24</sup> Abnormalities in these pathways are associated with cancer cell survival and proliferation. This p38 $\alpha$  inhibitory activity implies that the cytotoxicity of rooperol may be due to disruption of these irregular MAPK pathways. Preliminary studies by Mooberry, *et al.* at UT Health Science at San Antonio used immunofluorescence microscopy with rooperol in cancer cells lines and provided evidence that rooperol causes microtubule depolymerization, thus hindering the

replication of cancer cells (unpublished). These studies collectively suggest that rooperol may target several important pathways involved in cancer cell proliferation.

Phase I clinical trials of advanced-stage lung cancer patients dosed daily with hypoxoside showed that rooperol is a promising chemotherapeutic drug.<sup>25</sup> Several patients had positive responses to treatment, including prolonged survival and, in one patient, complete eradication of the cancer.<sup>25</sup> Most remarkably, there were no drug-induced toxicities reported from this therapy. In pharmacokinetic studies from this trial, hypoxoside and rooperol were not found to be circulating in the body, but were completely converted to inactive Phase II metabolites.<sup>26</sup> The major metabolite was a mixed sulfate/glucuronide and the two minor metabolites were the disulfate and the diglucuronide of rooperol.<sup>26, 27</sup> Though rooperol was shown to be extensively metabolized to these inactive forms, the positive results in the clinical trial suggests that rooperol still exhibits cytotoxic activity. A possible explanation for this contradiction is the conversion of the diglucuronide of rooperol back to active rooperol by the action of  $\beta$ -glucuronidase in tumor tissues. (Figure 2).  $\beta$ -Glucuronidase is a lysosomal enzyme that degrades glucuronic acid-containing molecules. It has been reported that tumors have higher levels of this enzyme, which may result in the localized activation of rooperol in tumor tissue.<sup>28</sup> Although the selective cytotoxicity of cancer cells is advantageous, the poor metabolic stability of rooperol results in only a small fraction of the active drug delivered to cancer cells. One way to increase the amount of circulating active rooperol is to slow the conversion to inactive metabolites. This can be achieved via synthetic analogues of the molecule with replacements for certain metabolically labile groups.

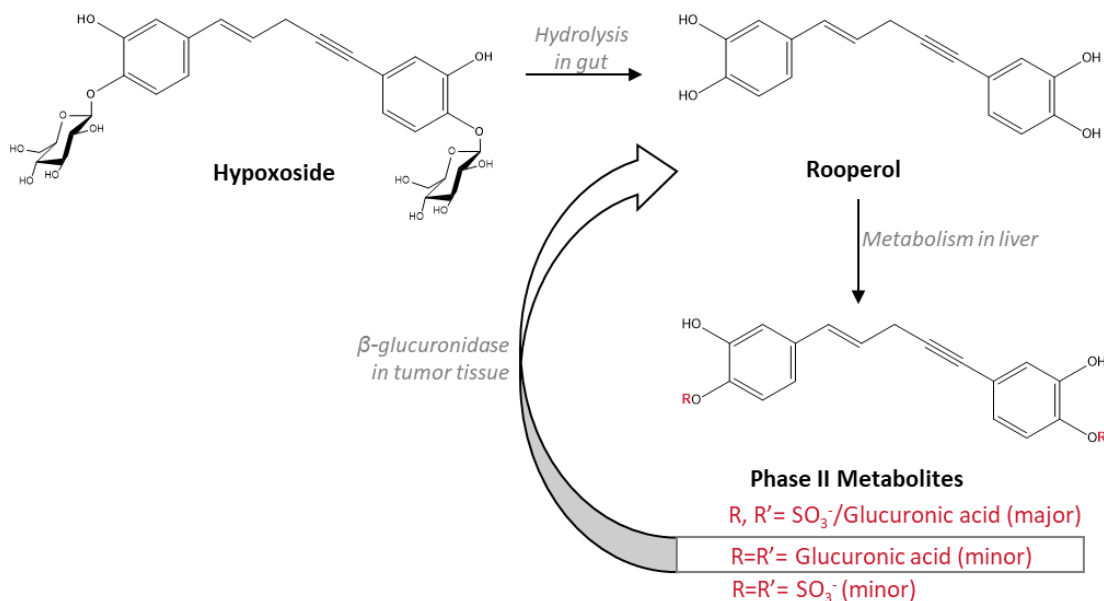
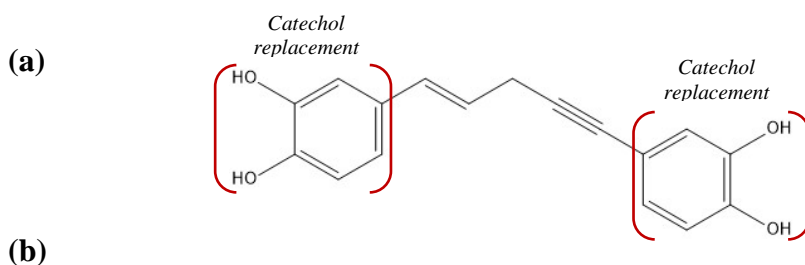


**Figure 2:** The Phase II Metabolism of Rooperol. When ingested, hypoxoside is hydrolyzed in the gut to the biologically active rooperol, which is quickly metabolized in the liver to produce several inactive Phase II metabolites. The minor diglucuronide of rooperol is hypothesized to be converted back to active rooperol by  $\beta$ -glucuronidase in tumor tissue.

#### 4. Rooperol Analogues

The synthesis of natural product analogues has been a common strategy for the development of new drugs. This typically involves the replacement of a particular group in a drug with its bioisostere. Bioisosteres are substituents that have similar chemical and physical characteristics and thus may have comparable biological activities.<sup>29</sup> Bioisosteric replacement may yield analogues that have similar pharmacological properties as the original drug but are improved in terms of absorption, metabolic stability, cytotoxicity, or safety.<sup>30, 31</sup> In the case of rooperol, the metabolic stability can be greatly improved. The catechol (3,4-dihydroxybenzene) groups of rooperol undergo extensive phase II metabolism. This leads to sulfate and glucuronide metabolites that are inactive and, due

to their hydrophilicity, are readily excreted from the body. Exchanging these catechols with bioisosteres could delay the production of inactive metabolites, allowing the active drug to remain in circulation. In addition, these analogues may display comparatively different biological activities and elucidate the many pathways that rooperol targets. Free hydroxyl groups are likely necessary for the biological activity of rooperol. In a previous study, a rooperol analogue with all hydroxyl groups of the catechol replaced with methoxy groups showed no activity in several cancer cell lines.<sup>13, 32</sup> An analogue with unsubstituted phenyl groups is also likely to be inactive, due to the absence of hydroxyl groups. Thus, catechol replacements with free hydroxyl groups at different positions in the ring were chosen for analogues. Fluorine replacements for hydroxyl groups were also considered, as fluorine has previously been shown to increase stability and biological activity when substituted into catechol-containing molecules.<sup>33</sup> Analogues have been prepared in our lab similarly to the recently published synthesis of rooperol, but with bioisosteric substituents in place of the catechols.<sup>34</sup> A variety of combinations of the substituents have been incorporated to create both symmetrical analogues, with the same replacement group, and asymmetrical analogues, with two different groups. Some representative rooperol analogues with catechol replacements are shown in Figure 3. To assess these new analogues, *in vitro* metabolism studies will be conducted to identify those with superior metabolic stability compared to rooperol.



### Representative Analogues

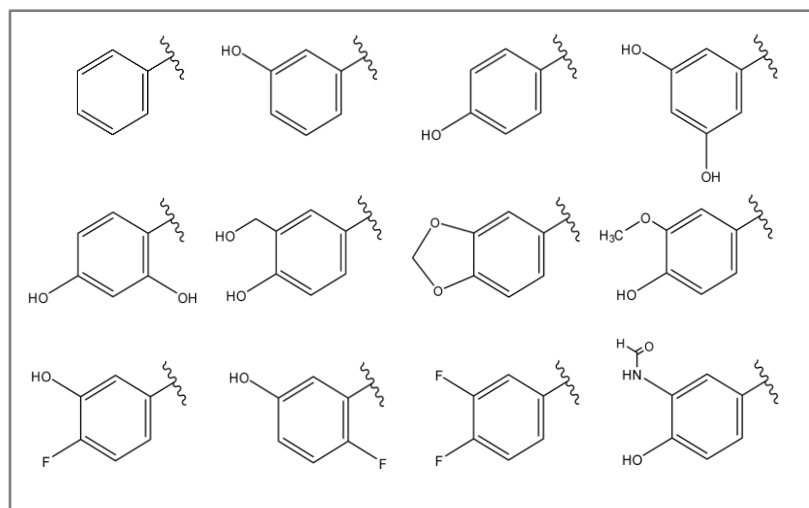


**Figure 3:** Rooperol Analogues (a) Structure of rooperol, with brackets denoting the metabolically labile catechol groups that will be replaced. (b) Some examples of the groups that will replace the catechols in rooperol analogues.

## 5. Drug Metabolism

Most drugs are nonpolar, lipophilic molecules that can easily cross biological membranes. These characteristics also account for the inability of some drugs to be excreted from the body in their native form. Therefore, metabolism into a more polar, hydrophilic form is crucial for inactivation and clearance of many drugs. This process is called biotransformation and is classified into Phase I and Phase II metabolic reactions, which mainly occur in the liver (Figure 4).<sup>35</sup> Phase I metabolism involves the transformation of a drug into a more polar compound via oxidation or hydrolysis.<sup>36</sup> This uncovers or adds reactive groups in the molecule that are necessary for Phase II

metabolism. The most important Phase I reaction is oxidation, which is usually catalyzed by the cytochrome P450 superfamily of enzymes.<sup>37</sup> However, not all drugs undergo Phase I metabolism. Those that already contain the appropriate functional groups may skip this phase and undergo Phase II conjugation reactions. For example, the hydroxyl groups in rooperol are suitable substrates for conjugation reactions. Thus, rooperol proceeds directly to Phase II metabolism. Phase II involves conjugation of a drug with another group to make the drug more hydrophilic and easily excreted.<sup>38</sup> These conjugation reactions include glucuronidation, sulfation, acetylation, and methylation as well as linkage to glutathione and amino acids.<sup>39</sup>

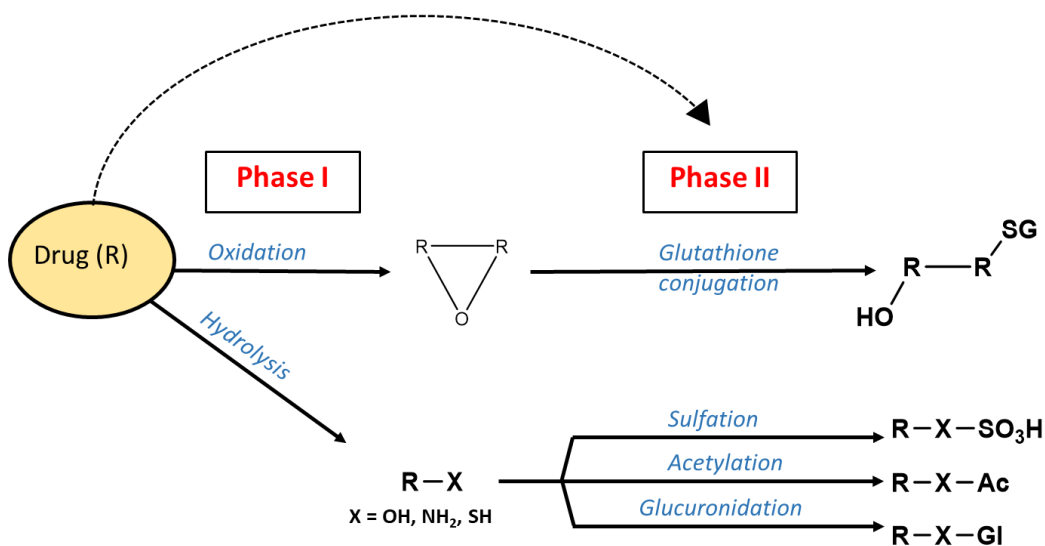


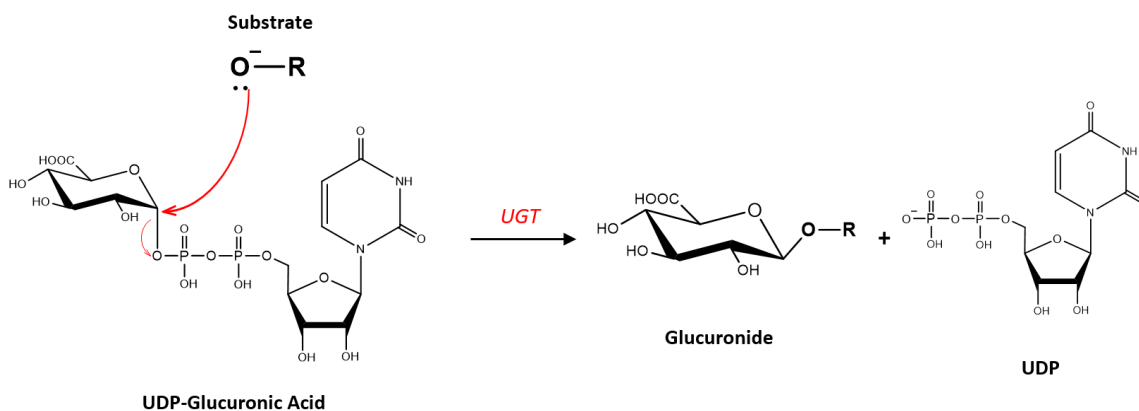
**Figure 4:** Phase I and II Drug Metabolism. Phase I involves oxidation and hydrolysis reactions while phase II consists of conjugation reactions. Alternatively, a drug with appropriate functional groups may proceed directly to phase II. Together, these reactions result in a species that is much more hydrophilic than the original drug.

## 6. Glucuronidation & UDP-Glucuronosyltransferase

Glucuronidation is the most important pathway for the detoxification and elimination of a majority of drugs.<sup>40</sup> The reaction is catalyzed by uridine 5'-diphosphoglucuronosyltransferase (UGT), which conjugates the drug with a glucuronic acid moiety derived from the cofactor UDP-glucuronic acid (Figure 5 (a)).<sup>40, 41</sup> UGTs are a superfamily of enzymes that play an important role in phase II metabolism. They are localized mostly in the liver and are involved in the detoxification of a diverse range of endogenous and foreign molecules. These enzymes are responsible for glucuronidation of lipophilic molecules, increasing their hydrophilicity and ease of excretion.<sup>42</sup> Substrates of UGTs include alcohols, phenols, carboxylic acids, amines and variety of other functional groups. In the cell, UGTs are associated with the endoplasmic reticulum (ER) membrane. It is generally believed that the C-terminal is anchored within the membrane while the majority of the UGT structure, including the active site, is present on the lumen-facing side of the membrane (Figure 5 (b)).<sup>43, 44</sup> Because the substrates of UGTs, including drugs, are usually lipophilic molecules, they pass freely through the phospholipid membrane into the lumen where glucuronidation takes place. UGT requires the cofactor UDPGA, which is synthesized in the cytosol and, due to its hydrophilic nature, cannot diffuse through the membrane. It is thought that UDPGA is shuttled into the ER by the action of an uptake transporter.<sup>45</sup> UDPGA provides the glucuronic acid moiety required for UGT-mediated conjugation of the substrate. The resulting glucuronide is much more polar and thus must be transported out of the membrane via a glucuronide efflux transporter.<sup>46</sup> In the case of phenolic compounds, glucuronidation reactions likely take place via an acid-base mechanism, where amino acids, such as histidine and aspartic acid,

respectively donate and accept protons allowing for a S<sub>N</sub>2 reaction to occur.<sup>47</sup> The histidine residue in UGT facilitates the deprotonation of the substrate oxygen, allowing for a nucleophilic attack on the C1 of the sugar in UDPGA (Figure 5 (a)). The leaving group, UDP, is subsequently protonated by the aspartic acid residue in UGT.<sup>48</sup>

(a)



(b)

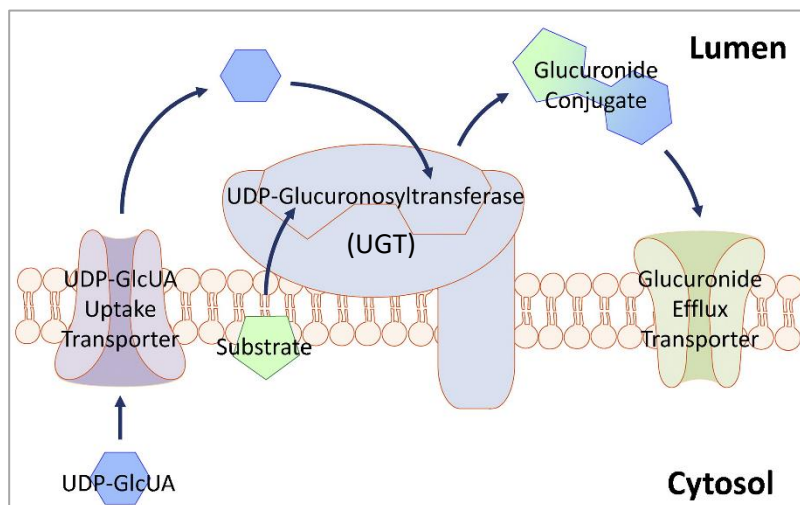


**Figure 5:** Glucuronidation Catalyzed by UGT (a) Glucuronidation reaction of an alcohol/phenol substrate catalyzed by UGT. (b) Diagram of the ER showing the hypothetical topology of UGT. Membrane transporters are believed to be involved in shuttling UDPGA (abbreviated in this figure as UDP-GlcUA) to the lumen-facing UGT active site and subsequent exportation of the glucuronide products to the cytosol.<sup>42</sup>

## 7. UGT Isoforms & Species Differences

The UGT enzymes responsible for drug metabolism are divided into two major subfamilies, UGT1 and UGT2, based on their amino acid sequences.<sup>49</sup> These subfamilies consist of numerous UGT isoforms with their own substrate specificities that are responsible for the metabolism of different compounds. For example, UGT1A1 is the only isoform capable of metabolizing bilirubin, a toxic byproduct from the breakdown of red blood cells.<sup>50</sup> UGT isoforms also vary amongst species, resulting in the inability of some animals to glucuronidate certain drugs. One important drug metabolizing isoform, UGT1A4, is responsible for the *N*-glucuronidation of amines. UGT1A4 is functional in humans but exists as pseudogenes in mice and rats.<sup>51</sup> UGT1A9, an important enzyme for acetaminophen and other phenolic glucuronidations, is functional in humans and mice, but not in rats.<sup>51, 52</sup> Most notably, felines lack several major UGT enzymes, including UGT1A6 and UGT1A9, which results in the poor metabolism of many drugs.<sup>53</sup> Thus, these differences must be considered carefully when studying drug metabolism in animal models.

## 8. Drug Metabolism Studies *In Vitro*

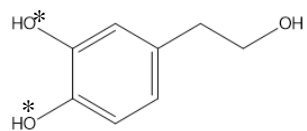
In drug development, *in vitro* metabolism studies are an important tool for predicting the pharmacokinetic behavior of drugs. Specifically, these studies help to elucidate drug metabolic pathways and resulting metabolites, serving as a precursor or replacement to *in vivo* studies. A common model used for *in vitro* metabolism studies is hepatic microsomes, due to the liver being the primary site of drug metabolism. Microsomes are fractions of the ER obtained from liver tissue by differential centrifugation, which involves lysing cells and fractioning cell components via

centrifugation. The microsomal fraction contains the ER-associated cytochrome P450s and UDP-glucuronosyltransferases, which are the most important drug metabolizing enzymes.<sup>54</sup> Therefore, microsomes can be used to carry out phase I and II reactions with a drug of interest. In phase II metabolism, glucuronidation is one of the major pathways of clearance for drugs. Thus, *in vitro* glucuronidation studies with microsomes are valuable for predicting the metabolic activity and stability of these drugs. Typical *in vitro* glucuronidation assays involve incubating hepatic microsomes with UDPGA and a drug of interest and monitoring the disappearance of the drug by HPLC. This method, referred to as the *in vitro*  $t_{1/2}$  method, allows for the determination of half-life and intrinsic clearance.<sup>55</sup> The *in vitro* half-life is useful for comparing the metabolic stability across several drugs. However, it is less suitable for predicting the metabolism of the drug *in vivo*. Instead, the *in vitro* intrinsic clearance calculated from microsomal incubations can be scaled up to more accurately predict the *in vivo* clearance of a drug.<sup>55</sup> There is some latency associated with UGT activity in hepatic microsomes that can cause underprediction in the clearance of drugs when compared to *in vivo* studies.<sup>46, 56</sup> One hypothesis for the observed latency in microsomes is that the glucuronide transport process that normally occurs within the ER membrane is disrupted.<sup>56</sup> Without these transporters, UDPGA may not be able to effectively pass through the membrane to access the active site of UGT. *In vitro* glucuronidation assays usually employ the use of detergents or pore-forming agents to disrupt the ER membrane and allow for access to the UGT active site.<sup>43, 57</sup> Alamethicin, a fungal pore-forming peptide, has been shown to increase glucuronidation activity when compared to detergents in rat liver microsomes.<sup>58</sup> Alamethicin is generally used to activate microsomes at a concentration of 50  $\mu\text{g}$  per mL

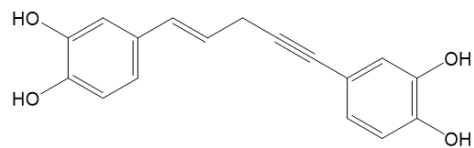
of microsomal protein.<sup>57</sup> Dithiothreitol (DTT), a reducing agent, may also combat the problem of latency. DTT has been shown to remove intramolecular disulfide bonds that are associated with latency in rat hepatic microsomes.<sup>59</sup> Overall, both alamethicin and DTT result in decreased microsomal latency and may provide more accurate estimates of UGT activity.

## 9. Research Aims

The goal of this project is to characterize the *in vitro* metabolic stability of rooperol and later use this method to rank rooperol analogues and related compounds based on half-life and intrinsic clearance. 3-Hydroxytyrosol (Figure 6) has previously been characterized in terms of its glucuronide metabolites.<sup>60</sup> This compound will be used to optimize the *in vitro* assay and will also serve as a positive control for experiments with rooperol. *In vitro* glucuronidation assays will be performed based on previously published methods.<sup>60-62</sup> Reactions will contain minipig liver microsomes suspended in TRIS-HCl buffer with the pore-forming peptide alamethicin, UDPGA cofactor, reducing agent dithiothreitol, MgCl<sub>2</sub>, and the drug of interest. The products will be separated by reversed-phase high-performance liquid chromatography (HPLC) and their identities validated by mass spectrometry (MS). We hypothesize that this *in vitro* study with rooperol will offer a reliable method for identifying rooperol analogues that display increased metabolic stability or are resistant to metabolism completely. Analogues that have longer half-lives and lower intrinsic clearance will be considered more metabolically stable. Rooperol analogues that display comparative antiproliferative characteristics to rooperol in cell lines will be selected as candidates to progress to *in vivo* testing.



**3-Hydroxytyrosol**



**Rooperol**

**Figure 6:** The Catechol-Containing Compounds 3-Hydroxytyrosol and Rooperol. Asterisks denote sites on hydroxytyrosol that have been shown to undergo glucuronidation.

## II. EXPERIMENTAL

### 1. Materials & Instruments

TRIS Ultra Pure was purchased from VWR, Gottingen minipig liver microsomes (Untreated, Male, Pool of 2) from XenoTech, alamethicin from Enzo, 2-(3,4-Dihydroxyphenyl)ethyl alcohol (3-hydroxytyrosol, >98.0%) from TCI, MgCl<sub>2</sub> and acetonitrile (HPLC grade) from Fisher, DL-dithiothreitol (99%) and acetic acid (ACS grade, 99.7%) from Sigma Aldrich, UDPGA•3Na, (99.9%) from Chem-Impex, caffeine (loaned from the Karen Lewis lab) from Eastman Organic Chemicals, ammonium acetate (HPLC grade) from EMD. Rooperol was synthesized in the Kerwin lab and estimated to be about 93% pure by HPLC (Appendix, Figure 13A).

All aqueous solutions were prepared with water from a Thermo Scientific Barnstead MicroPure Water Purification System. Other instruments include an eppendorf thermomixer (borrowed from the Whitten lab), a Fisher Scientific accuSpin Micro 17, a VWR Analog Vortex Mixer, and an eppendorf Vacufuge Plus. HPLC analysis was performed with a Thermo Scientific Dionex UltiMate 3000 HPLC. Two HPLC columns were used, an Accucore 2.6-C18, 2.1 x 100mm column for the kinetic assays and a Kromasil Eternity 5-C18, 4.6 x 250 mm column for HPLC/MS analysis. The HPLC was interfaced with an Advion expression compact mass spectrometer for identification of metabolite peaks. HPLC vials contained 300 µL capacity target inserts from Thermo Scientific.

## 2. Preparation of Stock Solutions

The reaction quencher consisted of about 2.76% acetic acid in methanol with a pH of 3.0. A TRIS-HCl buffer was prepared at 155 mM and the pH was adjusted to 7.1 at 37°C. Gottingen minipig microsomes were supplied at a concentration of 20 mg/mL in 0.5 mL of sucrose. The stock was thawed, divided into 20 µL aliquots, and then stored at -80°C. Alamethicin was supplied as 5 mg and was separated into 1 mg portions and stored at 4°C. A stock solution was prepared by dissolving the 1 mg aliquot of alamethicin in DMSO with a final concentration of 5 mg/mL and stored at -20°C. MgCl<sub>2</sub> was dissolved in water to give a concentration of 200 mM. Dithiothreitol (DTT) was made fresh daily and dissolved in TRIS-HCl pH 7.1 buffer with a final concentration of 40 mM. Three hydroxytyrosol stock solutions were prepared, 4 mM in 0.1 % DMSO, 5 mM in pure DMSO, and 0.5 mM in pure DMSO. The two rooperol stock solutions were prepared by dissolving in DMSO for a final concentration of either 5 mM or 0.5 mM. Additional stock solutions of hydroxytyrosol and rooperol were also prepared for the standard curves in methanol with a concentration of 1 mM that was diluted to 12 µM in methanol. UDPGA was supplied as 25 mg and TRIS-HCl buffer pH 7.1 was added to make a 20 mM stock. For the internal standard, caffeine was dissolved in water to give a final concentration 0.66 mM. The aqueous mobile phase for HPLC was 5 mM ammonium acetate solution in water and its pH was adjusted to 5.0.

## 3. Standard Curves

Standard curves were prepared with eleven concentrations of hydroxytyrosol or rooperol: 1, 5, 10, 20, 30, 50, 100, 150, 200, 300, and 500 µM. A 12 µM stock solution of the compounds was prepared and 1, 5, 12, 20 µL, etc. was added to the corresponding

tubes. The same amount of the internal standard caffeine (5  $\mu$ L of 0.66 mM) was added to each sample. The samples were dried with a vacufuge for about 30 minutes, the mobile phase was added (5% acetonitrile in 5 mM ammonium acetate buffer) for a final volume of 12  $\mu$ L, and each sample was transferred to an HPLC vial with an insert. HPLC analysis was performed on a 2.1 x 100 mm column, monitoring at 280 nm (hydroxytyrosol) or 260 nm (rooperol). The injection volume was 5  $\mu$ L and the flow rate was 0.2 mL/min. The mobile phase gradient is shown in Figure 7. The mobile phase composition was 5% acetonitrile for 5 minutes followed by a steep linear gradient up to 35% acetonitrile from 5-7 minutes with a total run time of 15 minutes (hydroxytyrosol) or 20 minutes (rooperol). The mobile phase was re-equilibrated to 5% acetonitrile for 20 minutes between each injection.

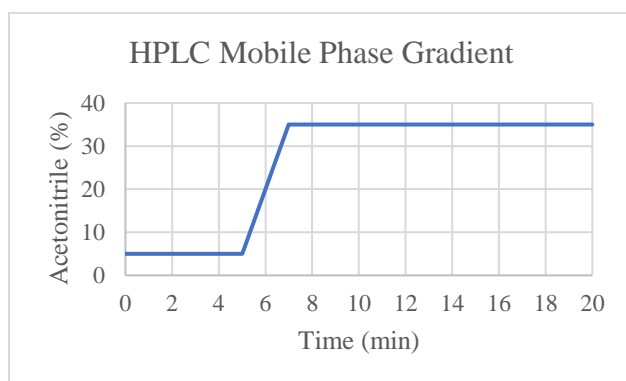


**Figure 7:** HPLC Mobile Phase Gradient. This gradient was used for HPLC analysis of standard curves and optimized *in vitro* assays with a 2.1 x 100 mm column. The mobile phase was 5 mM ammonium acetate pH 5 with an increasing amount of acetonitrile over time. The flow rate was 0.2 mL/min.

Caffeine was used as an internal standard to ensure uniformity across HPLC chromatograms as well as to account for losses in the product during the work-up phase of the *in vitro* assays. Preliminary assays carried out with caffeine added either before the work-up or just before HPLC analysis showed that better results were obtained when

adding the internal standard prior to the work-up (Appendix, Figure 1A). Thus, a peak area ratio was calculated for the drug/caffeine and was used to quantify the amount of the drug present in each HPLC chromatogram. A standard curve was prepared by plotting the peak area ratios of the drug and internal standard versus the drug and internal standard concentrations. The slope of the resulting line was used to calculate the concentration of the drug in the HPLC vial, allowing for the determination of the initial concentration in the reaction.

#### **4. Original *In Vitro* Assay with Hydroxytyrosol**

The assay was initially carried out based on a scaled-down version of a published procedure for the biocatalyzed synthesis of hydroxytyrosol glucuronides.<sup>60</sup> Hydroxytyrosol was used to optimize the *in vitro* glucuronidation assay and as a positive control for the rooperol assay. The general procedure involved combining 20  $\mu$ L of 25 mM hydroxytyrosol with a 180  $\mu$ L pre-reaction mixture containing 5 mM  $\text{CaCl}_2$ , 1 mM DTT, 100 mM TRIS-HCl buffer pH 8, 5 mM UDPGA, and 2.5 mg/mL microsomes. The final concentration of hydroxytyrosol was 2.5 mM. The reaction was carried out at 35°C in a thermomixer and 25  $\mu$ L aliquots were removed at 0, 5, 15, 30, 45, and 60 minutes. The reactions were quenched with 75  $\mu$ L of acidified methanol (2.7% acetic acid in methanol, pH 3). The internal standard, caffeine, was added (5  $\mu$ L of a 22 mM stock) and the tubes were centrifuged for 10 minutes at 10,000 x g. The supernatants were transferred to new tubes, evaporated under vacuum in a vacufuge, and stored at -80°C overnight. The samples were later dissolved in 125  $\mu$ L of mobile phase (7% acetonitrile in 5mM ammonium acetate, pH 5) and transferred to an HPLC vial with an insert. The samples were run on a 4.6 x 250 mm column and monitored at 280 nm. The injection

volume was 100  $\mu$ L and the flow rate was 1 mL/min of 7% acetonitrile in 5mM ammonium acetate, pH 5.

### **5. Optimized *In Vitro* Assay with Hydroxytyrosol and Rooperol**

The procedure described above was later optimized to more closely mimic physiological conditions. The new conditions were based on a published procedure for the glucuronidation of xenobiotics using the pore-forming peptide alamethicin.<sup>57</sup> To recapitulate physiological conditions,  $MgCl_2$  was substituted for  $CaCl_2$ , the pH of the buffer was lowered to 7.1, the final concentration of microsomes was reduced to 0.5 mg/mL, and the reaction was carried out at 37°C. A microsomal activation step was added before the reaction that involved combining microsomes with alamethicin (50  $\mu$ g/mg microsomal protein) on ice for 15 minutes. The reaction was pre-incubated at 37°C for 5 minutes after adding  $MgCl_2$ , DTT, and hydroxytyrosol and then UDPGA was used to initiate the reaction. The final concentration of hydroxytyrosol in the reaction was reduced from 2.5 mM to 0.1 mM, and the concentration of the caffeine stock solution was reduced from 22 mM to 0.66 mM.

This optimized procedure was used to study the *in vitro* metabolic stability of rooperol, with hydroxytyrosol serving as a positive control. All reactions were performed in triplicate. In a 1.5 mL microtube, TRIS-HCl buffer pH 7.1 (129  $\mu$ L for hydroxytyrosol or 130  $\mu$ L for rooperol), thawed microsomes (5  $\mu$ L), and alamethicin (1  $\mu$ L) were combined, gently vortexed, and placed on ice for 15 minutes.  $MgCl_2$  (5  $\mu$ L), DTT (5  $\mu$ L), and hydroxytyrosol (5  $\mu$ L of a 4 mM stock in 0.1% DMSO) or rooperol (4  $\mu$ L of 5 mM stock in pure DMSO) were added to the reaction tube and the mixture was pre-incubated in a thermomixer at 37°C and 900 rpm for 5 minutes. The reaction was initiated with

UDPGA (50  $\mu$ L) to give a final volume of 200  $\mu$ L. Final concentrations were 100 mM TRIS-HCl buffer, 0.5 mg/mL microsomes, 0.025 mg/mL alamethicin, 5 mM MgCl<sub>2</sub>, 1 mM DTT, 100  $\mu$ M drug, and 5 mM UDPGA. The first time point ( $t = 0$ ) was removed, and the reaction was incubated at 37°C and 900 rpm. Aliquots (30  $\mu$ L) were removed at 0, 5, 15, 30, 45, and 60 minutes for hydroxytyrosol or 0, 2, 4, 6, 8, and 10 minutes for rooperol. The aliquots were transferred to corresponding 0.65 mL microtubes containing quencher (75  $\mu$ L), vortexed, and placed on ice. After at least 30 minutes on ice, the internal standard caffeine (5  $\mu$ L of 0.66 mM) was added to each time point, which were then centrifuged at 10,000 x g for 10 minutes to precipitate the protein. Supernatants were transferred to 0.65 mL microtubes and dried in a vacufuge for about 2 hours. Samples were stored at -80°C overnight. The above assay was repeated for hydroxytyrosol dissolved in pure DMSO, (changed to 4  $\mu$ L of hydroxytyrosol and 130  $\mu$ L of TRIS-HCl buffer) The assay was also repeated for hydroxytyrosol and rooperol at a lower final concentration of 10  $\mu$ M in the reaction. The volume of each compound added to the assay was 4  $\mu$ L in DMSO and the volume of TRIS-HCl buffer used was 130  $\mu$ L. Stocks for both compounds were prepared at a concentration of 0.4 mM in pure DMSO.

## **6. Negative Controls for the *In Vitro* Assays**

Three negative controls were performed as described above with the vehicle (0.1% DMSO or DMSO), no UDPGA (only TRIS-HCl buffer pH 7.1), or heat-inactivated microsomes. For heat-inactivation, microsomes were placed in a water bath at 90°C for 5 minutes, vortexed, then placed in the water bath for another 5 minutes. Each negative control was performed in triplicate at three time points. The time points for hydroxytyrosol and rooperol experiments were 0, 15, and 60 minutes and 0, 4, and 10

minutes, respectively. For hydroxytyrosol, HPLC analysis was carried out on a 4.6 x 250 mm column and monitored at 280 nm. The injection volume was 100  $\mu$ L and the flow rate was 1 mL/min of 7% acetonitrile in 5mM ammonium acetate pH 5 with a total run time of 35 minutes. For rooperol, a 2.1 x 100 mm column was used, monitoring at 260 nm. The injection volume was 5  $\mu$ L and the flow rate was 0.2 mL/min. The mobile phase composition was 5% ACN in 5 mM ammonium acetate for 5 minutes, followed by a linear gradient up to 35% ACN from 5-7 minutes with a total run time of 20 minutes.

## **7. Half-life and Intrinsic Clearance Determination by HPLC**

The disappearance of the drug was monitored by HPLC in order to determine the first-order rate constant, which was used to calculate the *in vitro* half-life and intrinsic clearance. The HPLC analysis was originally performed on a 4.6 x 250 mm column. However, rooperol eluted much later than hydroxytyrosol and resulted in long analysis times for the rooperol *in vitro* assays. The column was changed to a 2.1 x 100 mm column with a gradient elution, which allowed for quicker analysis times and required less solvent. Reaction samples from the previous day were removed from the -80°C freezer, dissolved in 10  $\mu$ L of mobile phase (5% acetonitrile in 5 mM ammonium acetate, pH 5), and vortexed. Each sample was transferred to an HPLC vial containing an insert. The absorbance was monitored at 280 nm (hydroxytyrosol) or 260 nm (rooperol). The injection volume was 5  $\mu$ L and the flow rate was 0.2 mL/min. The mobile phase gradient used for *in vitro* assays was the same as described previously for standard curves and is illustrated in Figure 7.

The area under the peaks for both the drug and the internal standard caffeine were recorded for each injection. A peak area ratio (PAR) was calculated by dividing the peak area of the drug by the peak area of caffeine. The natural log of the PAR was plotted against time and resulted in a straight line, indicating a first-order reaction. The slope of the linear regression represents the first order rate constant (-k) and was used to calculate the half-life of the drug.<sup>63</sup>

$$t_{1/2} = \frac{\ln 2}{-k}$$

The half-life and the concentration of microsomal protein was used to calculate the *in vitro* intrinsic clearance ( $CL'_{int}$ ).<sup>55</sup>

$$CL'_{int} = \frac{\ln 2}{t_{1/2}} \times \frac{mL \text{ incubation}}{mg \text{ microsomal protein}}$$

## 8. Identification of Metabolites by HPLC/MS

An *in vitro* glucuronidation assay was performed as described above for both hydroxytyrosol and rooperol, but the reaction was permitted to proceed for a longer duration. This was to allow for maximum metabolite production for MS identification. For hydroxytyrosol, 50  $\mu$ L aliquots were removed at 4 hours. For rooperol, two 50  $\mu$ L aliquots were removed at 30 minutes and another two 50  $\mu$ L aliquots were removed after 60 minutes. The samples were centrifuged, the supernatants transferred and then dried in a vacufuge as before. After overnight storage at -80°C, the samples were dissolved in 25  $\mu$ L of mobile phase (5% acetonitrile in water) and transferred to HPLC vials containing inserts. The longer HPLC column (4.6 x 250 mm) was used to obtain better separation between the injection peak and any glucuronide metabolites. The injection volume was

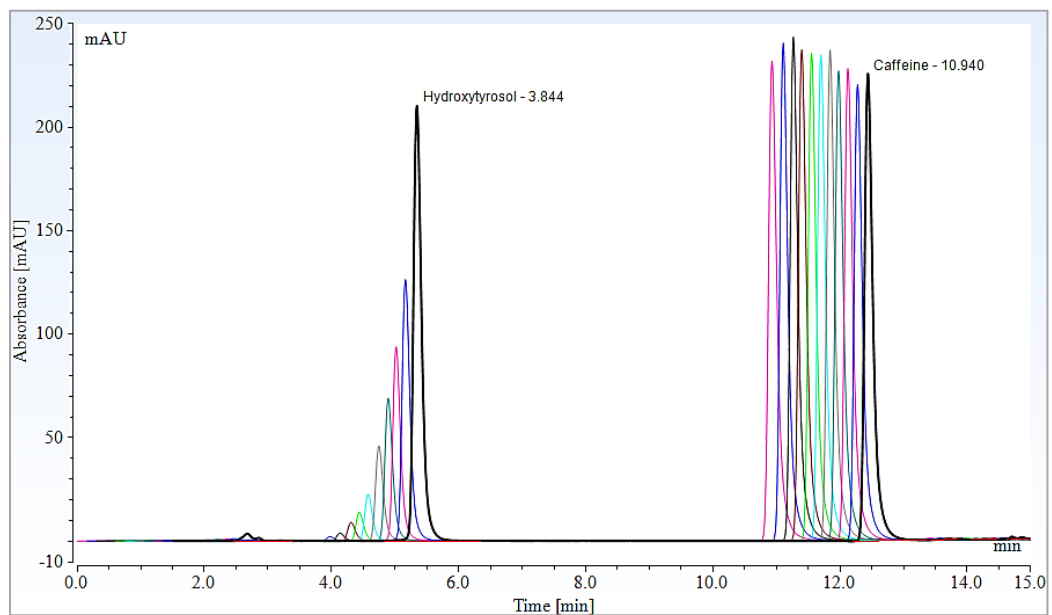
20  $\mu$ L and the flow rate was 1.0 mL/min. The absorbance was monitored at 280 nm (hydroxytyrosol) or 260 nm (rooperol). The mobile phase composition was 5% acetonitrile for 10 minutes, 5-35% acetonitrile from 10-20 minutes, and 35% acetonitrile for the remainder of the 30-minute run time. The HPLC was directly connected to the MS with an atmospheric-pressure chemical ionization (APCI) manifold monitoring with both APCI<sup>+</sup> and APCI<sup>-</sup> modes. The ionization conditions were a capillary temperature of 250°C, capillary voltage of 180 V, source gas temperature of 20°C, and APCI corona discharge of 0.1  $\mu$ A.

### III. RESULTS

#### 1. Standard Curves

The *in vitro*  $t_{1/2}$  method involves monitoring the disappearance of the drug by HPLC. In order to quantify the amount of drug present based on absorbance values, standard curves were constructed for both hydroxytyrosol and rooperol (Figures 8 and 9). An increasing concentration of the drug, hydroxytyrosol or rooperol, was spiked with the same concentration of the internal standard caffeine. The HPLC chromatograms (Figures 8 (a) and 9 (a)) for each drug concentration are overlaid to show the increase in absorbance associated with increasing concentration. The peak area (PA) ratio was then plotted against the concentration ratio of the drug and caffeine in each sample (Figure 8 (b) and 9 (b), For the corresponding table, see Appendix Figures 2A and 3A). The equation generated from the standard curve was used to determine the concentration of hydroxytyrosol or rooperol present in the *in vitro* assay. The concentrations calculated for each time point collected in the assays are listed in the corresponding data tables located in the Appendix.

(a)



(b)

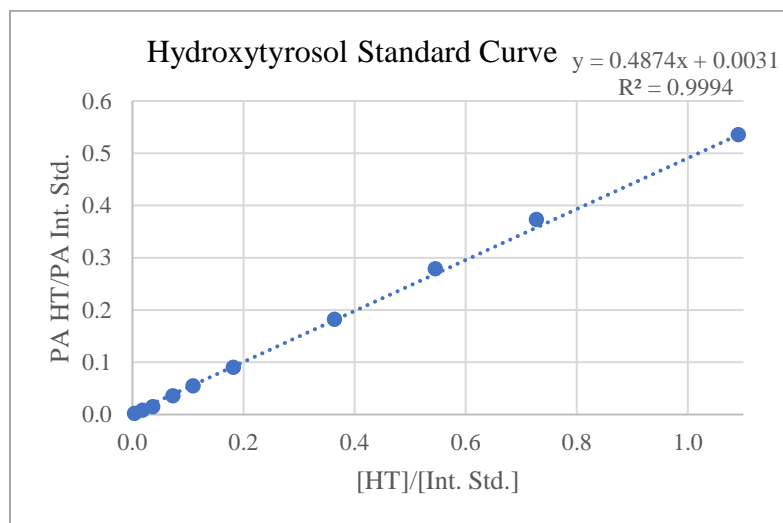
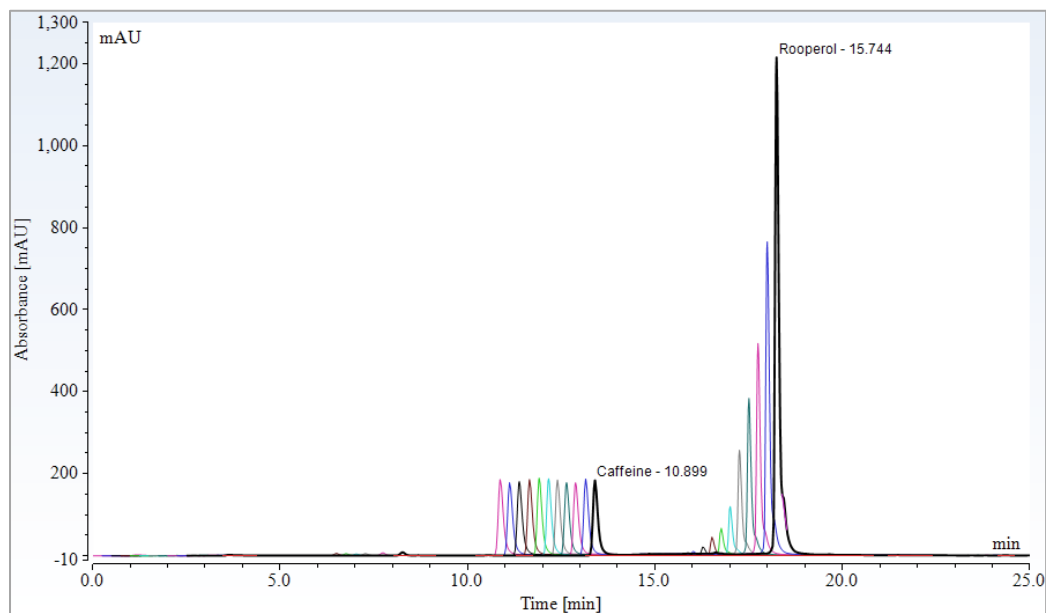


**Figure 8:** Standard Curve for Hydroxytyrosol. (a) An overlay of the HPLC chromatograms for eleven different concentrations of hydroxytyrosol (1, 5, 10, 20, 30, 50, 100, 150, 200, 300, and 500  $\mu\text{M}$ ) spiked with the same concentration of caffeine. (Overlay is shown with a time offset) (b) Plot of the peak area ratio versus the concentration ratio of hydroxytyrosol and caffeine.

(a)



(b)

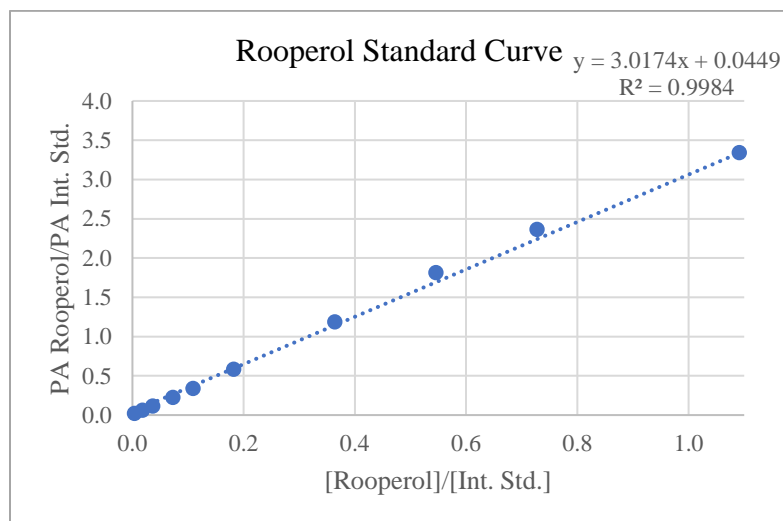
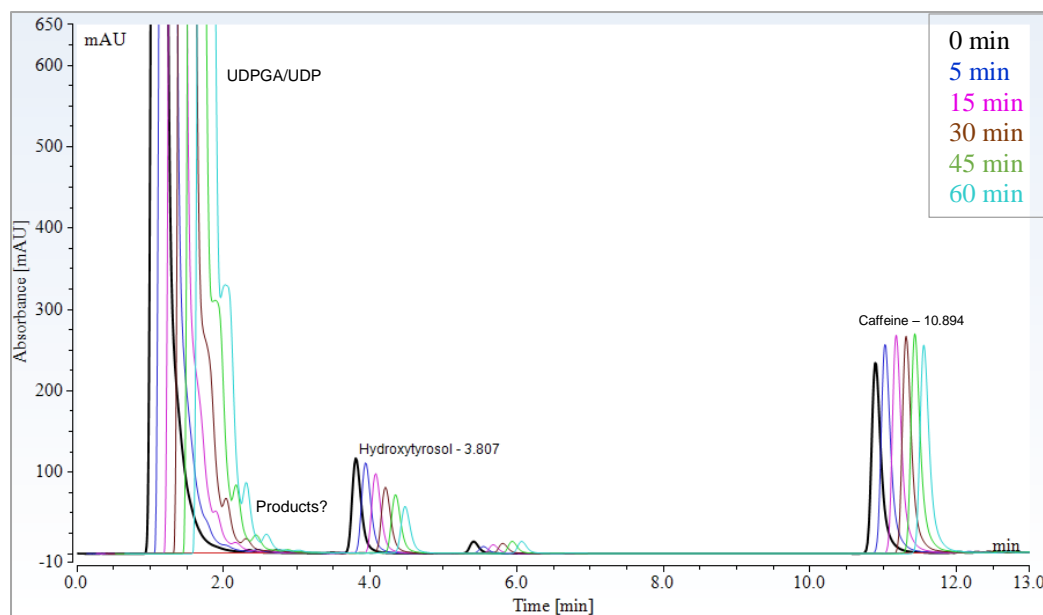


**Figure 9:** Standard Curve for Rooperol (a) An overlay of the HPLC chromatograms for eleven different concentrations of rooperol (1, 5, 10, 20, 30, 50, 100, 150, 200, 300, and 500  $\mu\text{M}$ ) spiked with the same concentration of caffeine. (Overlay is shown with a time offset) (b) Plot of the peak area ratio versus the concentration ratio of rooperol and caffeine.

## 2. *In Vitro* Assays with Hydroxytyrosol

Hydroxytyrosol was first used to optimize the *in vitro* metabolism assay reaction conditions, including pH and addition of alamethicin. Results from these experiments are shown in the Appendix, Figures 4A and 5A. After optimization of the assay, hydroxytyrosol was used as a positive control for experiments with rooperol. The results from one of the triplicate reactions with hydroxytyrosol (Replicate A) is shown in Figure 10. An overlay of the HPLC chromatograms obtained from each time point (see legend) with a time offset shows the disappearance of hydroxytyrosol and the subsequent appearance of metabolites (Figure 10 (a)). The large peak that elutes at a retention time (RT) of around 1.25 minutes is UDPGA. The magnitude of this peak is due to the 50-fold higher concentration of UDPGA compared to the drug to ensure no rate-limiting effects due to lack of the cofactor. The large, growing shoulder on the right side of the peak is likely UDP, which increases as the glucuronic acid moiety is removed from UDPGA. The smaller, growing shoulders on the UDPGA/UDP peak may correspond to hydroxytyrosol glucuronide metabolites, which are much more hydrophilic than hydroxytyrosol and elute between 1.5 and 2 minutes. Although the short HPLC column used here increased analysis time, a consequence of this column is poor separation of the early eluting UDPGA, UDP, and glucuronide metabolite peaks. The initial assays with hydroxytyrosol were analyzed with a longer column and showed two clearly separated peaks that correspond to two glucuronide products. The peak for hydroxytyrosol, with an RT of about 3.8 minutes, steadily decreases over time as the drug is metabolized. The peak at a RT of about 5.5 minutes is likely DTT since the oxidized form is cyclic and absorbs strongly at 280 nm.<sup>64</sup> In addition, this peak is present in HPLC

(a)



(b)

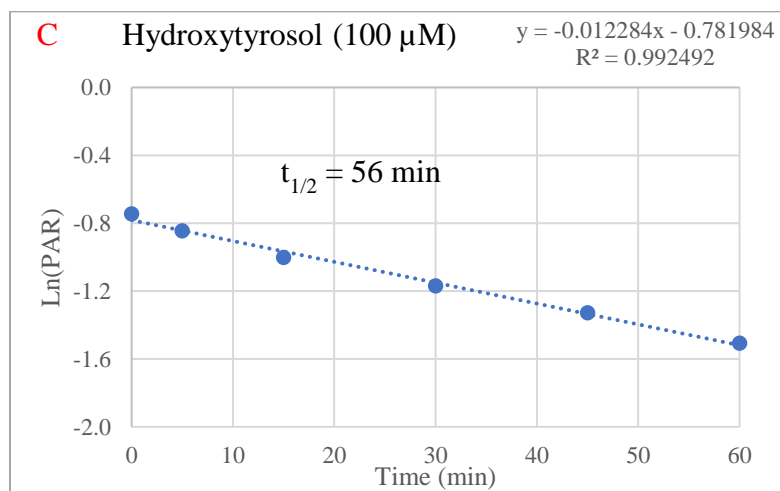


**Figure 10:** Results for the *In Vitro* Assay with 100  $\mu\text{M}$  Hydroxytyrosol (One replicate of the reactions performed in triplicate). (a) Overlay of the HPLC chromatograms of each time point during the reaction (shown with a time offset). (b) Log plot obtained from HPLC data showing the disappearance of hydroxytyrosol and the calculated half-life. (Replicate C is shown, See Appendix Figure 6A for all data from the triplicate reactions)

chromatograms for *in vitro* assays with both hydroxytyrosol and rooperol as well as all negative controls. The peak at a RT of about 10.9 minutes is the internal standard, caffeine. The same amount of caffeine is added to each time point, so fluctuations in these peak areas correspond to losses in product during the work-up of the reaction. The peak areas for hydroxytyrosol and caffeine were used to construct the log plot for the disappearance of hydroxytyrosol (Figure 10 (b)). The slope from the line of best fit was used to calculate the half-life. The half-life for this replicate was 59 minutes, with an average half-life of  $56 \pm 2$  minutes for the triplicate reactions. The half-lives were used to calculate an average *in vitro* intrinsic clearance ( $CL'_{int}$ ) of  $0.03 \pm 8 \times 10^{-4} \text{ mL} \cdot \text{mg}^{-1} \cdot \text{min}^{-1}$ . This experiment was a repeat of the *in vitro* assay with hydroxytyrosol on a separate day that had an average half-life of  $65 \pm 9$  min with an average  $CL'_{int}$  of  $0.02 \pm 3 \times 10^{-3} \text{ mL} \cdot \text{mg}^{-1} \cdot \text{min}^{-1}$ . These two triplicate assays (n=6) were combined to generate a different visual representation of the data based on the percent of the drug remaining over time (Figure 11). The average percent of hydroxytyrosol remaining at each time point was fit to an exponential curve and error bars were added to show the variability between reactions. During the 60 minutes of reaction time for these assays, one half-life of hydroxytyrosol was observed at about 57 minutes. The corresponding data table for this figure is shown in the Appendix, Figure 8A.

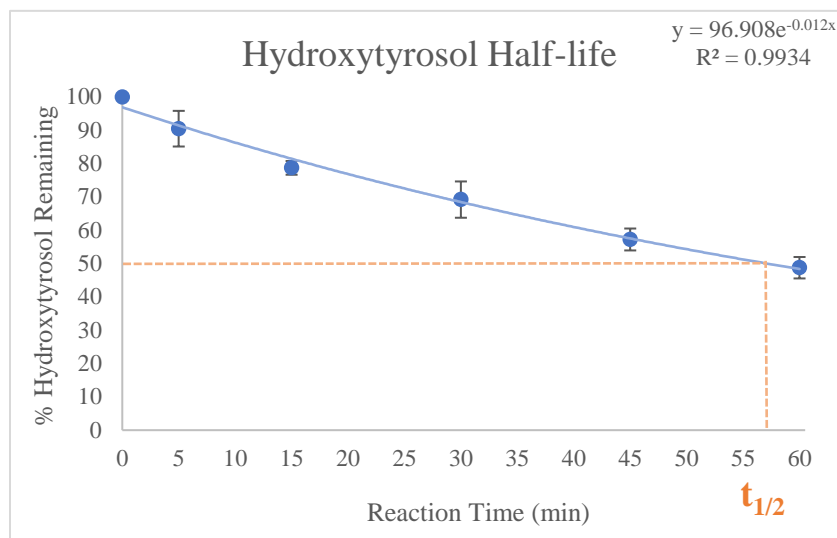
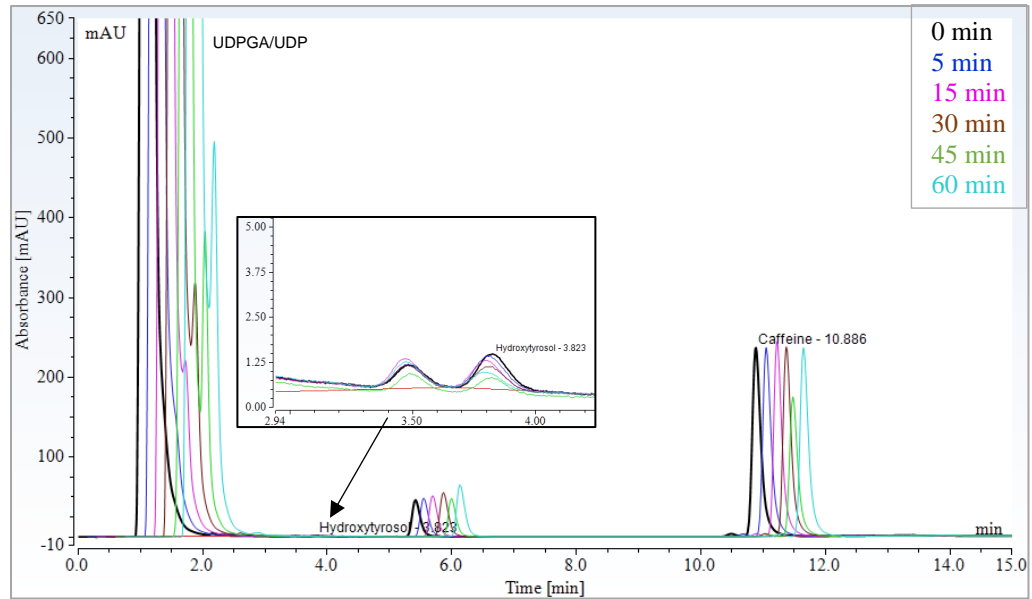


**Figure 11:** The Percent of Hydroxytyrosol Remaining Over Time. This was calculated from the averages of the triplicate *in vitro* assays with hydroxytyrosol from two different days (n=6). The concentration of hydroxytyrosol at each time point was normalized to time point 0, which was designated as 100%.

The derivation of the equation for half-life relies on the assumption that the substrate concentration is much lower than the  $K_m$ . To test how the concentration of hydroxytyrosol affects half-life, a low concentration of 10  $\mu\text{M}$  was used. This concentration is predicted to be lower than the  $K_m$  for hydroxytyrosol and is on the order of drug concentrations commonly used for *in vitro* metabolism assays.<sup>63, 65</sup> An overlay of the HPLC chromatograms for one replicate for the 10  $\mu\text{M}$  hydroxytyrosol assay is shown in Figure 12 (a). A consequence of the low concentration is that the peaks are very small and less distinguishable from baseline fluctuations. The inset in the chromatogram more clearly shows the hydroxytyrosol peaks present at an RT of 3.8 minutes. The inset chromatogram is overlaid with no time offset in order to discriminate the peak from the baseline. An issue with peaks this small is that the HPLC software can not automatically integrate these peaks accurately.

(a)



(b)

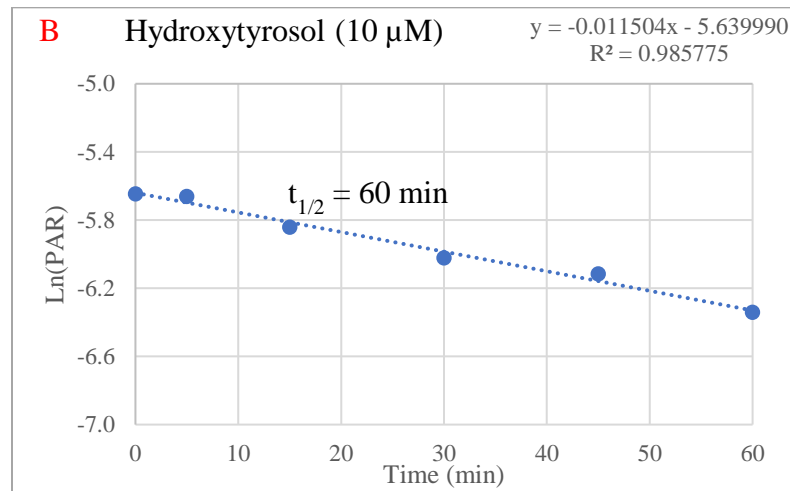


**Figure 12:** Results for the *In Vitro* Assay with 10  $\mu\text{M}$  Hydroxytyrosol (one replicate of the reactions performed in triplicate) (a) Overlay of the HPLC chromatograms for each time point (shown with a time offset). (b) Log plot obtained from HPLC data showing the disappearance of hydroxytyrosol and the calculated half-life. (Replicate B shown, See Appendix Figure 10A for all data from the triplicate reactions)

Manual integration was necessary and was done visually, ensuring that the limits chosen for the bases of the peaks were uniform across all time points. (See Appendix Figure 11A for comparison of the auto-integration versus manual integration). The peak areas from the manual integration gave surprisingly good results in the log plot (Figure 12 (b)), with  $R^2$  values between 0.93 and 0.98 for the triplicates. The average half-life for the triplicates with 10  $\mu\text{M}$  hydroxytyrosol was  $60 \pm 11$  min with an average  $\text{CL}'_{\text{int}} = 0.03 \pm 4 \times 10^{-3} \text{ mL} \cdot \text{mg}^{-1} \cdot \text{min}^{-1}$ . Based on these results, the change in concentration of hydroxytyrosol from 100  $\mu\text{M}$  to 10  $\mu\text{M}$  does not seem to largely influence the calculated half-life and intrinsic clearance. Negative controls were performed with either heat-inactivated microsomes, without UDPGA, or with only the vehicle (no hydroxytyrosol). When comparing the data from *in vitro* assays with hydroxytyrosol to that obtained for negative controls (Appendix, Figure 12A), it is apparent that the disappearance of hydroxytyrosol is due to enzymatic metabolism dependent on the presence of the glucuronic acid moiety from UDPGA. A summary of the results from all *in vitro* assays performed with hydroxytyrosol is shown in Table 1. The largest changes in calculated half-lives appear with the addition of alamethicin or when substituting  $\text{MgCl}_2$  and lowering the pH from 8.0 to 7.1. Overall, this data supports the conclusion that these reaction conditions have a much larger impact on UGT activity and half-life than the drug vehicle or concentration for these *in vitro* assays with hydroxytyrosol.

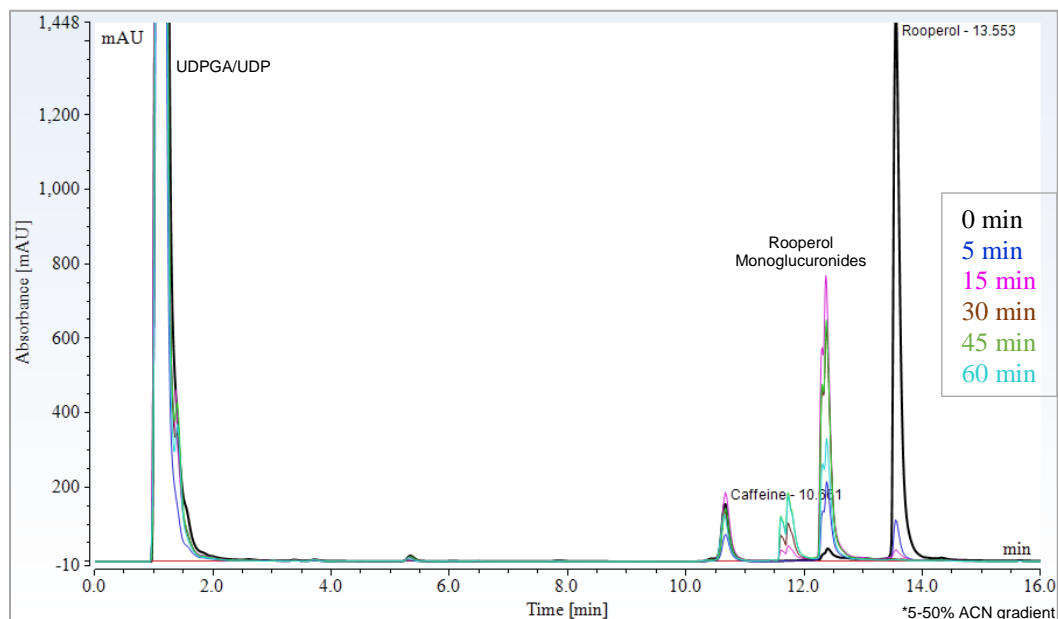
**Table 1:** Summary of results from *in vitro* assays with hydroxytyrosol at 100  $\mu\text{M}$  or 10  $\mu\text{M}$  in triplicate. The reaction conditions (alamethicin, pH, metal ion, and vehicle) changed during optimization of the *in vitro* assay are shown. Items in bold represent changes from the preceding experiment. The supporting data is located in the Appendix Section in the indicated figures.

Conc. ( $\mu\text{M}$ )	Reaction Conditions	Average $t_{1/2}$ (min)	Intrinsic Clearance ( $\text{mL}\cdot\text{mg}^{-1}\cdot\text{min}^{-1}$ )	Supp. Data
100	pH 8, $\text{CaCl}_2$ , 0.1% DMSO	$62 \pm 9$	$0.02 \pm 3 \times 10^{-3}$	Fig 4A
100	pH 8, $\text{CaCl}_2$ , 0.1% DMSO <b>alamethicin</b>	$47 \pm 1$	$0.03 \pm 9 \times 10^{-4}$	Fig 5A
100	<b>pH 7.1, <math>\text{MgCl}_2</math></b> , 0.1% DMSO alamethicin	$65 \pm 9$	$0.02 \pm 3 \times 10^{-3}$	Fig 6A
100	Same as above	$56 \pm 2$	$0.03 \pm 8 \times 10^{-4}$	Fig 7A
100	pH 7.1, $\text{MgCl}_2$ , <b>100% DMSO</b> alamethicin	$62 \pm 3$	$0.02 \pm 1 \times 10^{-3}$	Fig 9A
<b>10</b>	Same as above	$60 \pm 11$	$0.03 \pm 4 \times 10^{-3}$	Fig 10A

### 3. *In Vitro* Assays with Rooperol

All assays with rooperol were carried out using the optimized procedure. A preliminary *in vitro* assay with rooperol (100  $\mu\text{M}$ ) was performed using time points spanning 60 minutes as done previously with hydroxytyrosol. The results from this assay are shown in Figure 13. An overlay of the HPLC chromatograms obtained for this experiment is shown in Figure 13 (a), with no time offset. The mobile phase composition was 5-50% acetonitrile. All other HPLC analysis of rooperol assays was done using the 5-35% acetonitrile gradient (See Figure 7) to obtain better peak separation. With this HPLC method, rooperol eluted around 13.5 minutes. From the HPLC data, it was apparent that rooperol was metabolized exceptionally fast with an almost 90% reduction in the peak area by 5 minutes (See Appendix Figure 14A for data table).

(a)



(b)

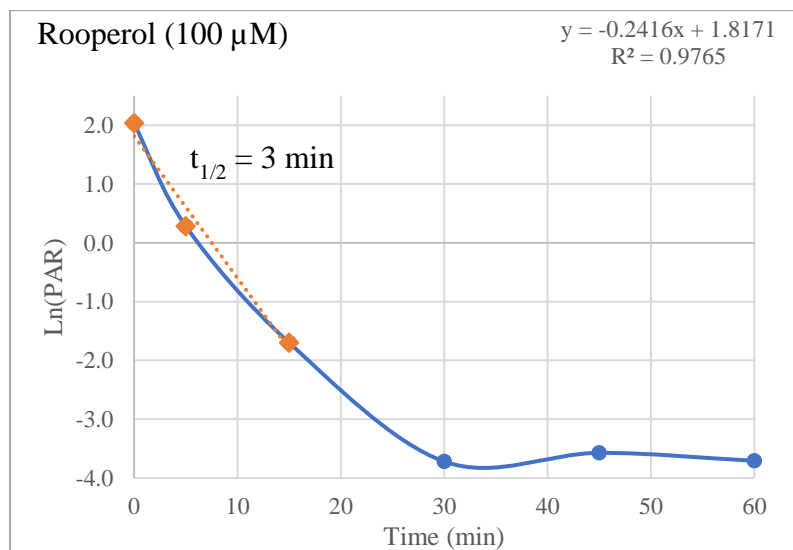


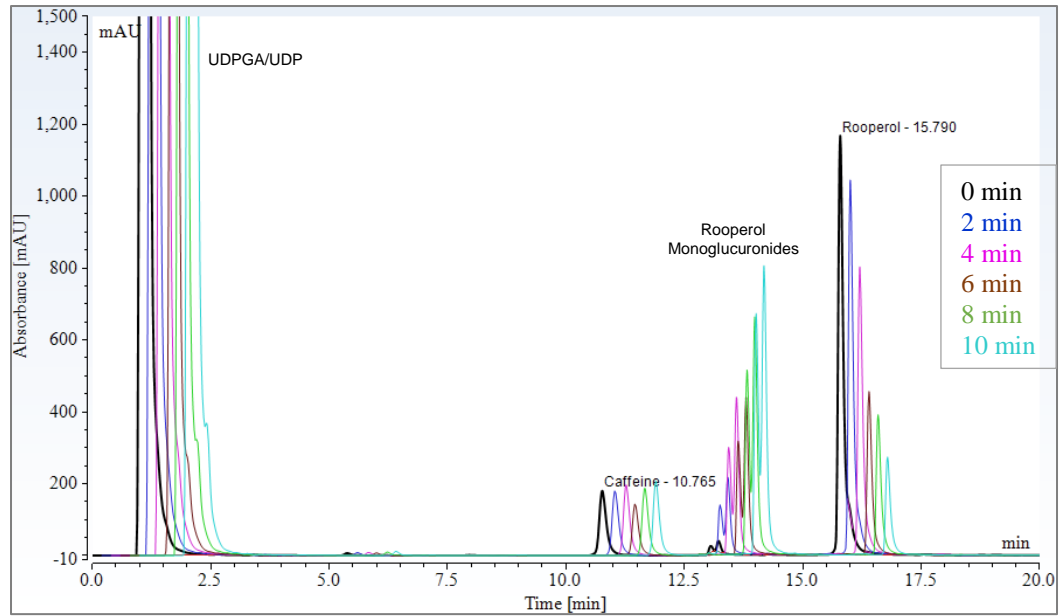
**Figure 13:** The Disappearance of Rooperol Over 60 Minutes. (a) An overlay of the HPLC chromatograms for each time point showing the rapid disappearance of the rooperol peak with a corresponding increase in rooperol glucuronides. (Note: The mobile phase gradient was 5-50% acetonitrile) (b) The log plot obtained from peak areas at each time point. Due to the short half-life of rooperol, the  $\text{Ln}(\text{PAR})$  vs. time plot is not linear. The approximate half-life of rooperol was estimated from the linear portion of the plot at time points 0, 5, 15 minutes (See Figure 14A in Appendix for data table).

Two closely eluting peaks at an RT of around 12.5 minutes increase in area from 0-15 min, then steadily decrease. This indicates that these are intermediates in the reaction, likely monoglucuronides. Another two closely eluting peaks first appear at 45 minutes and increase steadily. Because rooperol has four possible sites where glucuronide conjugation can occur, these four peaks (RTs between 11.75-12.5 minutes) may all be monoglucuronides of rooperol. The log plot (Figure 13 (b)) shows that the initial disappearance of rooperol is linear, but levels off around 30 minutes. The half-life of rooperol, 2.87 minutes, was estimated based on the linear portion of the plot with time points 0, 5, and 15 minutes. Based on the short half-life, the time points for the *in vitro* assay with rooperol were reduced to 0, 2, 4, 6, 8, and 10 minutes. An example of an assay with these new time points is shown in Figure 14. The HPLC chromatogram overlay (Figure 14 (a)) for one of the triplicate reactions (Replicate A) shows a steady decrease in the peak area of rooperol (RT  $\approx$  15.8 min) with a corresponding increase in the two monoglucuronide peaks (RT  $\approx$  13-13.5 min). At time point t=0, there should theoretically be no peak corresponding to the monoglucuronide intermediate. However, there is a slight delay that occurs between initiating the reaction, aliquoting, and quenching which accounts for the appearance of the monoglucuronide peak present in the chromatogram for time point zero. The log plot (Figure 14 (b)) was used to calculate a half-life of 4 minutes. The average half-life obtained for the assay in triplicate was  $4 \pm 0.5$  min with a  $CL'_{int}$  value of  $0.08 \pm 1 \times 10^{-2}$  mL $\cdot$ mg $^{-1}$  $\cdot$ min $^{-1}$ . This experiment was repeated on a separate day with an average half-life of  $3 \pm 0.5$  minutes and a  $CL'_{int}$  value of  $0.1 \pm 2 \times 10^{-2}$  mL $\cdot$ mg $^{-1}$  $\cdot$ min $^{-1}$ . These two triplicate assays (n=6) were combined to generate a different visual representation of the data based on the percent of the drug remaining over time

(Figure 15). The average percent of rooperol remaining at each time point was fit to an exponential curve and error bars were added to show the variability between reactions. During the 10 minutes of reaction time for these assays, two half-lives were observed for rooperol, at around 4 and 7 minutes. The corresponding data table for this figure is shown in the Appendix, Figure 17A.

The *in vitro* assay with a low concentration of rooperol, 10  $\mu\text{M}$ , is shown in Figure 16. The overlay of the HPLC chromatograms for one of the triplicates (Replicate A) in Figure 16 (a) shows the small peak for rooperol at an RT of about 15.8 minutes. The inset chromatogram more clearly shows the decrease in the rooperol peak size. This low concentration of rooperol resulted in peaks that were somewhat difficult to distinguish from the baseline, especially due to the increase in baseline noise normally seen after a gradient elution. As before, auto-integration by the HPLC software did not yield an equivalent characterization of the peak amongst all time points. Manual peak integration yielded adequate results, although the  $R^2$  values from the linear regression were much lower for rooperol compared to hydroxytyrosol. An example of auto-integration versus manual integration for rooperol peaks is shown in the Appendix, Figure 19A. The log plot shown in Figure 16 (b) was used to calculate the half-life of 3.81 minutes. The average half-life obtained for these triplicates at 10  $\mu\text{M}$  was  $4 \pm 0.5$  minutes with a  $CL'_{\text{int}}$  value of  $0.09 \pm 1 \times 10^{-2} \text{ mL} \cdot \text{mg}^{-1} \cdot \text{min}^{-1}$ .

(a)



(b)

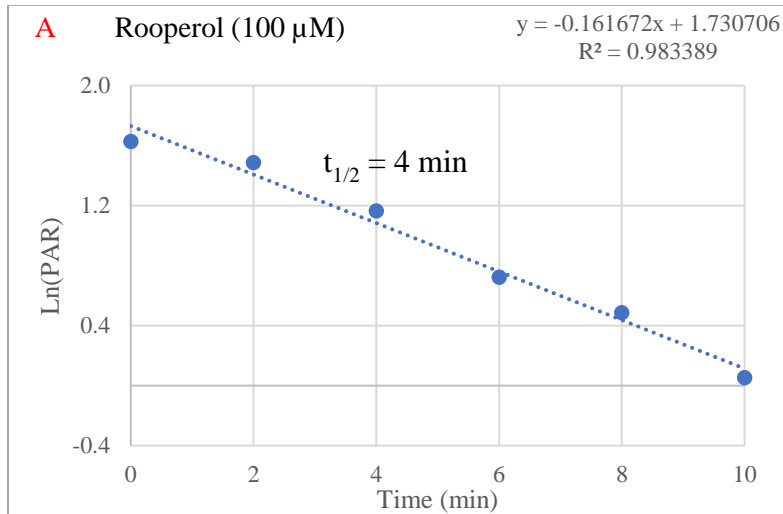


**Figure 14:** Results for the *In Vitro* Assay with 100  $\mu$ M Rooperol (one replicate of the reactions performed in triplicate). **(a)** Overlay of the HPLC chromatograms for each time point (shown with a time offset). **(b)** Log plot obtained from HPLC data showing the disappearance of rooperol and the calculated half-life. (Replicate A shown, See Appendix Figure 16A for all data from the triplicate reactions)

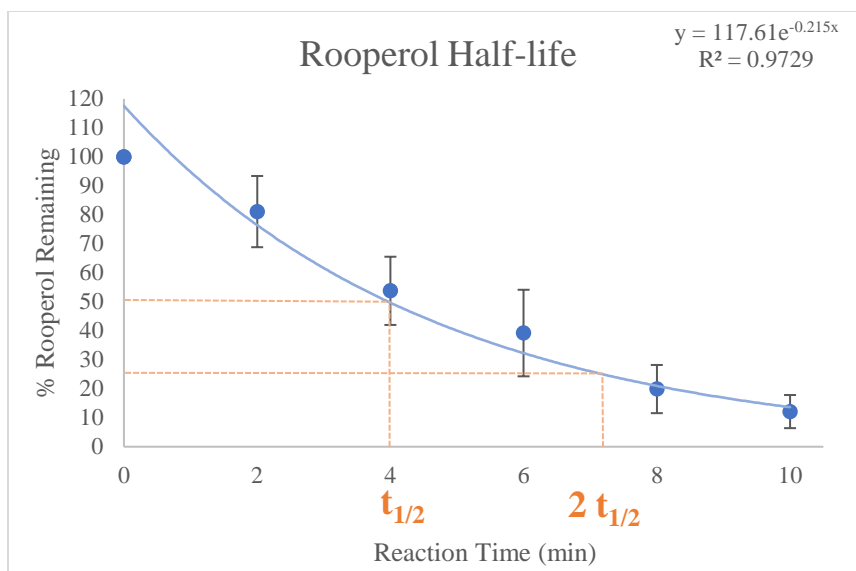
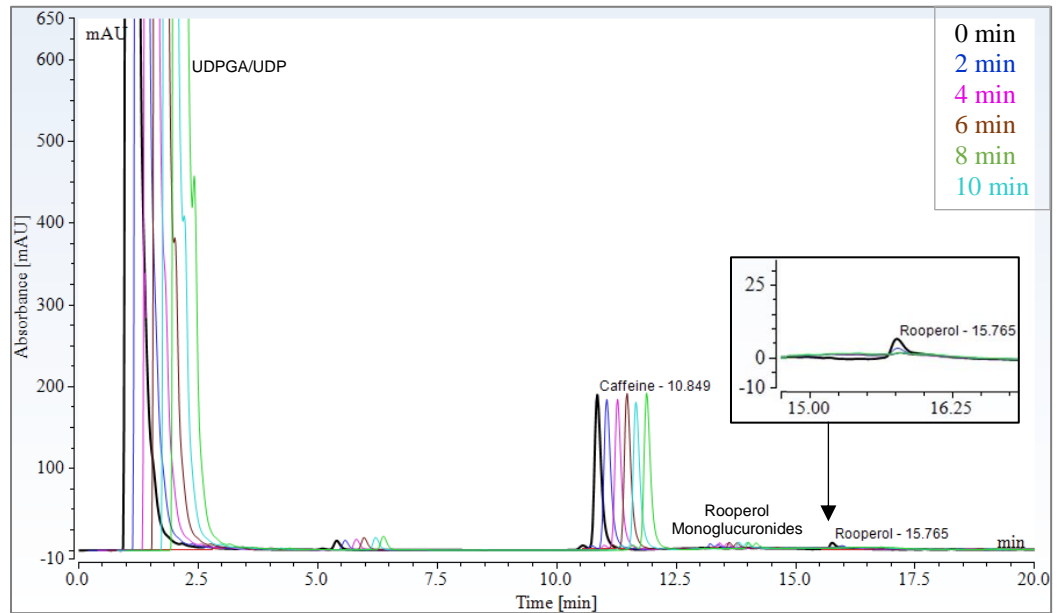


**Figure 15:** The Percent of Rooperol Remaining Over Time. This was calculated from the averages of the triplicate *in vitro* assays with rooperol from two different days (n=6). The concentration of rooperol at each time point was normalized to time point 0, which was designated as 100%.

Negative controls for rooperol *in vitro* assays consisted of heat-inactivated microsomes, no UDPGA cofactor, or the vehicle with no rooperol (Appendix, Figure 20A). These results confirmed that the disappearance of rooperol does not occur when microsomal enzymes are inactivated or without the presence of the UDPGA cofactor. A summary of the results obtained from all *in vitro* assays with rooperol is shown in Table 2. The initial prediction of a half-life of about 3 minutes from the disappearance of rooperol over 60 minutes agrees with the half-lives calculated for the disappearance of rooperol over 10 minutes. In addition, the decrease in the reaction concentration from 100  $\mu\text{M}$  to 10  $\mu\text{M}$  did not impact the calculated half-life and intrinsic clearance.

(a)



(b)

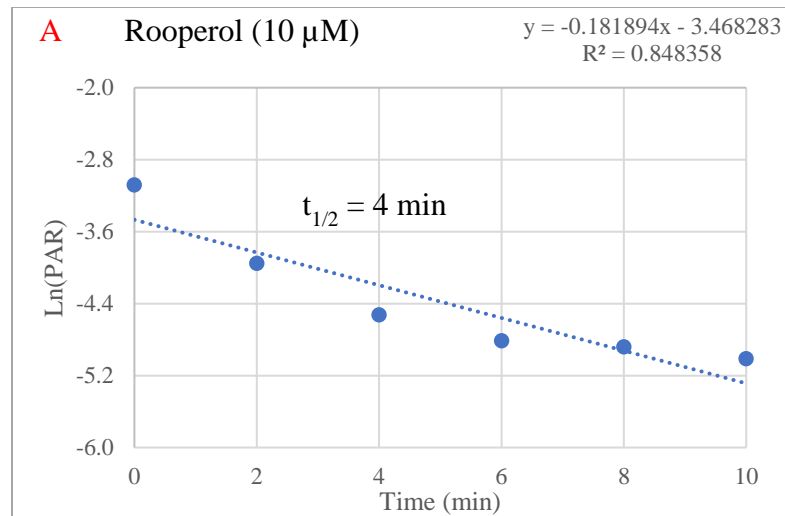


**Figure 16:** Results from the *in vitro* assay with 10  $\mu\text{M}$  rooperol (one replicate of the reactions performed in triplicate). **(a)** Overlay of the HPLC chromatograms for each time point (shown with a time offset). **(b)** Log plot obtained from HPLC data showing the disappearance of rooperol and the calculated half-life. (Replicate A shown, See Appendix Figure 18A for all data from the triplicate reactions)

**Table 2:** Summary of results from *in vitro* assays with rooperol at 100  $\mu\text{M}$  or 10  $\mu\text{M}$  in triplicate. The supporting data is located in the Appendix section in the indicated figures.

Conc. ( $\mu\text{M}$ )	Reaction Conditions	Average $t_{1/2}$ (min)	Intrinsic Clearance ( $\text{mL}\cdot\text{mg}^{-1}\cdot\text{min}^{-1}$ )	Supp. Data
100	pH 7.1, $\text{MgCl}_2$ , 100% DMSO alamethicin	3*	0.1*	Fig 14A
100	Same as above	$3 \pm 0.5$	$0.1 \pm 2 \times 10^{-2}$	Fig 15A
100	Same as above	$4 \pm 0.5$	$0.08 \pm 1 \times 10^{-2}$	Fig 16A
<b>10</b>	Same as above	$4 \pm 0.5$	$0.09 \pm 1 \times 10^{-2}$	Fig 18A

\*Calculated from the plot for disappearance of rooperol over 60 minutes. (Fig. 13 (b))

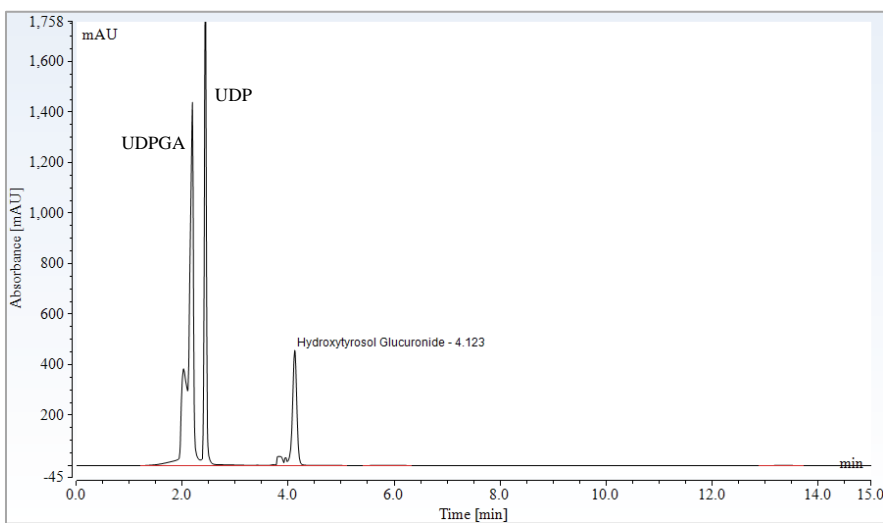
#### 4. HPLC/MS of Glucuronide Metabolites

The identities of the products of the *in vitro* glucuronidation assay were verified by HPLC/MS. Molecular weights of all species are shown in Table 3. Analysis was performed on the longer, 4.6 x 250 mm HPLC column to separate any early eluting metabolite peaks from the large UDPGA/UDP peaks. The HPLC chromatogram for in the *in vitro* assay with hydroxytyrosol after a reaction time of four hours is shown in Figure 17 (a). At 4 hours, hydroxytyrosol has been converted to one product, at an RT of about 4.12 minutes. Figure 17 (b) shows the MS spectrum acquired for this peak. The signal at 329.1 corresponds to a hydroxytyrosol glucuronide ( $[\text{M}-\text{H}]^-$ ). The addition of a glucuronide group adds about 176 mass units to hydroxytyrosol and results in a molecular weight of 330.29.

**Table 3:** Molecular weights of hydroxytyrosol, rooperol, and their corresponding glucuronides. The addition of a glucuronide group adds about 176 mass units to the molecular weight of the parent compound.

Species	Molecular Weight
Glucuronide Group	~176
Hydroxytyrosol	154.17
Hydroxytyrosol Glucuronide	330.29
Rooperol	282.30
Rooperol Monoglucuronide	458.42
Rooperol Diglucuronide	634.54

(a)



(b)

Hydroxytyrosol Glucuronide, MW = 330.29

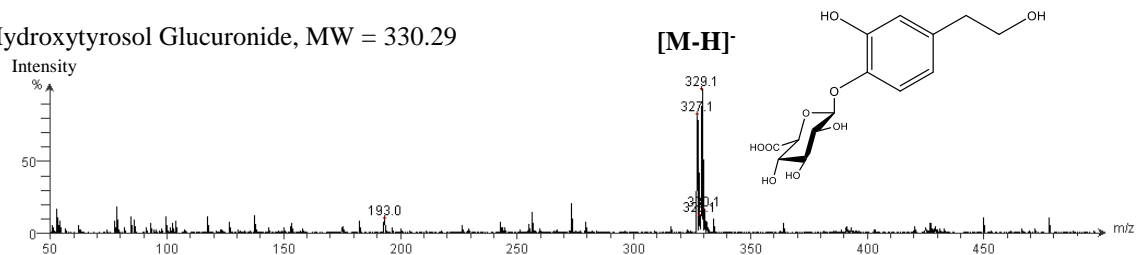
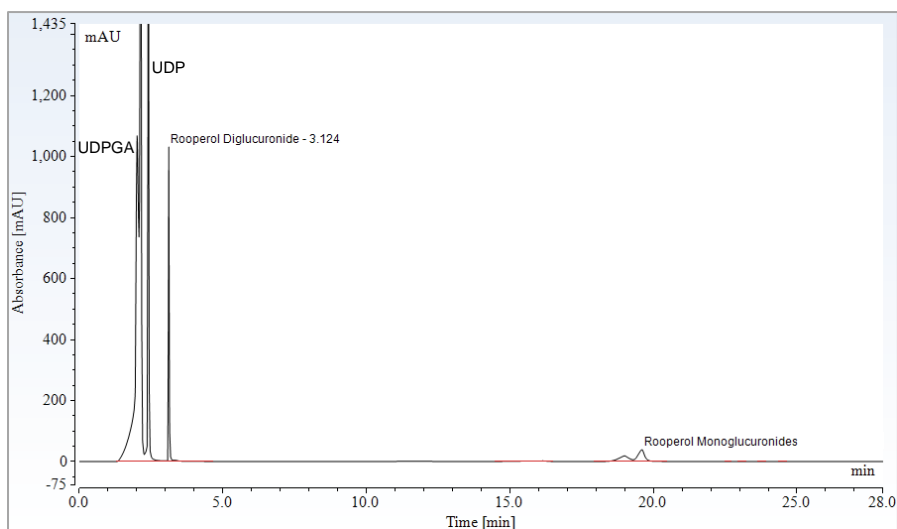


**Figure 17:** HPLC/MS of hydroxytyrosol metabolites. The reaction was allowed to proceed for four hours. (a) HPLC chromatogram (b) MS spectrum for the glucuronide metabolite of hydroxytyrosol. The molecular structure shown is an example of one possible position of the glucuronide moiety on hydroxytyrosol.

The HPLC chromatogram for the *in vitro* assay with rooperol after a reaction time of 60 minutes (Figure 18 (a)) shows one product at a RT of 3.12 minutes as well as two later eluting peaks around 18.5-20 minutes. Figure 18 (b) shows the MS spectrum obtained for the early eluting metabolite peak (RT = 3.12 minutes). The MS signal at 633.7 corresponds to rooperol plus two glucuronide groups (~176 each) which results in a molecular weight of 634.54.

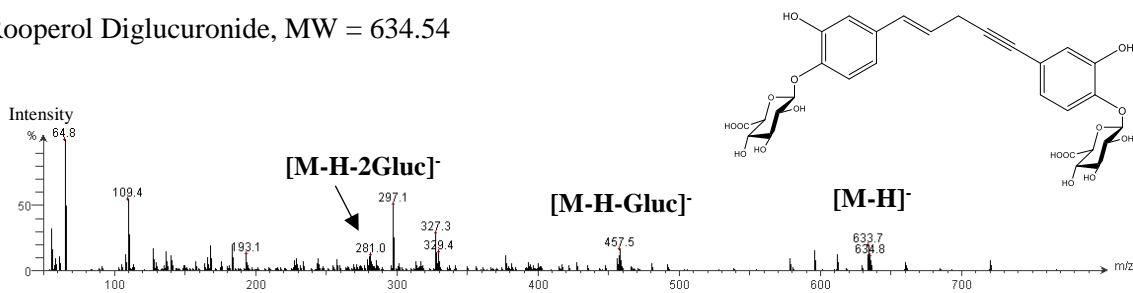
Fragments of the rooperol diglucuronide can also be seen from the MS signals at 475.5 and 281.0, corresponding the loss of one and two glucuronide moieties, respectively. The MS spectrum obtained for both of the later eluting peaks have three major signals at 457.4, 281.3, and 175.1. The signal at 457.5,  $[M-H]^-$ , corresponds to rooperol plus one glucuronide group and indicates the presence of a monoglucuronide of rooperol, which has a molecular weight of 458.42. The other two signals correspond to the fragmentation of the rooperol monoglucuronide, giving rise to rooperol  $[M-H-Gluc]^-$  and a glucuronide group  $[Gluc-H]^-$ . This HPLC/MS data for rooperol *in vitro* assays supports the conclusion that both of the late eluting peaks are monoglucuronide intermediates that give rise to at least one diglucuronide metabolite of rooperol. All HPLC/MS data for UDGPA/UDP and glucuronides of hydroxytyrosol and rooperol can be found in the Appendix section in Figures 21A and 22A.

(a)



(b)

Rooperol Diglucuronide, MW = 634.54



(c)

Rooperol Monoglucuronide, MW = 458.42

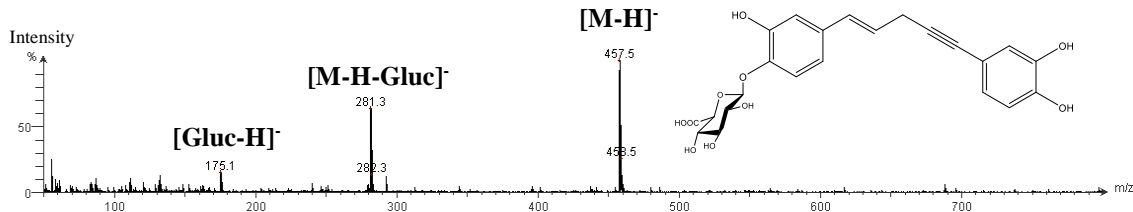


**Figure 18:** HPLC/MS of rooperol metabolites. The reaction was allowed to proceed for 60 minutes. (a) HPLC chromatogram (b) MS spectrum for the monoglucuronide metabolite of rooperol. (c) MS spectrum for the diglucuronide metabolite of rooperol. Note: The molecular structures shown are examples of one possible position of the glucuronide moiety on rooperol.

## IV. DISCUSSION

*In vitro* glucuronidation assays are a useful approach for characterizing the metabolic stability of drugs. This method can be used to predict human hepatic clearance of a drug and to determine its suitability for further *in vivo* testing. It is also a valuable method for comparing the metabolic properties between different compounds or analogues of a parent compound. An *in vitro* glucuronidation assay was utilized in this study to characterize the metabolic stability of rooperol, a compound known to extensively undergo Phase II metabolism<sup>26</sup> This metabolic assay for rooperol will later be employed with rooperol analogues containing catechol replacements. The analogues will be ranked based on half-life and intrinsic clearance in order to find a compound with similar cytotoxic properties and increased metabolic stability compared to rooperol.

The *in vitro* assay was optimized with hydroxytyrosol, a catechol-containing compound, based on a previously published biosynthesis of hydroxytyrosol glucuronides.<sup>60</sup> The assay was later adjusted to mimic physiological conditions based on a procedure for the *in vitro* glucuronidation of several drugs using alamethicin.<sup>57</sup> Porcine liver microsomes were utilized in this assay and contain the enzyme UGT, which is responsible for the glucuronidation of drugs. Minipig liver microsomes were chosen as an animal model as for this *in vitro* assay. Although minipigs differ in their degree of glucuronidation when compared to humans, they have no deficiency in the UGT isoforms required to glucuronidate a variety of drugs.<sup>66-68</sup> Similar glucuronidation activity has been observed for hydroxytyrosol with human, rat, and pig liver microsomes, although pig microsomes resulted in a higher preference for one glucuronidation product over another.<sup>60</sup> Reaction conditions were chosen so that they would most closely mimic the

physiological environment of UGT in the lumen of the endoplasmic reticulum. The TRIS-HCl buffer was adjusted to pH 7.1, which is the reported pH of the ER lumen.<sup>69</sup> The incorporation of 1 mM MgCl<sub>2</sub> was based on the presence of endogenous magnesium in the ER lumen. Mg<sup>2+</sup> has been observed to increase UGT activity in microsomes and facilitates the transport of UDPGA to the active site of UGT.<sup>70</sup> Likewise, the pore-forming peptide, alamethicin, was incorporated in order to promote the diffusion of the UDPGA cofactor into the microsomal membrane. This more appropriately simulates the ER membrane *in vivo*, where transporters are thought to facilitate the transfer of hydrophilic molecules across the membrane.<sup>56</sup> When comparing hydroxytyrosol *in vitro* assays, either in the presence or absence of alamethicin, the half-life was much shorter when alamethicin was added, 47 minutes, compared to without, around 62 minutes. (Appendix, Figures 4A and 5A). This suggests that alamethicin does increase the observed activity of UGT. However, when lowering the pH of the reaction from 8 to 7.1 and substituting MgCl<sub>2</sub> for CaCl<sub>2</sub> in the presence of alamethicin, the half-life returned to around 60 minutes. Together, these observations indicate that alamethicin, the metal cofactor, and the pH of the buffer may have the largest influence on half-life.

An obstacle that is frequently encountered during drug testing is solubility issues. A low concentration of DMSO can help combat the poor solubility of drugs. However, a high concentration of DMSO is known to inhibit enzyme activity, an effect that has been well characterized in the Phase I cytochrome P450 enzymes.<sup>71, 72</sup> A 0.1% DMSO solution was suitable for hydroxytyrosol. However, rooperol is much more insoluble in water and only pure DMSO could be used as a vehicle for this compound. In order to determine whether pure DMSO has a significant effect on the observed half-life in our *in vitro*

assays, experiments were carried out with hydroxytyrosol in pure DMSO (Appendix, Figure 9A). Based on the half-life for hydroxytyrosol in pure DMSO,  $62 \pm 3$  minutes, the amount of DMSO in the vehicle does not seem to have a significant effect on the half-life of hydroxytyrosol compared to with 0.1% DMSO (combined average of about 61 minutes) for these assays.

Another important consideration for this assay is the concentration of the drug of interest. If the drug concentration is much greater than the  $K_m$ , the reaction proceeds in a zero-order fashion and the rate of the reaction is independent of the substrate concentration. Conversely, if the concentration of the drug is much lower than the  $K_m$ , the reaction is first-order and a decrease in the amount of the substrate results in a proportional decrease in the rate of the reaction.<sup>71</sup> In a first order reaction, the half-life is constant and does not depend on the substrate concentration. Therefore, the half-life can be determined directly from the slope of a first-order reaction. Thus, the drug concentration must be chosen so that it is lower than the  $K_m$ . Although the *in vitro* assays for hydroxytyrosol and rooperol both yielded results typical of a first-order reaction, the assays were repeated at a lower concentration of 10  $\mu\text{M}$ . This was to ensure that the concentration was below  $K_m$  and that substrate concentration would not affect the calculated half-life. The half-lives calculated for the optimized *in vitro* assay with hydroxytyrosol at 100  $\mu\text{M}$  yielded half-lives of  $65 \pm 7$  and  $56 \pm 1$  minutes on two separate occasions. The assay with 10  $\mu\text{M}$  hydroxytyrosol resulted in a similar half-life of  $61 \pm 10$  minutes. Similarly, 100  $\mu\text{M}$  rooperol assays yielded half-lives of  $3 \pm 0.4$  and  $4 \pm 0.4$  on separate occasions while 10  $\mu\text{M}$  resulted in a half-life of  $4 \pm 0.4$ . This data supports the conclusion that substrate concentration does not affect the half-life for these

*in vitro* assays in the range of 10-100  $\mu\text{M}$  of the drug. The log plots for rooperol at 10  $\mu\text{M}$  (Appendix, Figure 18A (b)) have a slightly curved appearance with lower  $R^2$  values, which may be due to reaching the lower limit of detection on the HPLC. The area where rooperol elutes exhibited a significant amount of baseline noise in the region, likely influenced by the mobile phase gradient (Appendix, Figure 19A). Thus, higher concentrations of the drug of interest ( $>10 \mu\text{M}$ ) is more desirable for these assays for more accurate determination of peak areas by HPLC.

Although hydroxytyrosol and rooperol both contain metabolically labile catechol groups, a significant difference in the half-lives of these compounds was observed. Hydroxytyrosol had a calculated half-life of around 61 minutes, while rooperol had a strikingly shorter half-life of about 3 minutes. This substantial difference in half-lives is influenced by the lipophilicity of the compounds, which can be predicted using logP values. This is a measure of how a compound partitions between organic and aqueous layers and is therefore related to membrane permeability.<sup>73</sup> The higher the logP value, the more lipophilic the compound is. LogP values were obtained for hydroxytyrosol and rooperol using an online software that can predict the logP for any compound.<sup>74</sup> The predicted logP values for hydroxytyrosol and rooperol are 0.13 and 3.22, respectively. This roughly 25x increase in the logP value for rooperol indicates that it is much more lipophilic than hydroxytyrosol. This difference in lipophilicity is also apparent when comparing the retention times of these compounds in the reversed-phase HPLC method used in this study. Hydroxytyrosol elutes very early (RT = 3.8 min) at a low concentration of organic solvent (5% acetonitrile). Conversely, rooperol elutes much later (RT = 15.8 min) only after increasing the concentration of the organic solvent to 35%

acetonitrile. This difference in lipophilicity directly influences half-life because of its effect on membrane permeability. More lipophilic compounds tend to more easily diffuse across the microsomal ER membrane. As a result, they can more readily access the lumen-facing active site of UGT and can be metabolized much more quickly. Therefore, the lipophilicity of rooperol is a significant factor contributing to its exceptionally short half-life.

The HPLC/MS data verified that the identity of the observed products of the *in vitro* assays were indeed glucuronides. One glucuronide product was identified for hydroxytyrosol by HPLC/MS using the optimized *in vitro* assay (Figure 15). However, in the chromatogram overlay showing the time-dependent disappearance of hydroxytyrosol, there appear to be two peaks that may correspond to glucuronide metabolites. Furthermore, in original assays with hydroxytyrosol at pH 8, an additional peak was present in the HPLC chromatogram (Appendix, Figure 5A (d)). The two peaks, in an approximate ratio of 3:1, are suspected to be two glucuronide products of hydroxytyrosol (Appendix, Figure 5A (c)). The results from our assay at pH 8 agrees with the previously published findings for hydroxytyrosol, which reported a major 4'-*O*- $\beta$ -D-glucuronide and a minor 3'-*O*- $\beta$ -D-glucuronide of hydroxytyrosol with a regioisomer ratio of 3.0 in porcine liver microsomes at pH 8.<sup>60</sup> In our optimized assays, at pH 7.1, the HPLC/MS data indicates the presence of only one hydroxytyrosol glucuronide. This suggests that the lower pH may favor the production of only the major glucuronide of hydroxytyrosol. This conclusion is based off HPLC/MS data from one sample, however, and further testing is necessary to resolve this apparent contradiction. HPLC/MS of the products from the *in vitro* assay with rooperol verified the presence of both monoglucuronides and

at least one diglucuronide. Four species of monoglucuronides are possible for rooperol since there are two sites for glucuronide conjugation on each catechol. The HPLC chromatogram overlay for the disappearance of rooperol over 60 minutes (Figure 13 (a)) shows four peaks that may correspond to each possible monoglucuronide species. These peaks consist of a pair of coeluting peaks that appear immediately (RT  $\approx$  12.5 min), and another pair of coeluting peaks that only appear at the 15-minute time point (RT  $\approx$  11.75 min). This suggests that there are two major and two minor monoglucuronide intermediates. However, only one diglucuronide peak appears on the HPLC chromatogram in Figure 18 (a). It cannot be concluded from the chromatogram alone that there is only one product, since rooperol diglucuronides may be coeluting with each other or with UDPGA/UDP. In addition, this reaction was only allowed to proceed for 60 minutes, with intermediate monoglucuronides still present in the HPLC chromatogram. It is possible that the diglucuronide product observed in the HPLC chromatogram is simply the major product for the *in vitro* glucuronidation of rooperol.

## V. CONCLUSION

An *in vitro* metabolism assay was employed to characterize the phase II metabolism of catechol-containing compounds. The reaction conditions and the HPLC/MS method for this assay were optimized with 3-hydroxytyrosol. The disappearance of hydroxytyrosol monitored by HPLC consistently yielded a half-life of about 61 minutes and the identity of a glucuronide metabolite was verified by HPLC/MS. These results confirmed the suitability of this *in vitro* assay to characterize the metabolic stability of rooperol, a cytotoxic agent known to exhibit poor metabolic stability *in vivo*. Indeed, the *in vitro* assay with rooperol revealed an exceptionally short half-life of about 3 minutes. The identities of Phase II monoglucuronide and diglucuronide metabolites were verified with HPLC/MS. Initially, rooperol is quickly metabolized into two major monoglucuronide intermediates, followed by the production of at least one diglucuronide metabolite. The metabolic lability of rooperol has led to a search for rooperol analogues and related compounds that may exhibit increased metabolic stability. This *in vitro* assay established with hydroxytyrosol and rooperol will be employed to identify related compounds that display both cytotoxic activity and superior metabolic stability compared to rooperol.

## APPENDIX SECTION

	Page
1. Standard Curves .....	52
Figure 1A – Determining the Best Time to Add the Internal Standard .....	52
Figure 2A – Standard Curve Data Table for Hydroxytyrosol.....	53
Figure 3A – Standard Curve Data Table for Rooperol .....	53
2. Hydroxytyrosol <i>In Vitro</i> Data .....	54
Figure 4A – Preliminary Hydroxytyrosol <i>In Vitro</i> Assay.....	54
Figure 5A – Preliminary Hydroxytyrosol <i>In Vitro</i> Assay Supplemented with Alamethicin and Two Products Identified for Hydroxytyrosol .....	56
Figure 6A – Hydroxytyrosol (100 $\mu$ M) <i>In Vitro</i> Assay .....	59
Figure 7A – Hydroxytyrosol (100 $\mu$ M) <i>In Vitro</i> Assay on a Separate Day .....	61
Figure 8A – The Percent of Hydroxytyrosol Remaining Over Time .....	63
Figure 9A – Hydroxytyrosol (100 $\mu$ M) <i>In Vitro</i> Assay with DMSO Vehicle.....	63
Figure 10A – Hydroxytyrosol (10 $\mu$ M) <i>In Vitro</i> Assay .....	65
Figure 11A – Auto-Integration vs. Manual Integration of Hydroxytyrosol Peaks .....	67
Figure 12A – Negative Controls for the Hydroxytyrosol <i>In Vitro</i> Assay .....	68
3. Rooperol <i>In Vitro</i> Data.....	70
Figure 13A – Rooperol Purity.....	70
Figure 14A – Preliminary Rooperol <i>In Vitro</i> Assay .....	71
Figure 15A – Rooperol (100 $\mu$ M) <i>In Vitro</i> Assay .....	72
Figure 16A – Rooperol (100 $\mu$ M) <i>In Vitro</i> Assay on a Separate Day .....	74
Figure 17A – The Percent of Rooperol Remaining Over Time .....	76
Figure 18A – Rooperol (10 $\mu$ M) <i>In Vitro</i> Assay .....	76
Figure 19A – Auto-Integration vs. Manual Integration of Rooperol Peaks .....	78
Figure 20A - Negative Controls for the Rooperol <i>In Vitro</i> Assay .....	79
4. HPLC/MS Data.....	81
Figure 21A – HPLC/MS of Hydroxytyrosol Metabolites.....	81
Figure 22A – HPLC/MS of Rooperol Metabolites .....	83

## 1. Standard Curves

### Figure 1A: Determining the Best Time to Add the Internal Standard

(a) Data table and (b) plots with caffeine added immediately after quenching or just before HPLC analysis for three different concentrations of hydroxytyrosol.

(a)

Time Caffeine is Added	[HT] ( $\mu\text{M}$ )	HT Peak Area ( $\text{mAU}\cdot\text{min}$ )	Caffeine Peak Area ( $\text{mAU}\cdot\text{min}$ )	PA HT/PA Caffeine
Immediately	1	0.12	1.10	0.1133
	3	0.83	1.05	0.7924
	10	2.71	1.04	2.6217
Before HPLC analysis	1	0.15	1.23	0.1240
	3	1.19	1.20	0.9967
	10	2.72	1.11	2.4369

(b)

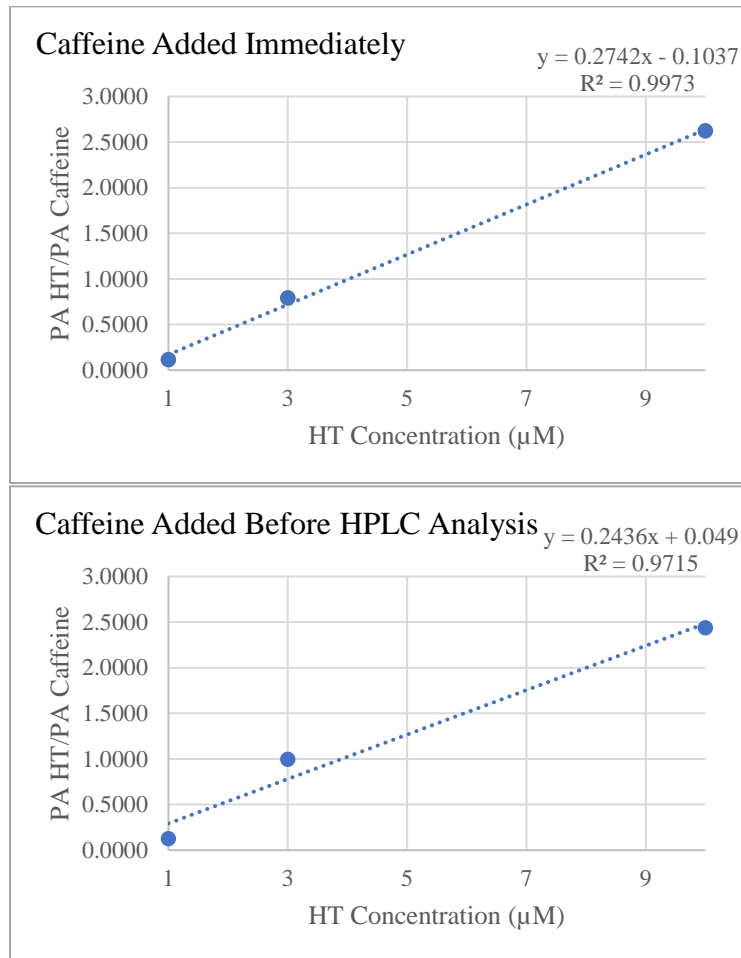


**Figure 2A: Standard Curve Data for Hydroxytyrosol**

HPLC peak areas were obtained from increasing concentrations of hydroxytyrosol (HT) with the internal standard caffeine.

[HT] ( $\mu\text{M}$ )	HT Peak Area (mAU $\cdot$ min)	[Caffeine] ( $\mu\text{M}$ )	Caffeine Peak Area (mAU $\cdot$ min)	[HT]/ [Caffeine]	PA HT/ PA Caffeine
1	0.0735	275	37.864	0.0036	0.0019
5	0.3138	275	37.988	0.0182	0.0083
10	0.5630	275	37.808	0.0364	0.0149
20	1.3530	275	37.951	0.0727	0.0357
30	2.0647	275	37.560	0.1091	0.0550
50	3.3740	275	37.386	0.1818	0.0902
100	6.8936	275	37.805	0.3636	0.1823
150	10.3585	275	37.171	0.5455	0.2787
200	13.8934	275	37.216	0.7273	0.3733
300	19.0493	275	35.565	1.0909	0.5356
500	31.8264	275	36.169	1.8182	0.8799

**Figure 3A: Standard Curve Data for Rooperol.**

HPLC peak areas were obtained from increasing concentrations of rooperol with the internal standard caffeine.

[Rooperol] ( $\mu\text{M}$ )	Rooperol Peak Area (mAU $\cdot$ min)	[Caffeine] ( $\mu\text{M}$ )	Caffeine Peak Area (mAU $\cdot$ min)	[Rooperol]/ [Caffeine]	PA Rooperol/ PA Caffeine
1	0.66	275	32.42	0.0036	0.0203
5	1.88	275	31.21	0.0182	0.0602
10	3.56	275	31.38	0.0364	0.1134
20	7.00	275	31.26	0.0727	0.2240
30	10.63	275	31.60	0.1091	0.3362
50	18.13	275	31.01	0.1818	0.5847
100	36.94	275	31.13	0.3636	1.1865
150	54.96	275	30.32	0.5455	1.8128
200	71.95	275	30.44	0.7273	2.3635
300	104.34	275	31.22	1.0909	3.3418
500	165.09	275	30.35	1.8182	5.4390

## 2. Hydroxytyrosol *In vitro* Data

### Figure 4A: Preliminary Hydroxytyrosol *In Vitro* Assay

(a) Data tables and (b) corresponding plots for the assay with hydroxytyrosol (100  $\mu$ M) in triplicate using initial reactions conditions (e.g. TRIS-HCl buffer pH 8, 1 mM CaCl<sub>2</sub>, no alamethicin) and the 4.6 x 250 mm HPLC column.

(a)

Replicate	Time Point (min)	Hydroxytyrosol Peak Area <sup>a</sup> (mAU•min)	Caffeine Peak Area <sup>a*</sup> (mAU•min)	Ln(PAR)	
<b>A</b>	0	9.16	617.90	-4.2117	$t_{1/2} = 55 \text{ min}$ $CL'_{\text{int}} = 0.03^b$
	5	8.87	693.16	-4.3587	
	15	7.30	722.47	-4.5943	
	30	6.22	710.82	-4.7381	
	45	5.10	641.83	-4.8358	
	60	4.94	759.87	-5.0352	
<b>B</b>	0	9.77	704.88	-4.2785	$t_{1/2} = 59 \text{ min}$ $CL'_{\text{int}} = 0.03^b$
	5	9.24	743.78	-4.3878	
	15	7.81	703.02	-4.4998	
	30	6.47	681.44	-4.6565	
	45	5.67	739.47	-4.8704	
	60	4.93	722.61	-4.9866	
<b>C</b>	0	10.88	752.83	-4.2368	$t_{1/2} = 72 \text{ min}$ $CL'_{\text{int}} = 0.02^b$
	5	9.90	748.87	-4.3262	
	15	8.36	765.60	-4.5171	
	30	7.65	797.93	-4.6480	
	45	6.35	692.45	-4.6921	
	60	5.69	727.96	-4.8514	
					$t_{1/2} = 62 \pm 9 \text{ min}$ $CL'_{\text{int}} = 0.02 \pm 3 \times 10^{-3b}$

<sup>a</sup> Monitored at 280 nm

<sup>b</sup> Intrinsic clearance units are mL•mg<sup>-1</sup>•min<sup>-1</sup>

\*A higher concentration of caffeine was mistakenly used for the internal standard

(b)

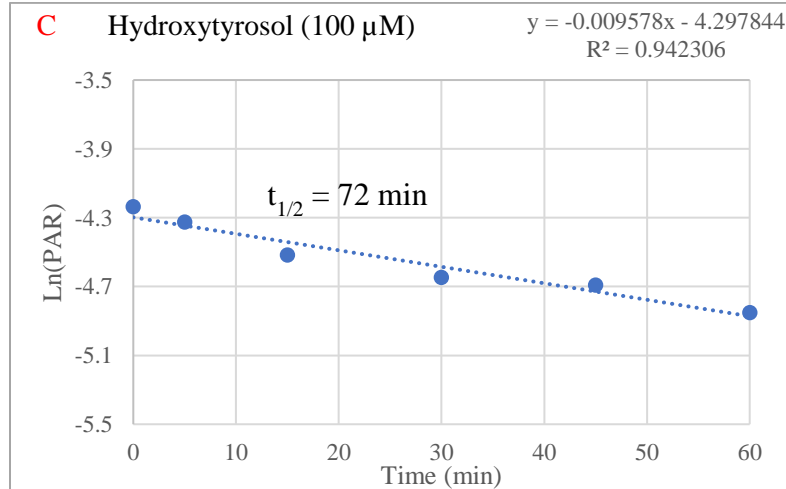
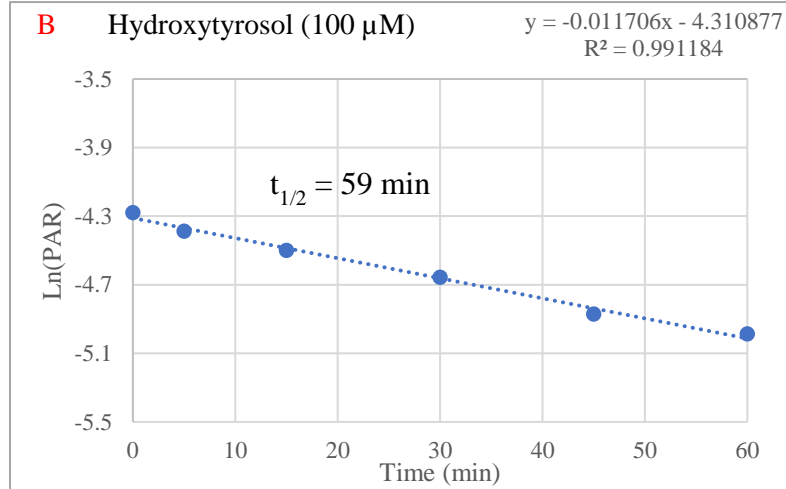
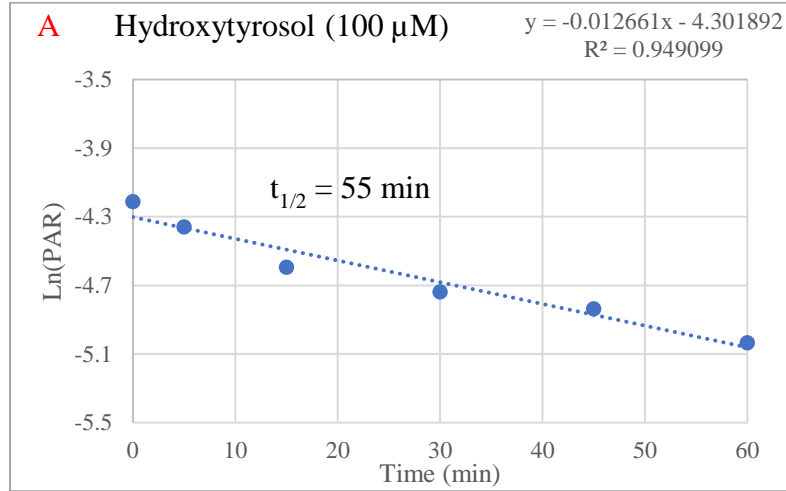


**Figure 5A: Hydroxytyrosol *In Vitro* Assay Supplemented with Alamethicin and Two Products Identified for Hydroxytyrosol**

(a) Data tables and (b) corresponding plots for the *in vitro* assay with hydroxytyrosol (100  $\mu$ M) in triplicate using initial reactions conditions (e.g. TRIS-HCl buffer pH 8, 1 mM CaCl<sub>2</sub>) in the presence of alamethicin and with a 4.6 x 250 mm HPLC column. (c) Peak areas obtained for the possible glucuronide products with the calculated product ratio. (d) HPLC chromatogram showing the presence of two possible glucuronide products of hydroxytyrosol.

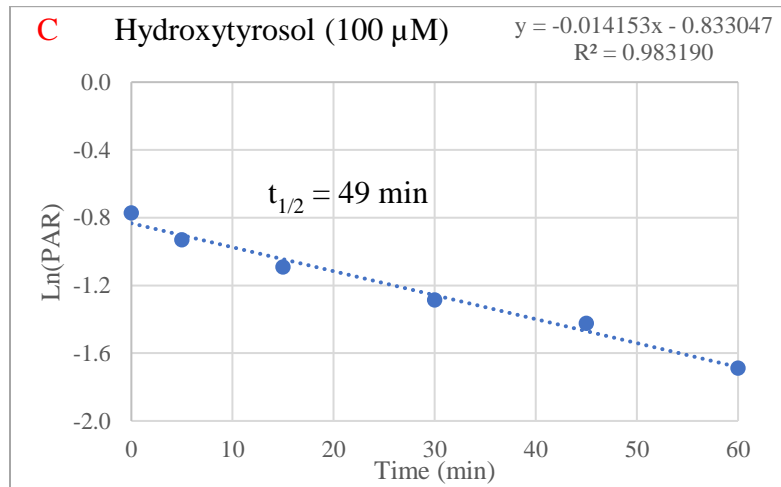
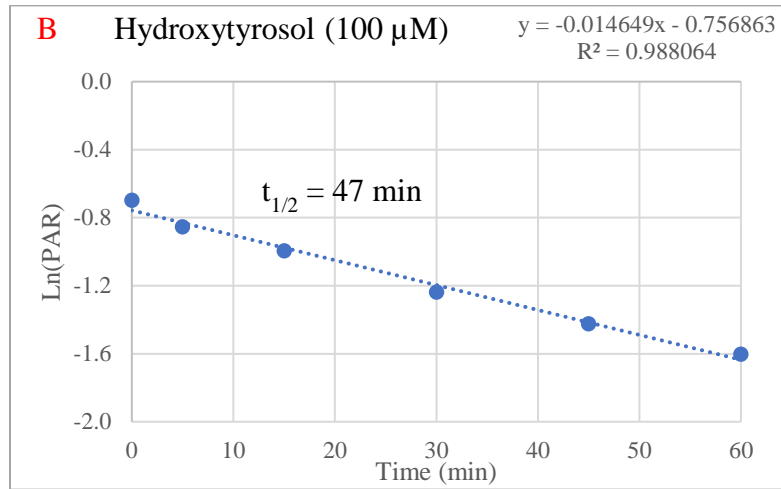
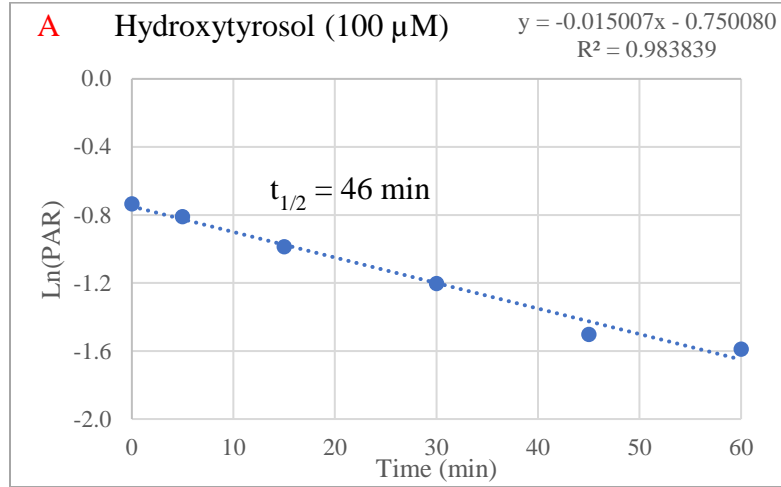
(a)

Replicate	Time Point (min)	Hydroxytyrosol Peak Area <sup>a</sup> (mAU•min)	Caffeine Peak Area <sup>a</sup> (mAU•min)	Ln(PAR)	
<b>A</b>	0	8.70	18.13	-0.7344	$t_{1/2} = 46 \text{ min}$ $CL'_{\text{int}} = 0.03^{\text{b}}$
	5	8.40	18.88	-0.8103	
	15	7.38	19.78	-0.9863	
	30	5.59	18.63	-1.2037	
	45	4.59	20.64	-1.5024	
	60	3.91	19.18	-1.5895	
<b>B</b>	0	9.22	18.54	-0.6985	$t_{1/2} = 47 \text{ min}$ $CL'_{\text{int}} = 0.03^{\text{b}}$
	5	8.41	19.74	-0.8537	
	15	7.12	19.27	-0.9956	
	30	5.75	19.81	-1.2376	
	45	4.52	18.76	-1.4239	
	60	3.61	17.93	-1.6026	
<b>C</b>	0	8.73	18.88	-0.7716	$t_{1/2} = 49 \text{ min}$ $CL'_{\text{int}} = 0.03^{\text{b}}$
	5	7.64	19.37	-0.9301	
	15	6.75	20.11	-1.0916	
	30	5.10	18.46	-1.2857	
	45	4.34	18.06	-1.4246	
	60	3.37	18.23	-1.6885	
					$t_{1/2} = 47 \pm 1 \text{ min}$ $CL'_{\text{int}} = 0.03 \pm 9 \times 10^{-4\text{b}}$

<sup>a</sup> Monitored at 280 nm

<sup>b</sup> Intrinsic clearance units are mL•mg<sup>-1</sup>•min<sup>-1</sup>

(b)



(c)

Replicate	Time Point (min)	Product 1 Peak Area <sup>a</sup> (mAU•min)	Product 2 Peak Area <sup>a</sup> (mAU•min)	Product 1/ Product 2
A	0	0.0546	0	N/A
	5	0.4839	0.1494	3.2390
	15	1.2852	0.4392	2.9262
	30	2.0591	0.7299	2.8210
	45	2.6605	0.9249	2.8765
	60	3.1559	1.0910	2.8927
B	0	0.0589	0	N/A
	5	0.4913	0.1599	3.0725
	15	1.3161	0.4457	2.9529
	30	2.2752	0.7723	2.9460
	45	2.8572	0.9701	2.9452
	60	3.2091	1.0870	2.9523
C	0	0.0654	0	N/A
	5	0.4553	0.1452	3.1357
	15	1.2484	0.4153	3.0060
	30	2.0351	0.6798	2.9937
	45	2.6958	0.9077	2.9700
	60	2.8989	0.9682	2.9941

<sup>a</sup> Monitored at 280 nm  
Average product ratio = 2.9816

(d)

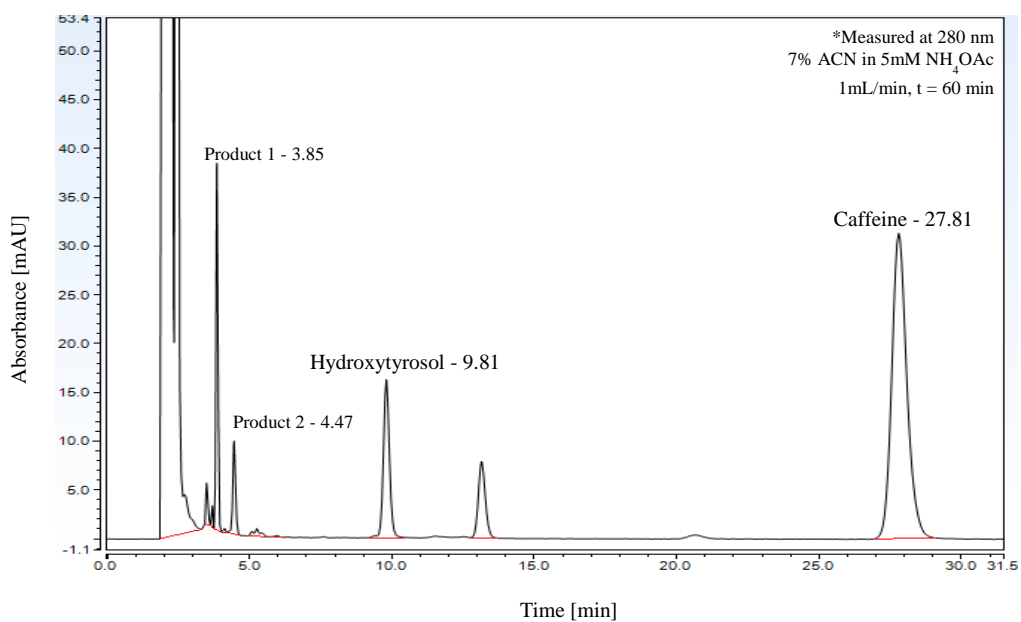


**Figure 6A: Hydroxytyrosol (100  $\mu$ M) *In Vitro* Assay**

(a) Data tables and (b) corresponding plots for the assay with hydroxytyrosol in triplicate using the optimized conditions (e.g. pH 7.1, MgCl<sub>2</sub>, alamethicin, and a 2.1 x 100 mm HPLC column).

(a)

Replicate	Time Point (min)	Hydroxytyrosol Peak Area <sup>a</sup> (mAU•min)	Caffeine Peak Area <sup>a</sup> (mAU•min)	Ln(PAR)	Conc. from Standard Curve ( $\mu$ M)	
<b>A</b>	0	23.37	40.10	-0.5399	130.81	$t_{1/2} = 63 \text{ min}$ $CL'_{\text{int}} = 0.02^{\text{b}}$
	5	15.46	31.05	-0.6972	111.66	
	15	16.58	36.68	-0.7938	101.32	
	30	15.79	34.09	-0.7698	103.80	
	45	11.31	33.78	-1.0941	74.85	
	60	11.56	40.90	-1.2638	63.06	
<b>B</b>	0	20.14	42.09	-0.7372	107.26	$t_{1/2} = 74 \text{ min}$ $CL'_{\text{int}} = 0.02^{\text{b}}$
	5	18.54	42.91	-0.8390	96.81	
	15	16.41	42.06	-0.9410	87.35	
	30	14.34	40.99	-1.0503	78.23	
	45	11.64	38.21	-1.1890	68.01	
	60	8.69	32.80	0.2648	59.05	
<b>C</b>	0	17.62	37.13	-0.7454	106.38	$t_{1/2} = 56 \text{ min}$ $CL'_{\text{int}} = 0.02^{\text{b}}$
	5	17.60	41.03	-0.8462	96.11	
	15	15.43	42.03	-1.0019	82.15	
	30	12.90	41.50	-1.1687	69.42	
	45	11.36	42.85	-1.3275	59.12	
	60	9.12	41.11	-1.5062	49.33	

<sup>a</sup> Monitored at 280 nm

<sup>b</sup> Intrinsic clearance units are mL•mg<sup>-1</sup>•min<sup>-1</sup>

$t_{1/2} = 65 \pm 9 \text{ min}$   
 $CL'_{\text{int}} = 0.02 \pm 3 \times 10^{-3\text{b}}$

(b)

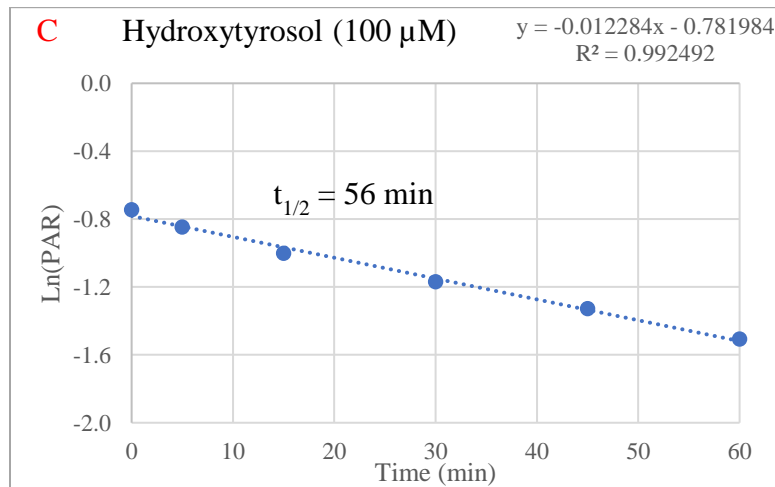
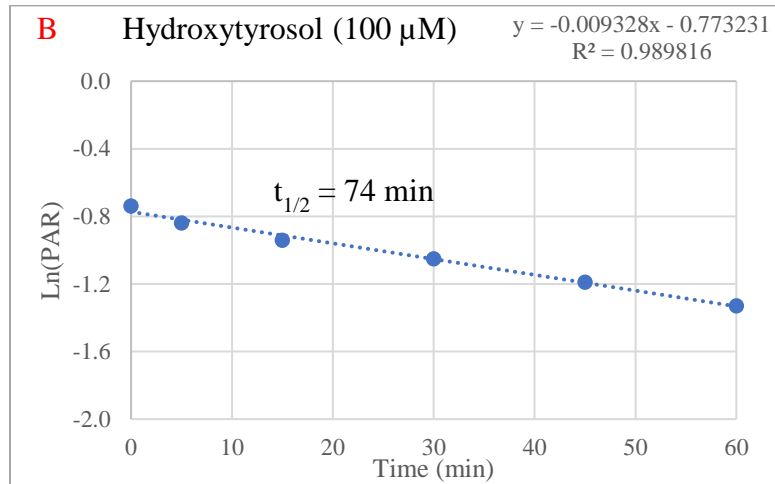
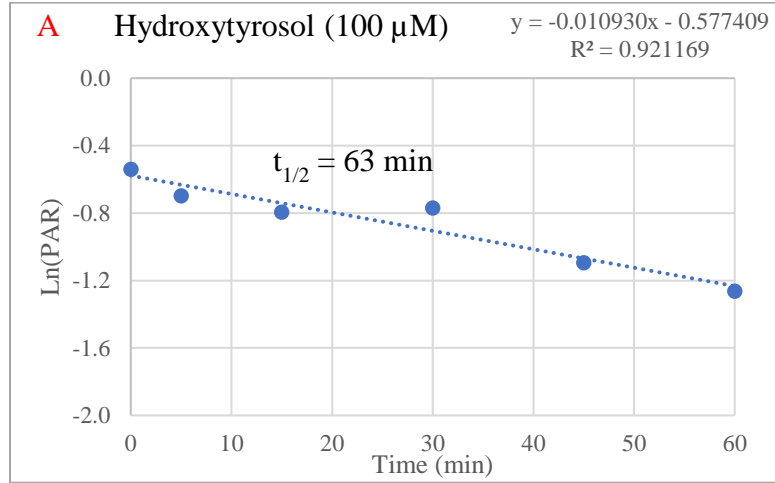


**Figure 7A: Hydroxytyrosol (100  $\mu$ M) *In Vitro* Assay on a Separate Day**

(a) Data tables and (b) corresponding plots for the *in vitro* assay with hydroxytyrosol in triplicate on a different day than the figure above.

(a)

Replicate	Time Point (min)	Hydroxytyrosol Peak Area <sup>a</sup> (mAU*min)	Caffeine Peak Area <sup>a</sup> (mAU*min)	Ln(PAR)	Conc. from Standard Curve ( $\mu$ M)	
<b>A</b>	0	23.51	33.25	-0.3467	158.84	$t_{1/2} = 59 \text{ min}$ $CL'_{\text{int}} = 0.02^{\text{b}}$
	5	16.78	27.40	-0.4903	137.50	
	15	15.55	29.04	-0.6243	120.16	
	30	19.73	44.09	-0.8042	100.26	
	45	16.61	43.11	-0.9537	86.24	
	60	14.46	42.84	-1.0860	75.46	
<b>B</b>	0	17.86	40.45	-0.8176	98.92	$t_{1/2} = 55 \text{ min}$ $CL'_{\text{int}} = 0.03^{\text{b}}$
	5	16.59	36.93	-0.8006	100.63	
	15	15.17	42.75	-1.0362	79.35	
	30	11.18	37.88	-1.2208	65.86	
	45	8.99	34.27	-1.3387	58.45	
	60	*	*	*	15.77	
<b>C</b>	0	18.38	42.00	-0.8266	98.03	$t_{1/2} = 56 \text{ min}$ $CL'_{\text{int}} = 0.02^{\text{b}}$
	5	12.84	33.11	-0.9468	86.84	
	15	8.21	23.32	-1.0438	78.75	
	30	12.39	41.56	-1.2099	66.59	
	45	10.14	42.84	-1.4406	52.72	
	60	8.22	39.99	-1.5816	45.70	
					<b><math>t_{1/2} = 56 \pm 2 \text{ min}</math></b> <b><math>CL'_{\text{int}} = 0.03 \pm 8 \times 10^{-4\text{b}}</math></b>	

<sup>a</sup> Monitored at 280 nm

<sup>b</sup> Intrinsic clearance units are  $\text{mL} \cdot \text{mg}^{-1} \cdot \text{min}^{-1}$

\*The time point at 60 minutes in replicate B was unable to be collected and is excluded from the plot.

(b)

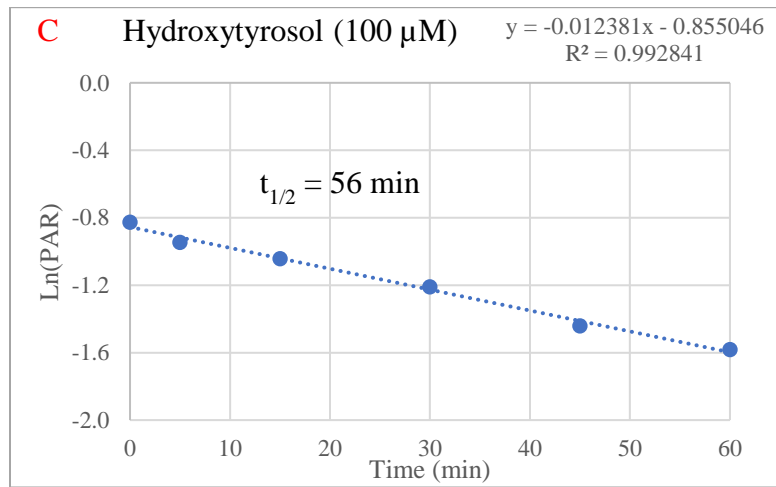
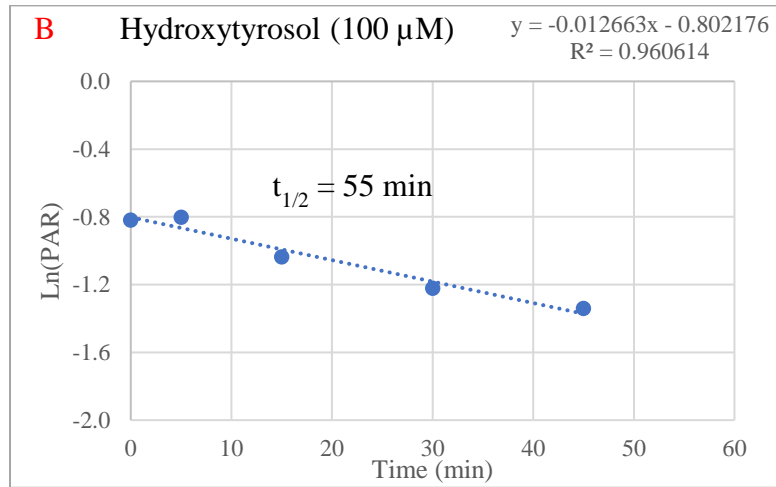
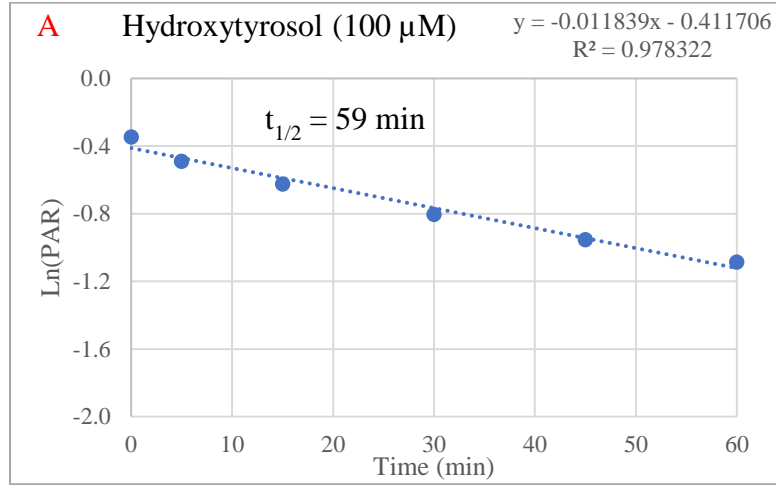


**Figure 8A: The Percent of Hydroxytyrosol Remaining Over Time.**

The percent of hydroxytyrosol was calculated for each replicate (3) from two different days for an n=6. The average of the percent of hydroxytyrosol remaining for each time point was averaged and plotted versus reaction time.

Time Point (min)	Average % Hydroxytyrosol Remaining	Std. Dev. (±)
0	100.00	0.00
5	90.48	5.35
15	78.72	2.06
30	69.20	5.44
45	57.23	3.29
60	48.75	3.22

**Figure 9A: Hydroxytyrosol (100 µM) *In Vitro* Assay with DMSO Vehicle**

(a) Data tables and (b) corresponding plots for the *in vitro* assay with hydroxytyrosol at a lower concentration in triplicate.

(a)

Replicate	Time Point (min)	Hydroxytyrosol Peak Area <sup>a</sup> (mAU*min)	Caffeine Peak Area <sup>a</sup> (mAU*min)	Ln(PAR)	Conc. from Standard Curve (µM)	
<b>A</b>	0	12.82	37.32	-1.0688	76.79	$t_{1/2} = 58 \text{ min}$ $CL'_{int} = 0.02^b$
	5	14.69	46.88	-1.1602	70.02	
	15	13.48	47.64	-1.2623	63.15	
	30	10.67	47.25	-1.4882	50.24	
	45	8.64	44.96	-1.6491	42.67	
	60	7.83	46.04	-1.7711	37.69	
<b>B</b>	0	16.04	48.04	-1.0971	74.63	$t_{1/2} = 62 \text{ min}$ $CL'_{int} = 0.02^b$
	5	15.18	48.01	-1.1516	70.63	
	15	13.47	48.24	-1.2755	62.31	
	30	11.50	47.63	-1.4212	53.77	
	45	9.47	47.17	-1.6061	44.57	
	60	8.03	47.30	-1.7735	37.59	
<b>C</b>	0	16.05	46.62	-1.0664	76.97	$t_{1/2} = 65 \text{ min}$ $CL'_{int} = 0.02^b$
	5	15.36	46.49	-1.1073	73.86	
	15	14.29	47.84	-1.2081	66.71	
	30	12.04	47.44	-1.3709	56.58	
	45	10.86	50.36	-1.5344	47.94	
	60	8.75	48.18	-1.7061	40.26	

<sup>a</sup> Monitored at 280 nm

<sup>b</sup> Intrinsic clearance units are  $\text{mL}\cdot\text{mg}^{-1}\cdot\text{min}^{-1}$

$t_{1/2} = 62 \pm 3 \text{ min}$   
 $CL'_{int} = 0.02 \pm 1 \times 10^{-3b}$

(b)

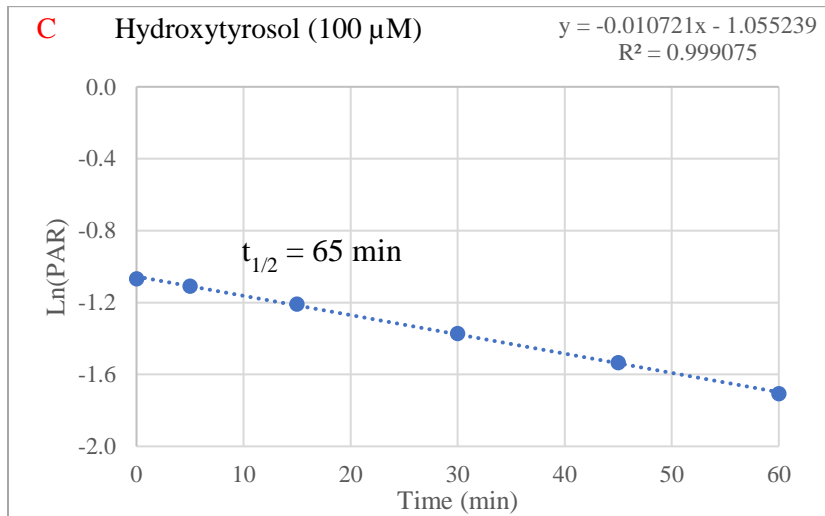
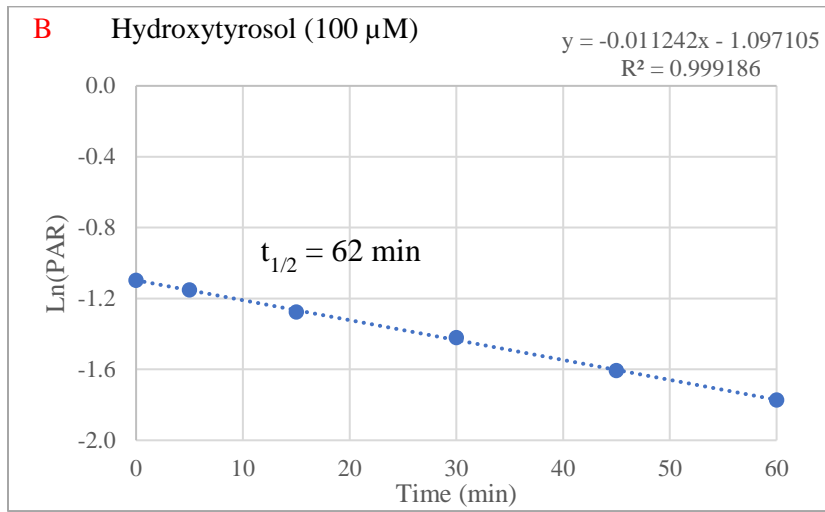
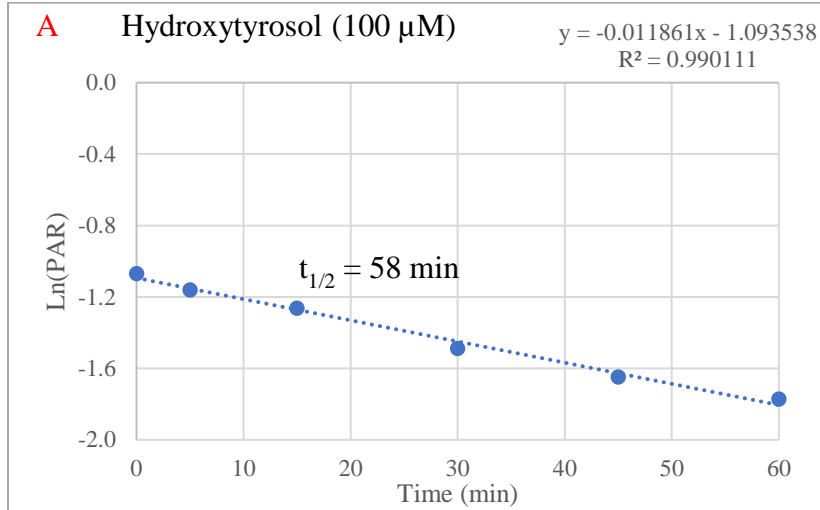


**Figure 10A: Hydroxytyrosol (10  $\mu$ M) *In Vitro* Assay**

(a) Data tables and (b) corresponding plots for the *in vitro* assay with hydroxytyrosol at a lower concentration in triplicate.

(a)

Replicate	Time Point (min)	Hydroxytyrosol Peak Area <sup>a</sup> (mAU•min)	Caffeine Peak Area <sup>a</sup> (mAU•min)	Ln(PAR)	Conc. from Standard Curve ( $\mu$ M)	
<b>A</b>	0	*	*	*	*	$t_{1/2} = 74$ min $CL'_{int} = 0.02^b$
	5	0.1175	36.77	-5.7461	0.0184	
	15	0.1077	38.79	-5.8865	-0.0852	
	30	0.0899	40.28	-6.1049	-0.2267	
	45	0.0810	40.06	-6.2038	-0.2394	
	60	0.0774	40.27	-6.2544	-0.2816	
<b>B</b>	0	0.1403	39.70	-5.6454	0.1093	$t_{1/2} = 60$ min $CL'_{int} = 0.02^b$
	5	0.1372	39.42	-5.6606	0.0858	
	15	0.1150	39.54	-5.8403	-0.0313	
	30	0.0931	38.37	-6.0213	-0.1349	
	45	0.0636	28.81	-6.1160	-0.2218	
	60	0.0694	39.32	-6.3396	-0.2984	
<b>C</b>	0	0.1389	37.71	-5.6039	0.1317	$t_{1/2} = 50$ min $CL'_{int} = 0.03^b$
	5	0.0987	32.67	-5.8023	-0.0179	
	15	0.1041	40.09	-5.9535	-0.1136	
	30	0.0876	39.86	-6.1203	-0.2036	
	45	0.0683	40.81	-6.3929	-0.3220	
	60	0.0615	38.77	-6.4462	-0.3416	
					<b><math>t_{1/2} = 60 \pm 11</math> min</b> <b><math>CL'_{int} = 0.03 \pm 4 \times 10^{-3b}</math></b>	

<sup>a</sup> Monitored at 280 nm

<sup>b</sup> Intrinsic clearance units are mL•mg<sup>-1</sup>•min<sup>-1</sup>

\*The time point at 0 minutes in replicate A had no HPLC signal and was excluded from the plot

Note: Concentrations are negative because they are under the lower limit of the standard curve (e.g. < 1  $\mu$ M)

(b)

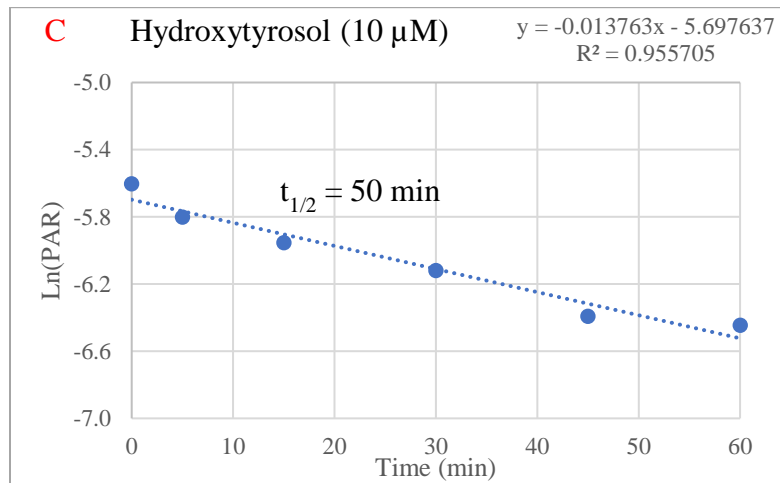
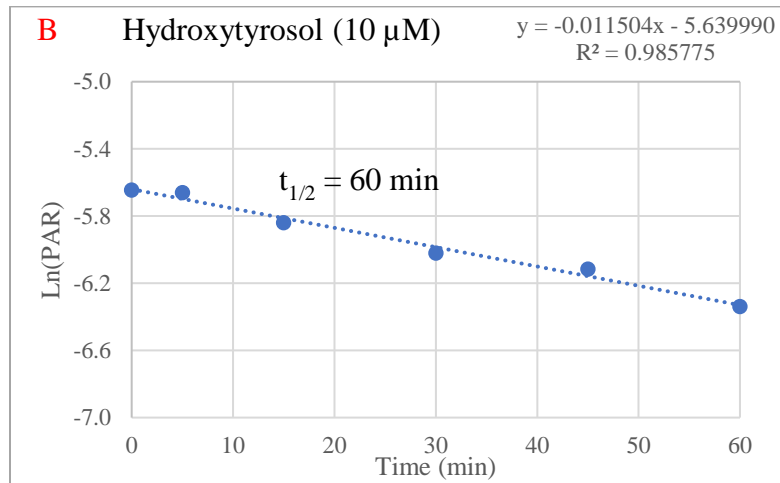
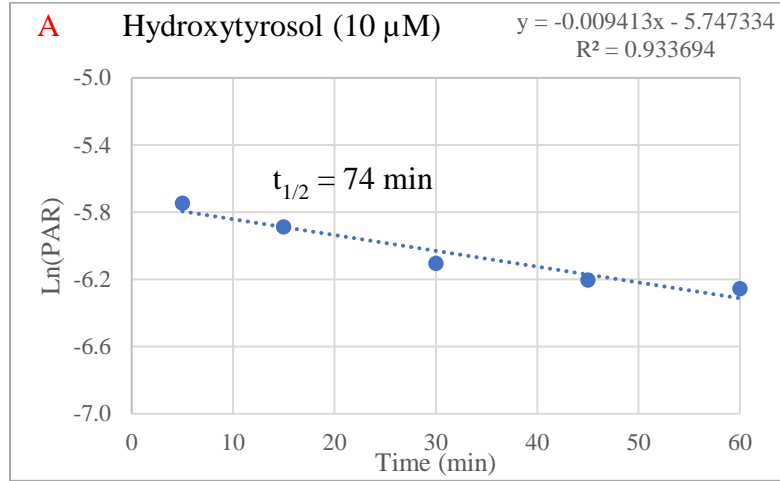
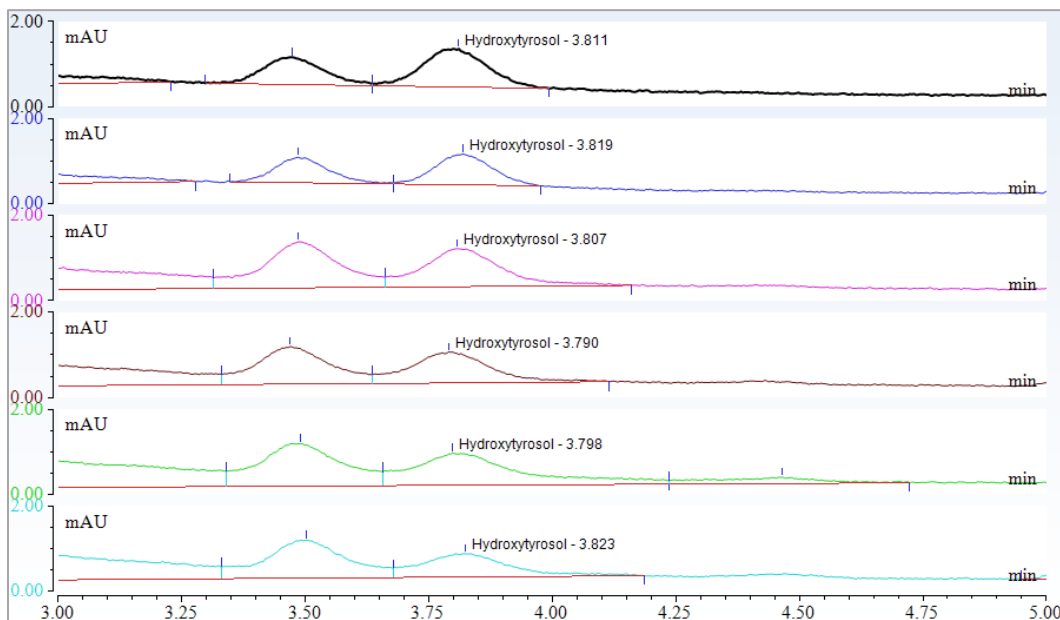


### Figure 11A: Auto-Integration vs. Manual Integration of Hydroxytyrosol Peaks

Comparison of (a) autointegration of the peaks by the HPLC software versus (b) manual peak integration for the peaks at RT  $\approx$  3.8 minutes for replicate B with 10  $\mu$ M hydroxytyrosol. The positions of the baselines (red) were increased vertically in the last four chromatograms to intersect the peak valleys. The peak delimiters (blue) were adjusted horizontally to be uniform across all chromatograms.

(a)



(b)

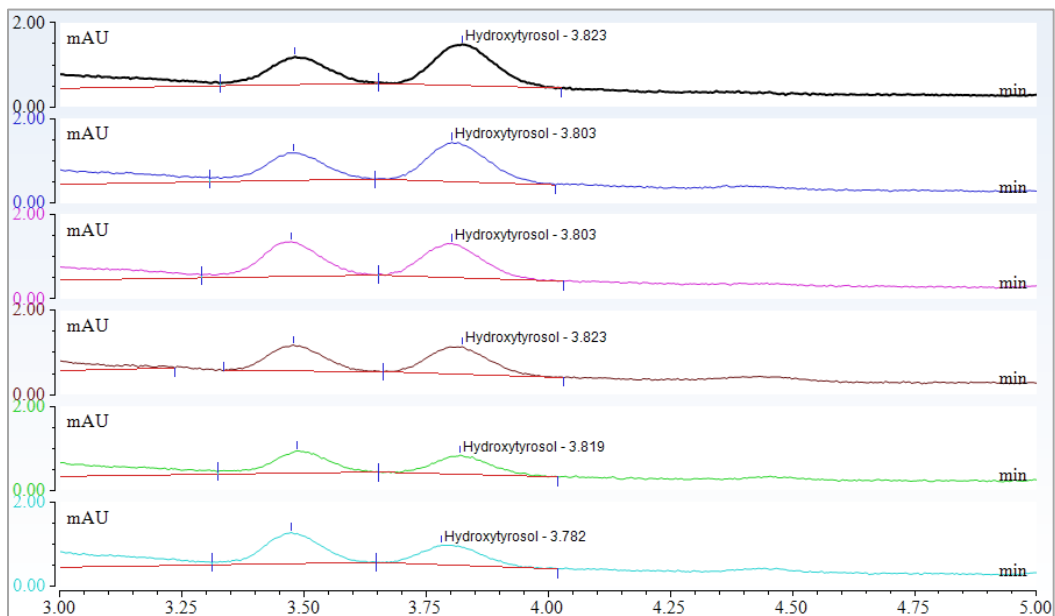
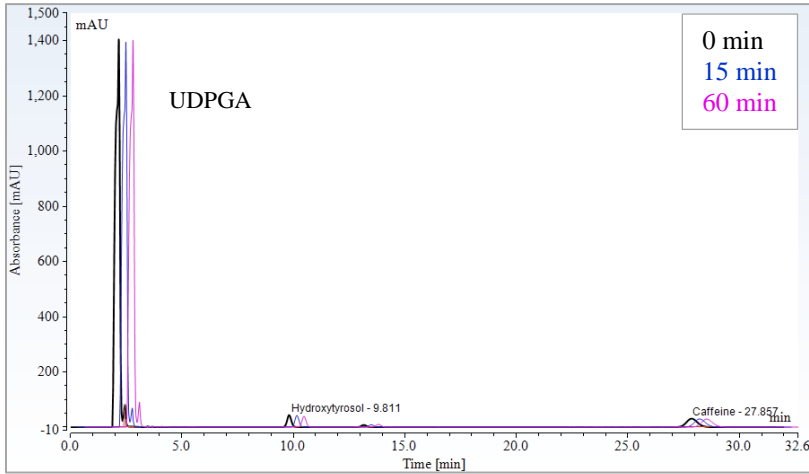


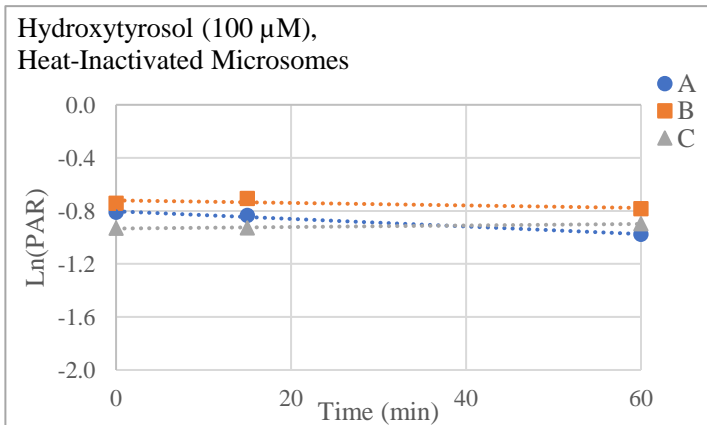
**Figure 12A: Negative Controls for Hydroxytyrosol *In Vitro* Assay**

The HPLC chromatogram overlay (one replicate) and the data table and log plot for the triplicate reactions with (a) heat-inactivated microsomes and (b) no UDPGA. (c) The HPLC chromatogram overlay (one replicate) with the vehicle. The HPLC mobile phase was 5% ACN in 5mM ammonium acetate, 1 mL/min, with a 4.6 x 250 mm column.

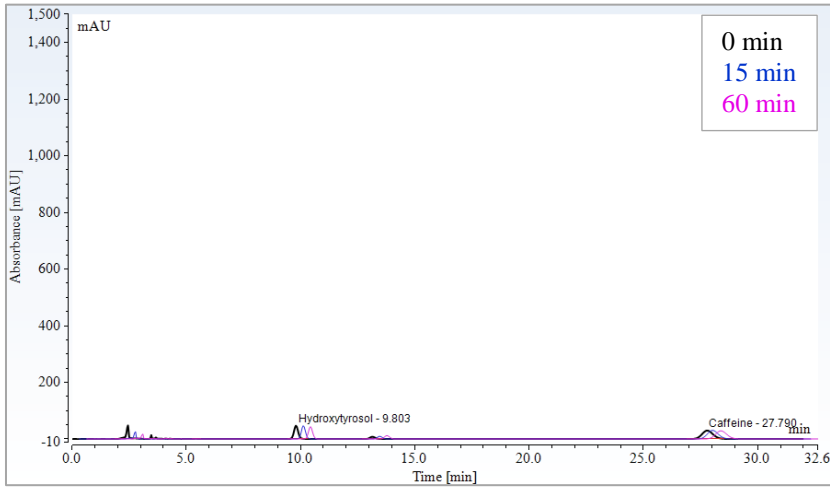
(a)



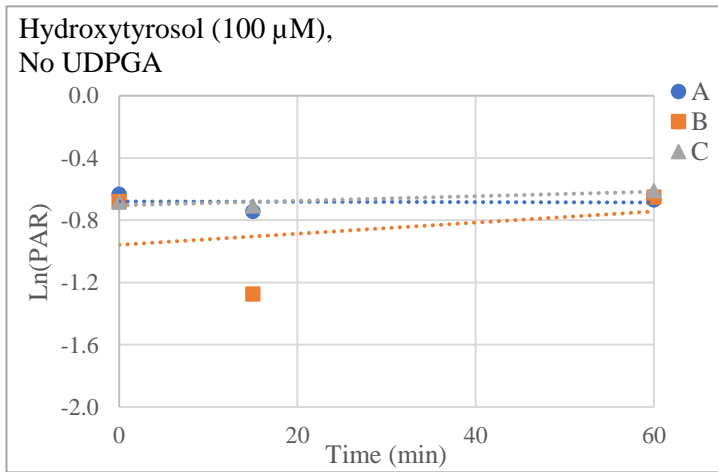
Replicate	Time Point (min)	Hydroxytyrosol Peak Area <sup>a</sup> (mAU•min)	Caffeine Peak Area <sup>a</sup> (mAU•min)	Ln(PAR)	Conc. from Standard Curve (μM)
<b>A</b>	0	6.58	14.81	-0.8118	99.50
	15	6.96	16.04	-0.8352	97.18
	60	6.06	16.12	-0.9778	84.17
<b>B</b>	0	8.09	16.99	-0.7418	106.76
	15	8.26	16.76	-0.7076	110.50
	60	6.44	14.12	-0.7848	102.24
<b>C</b>	0	6.35	16.11	-0.9305	88.28
	15	6.57	16.63	-0.9283	88.48
	60	6.53	16.02	-0.8978	91.24



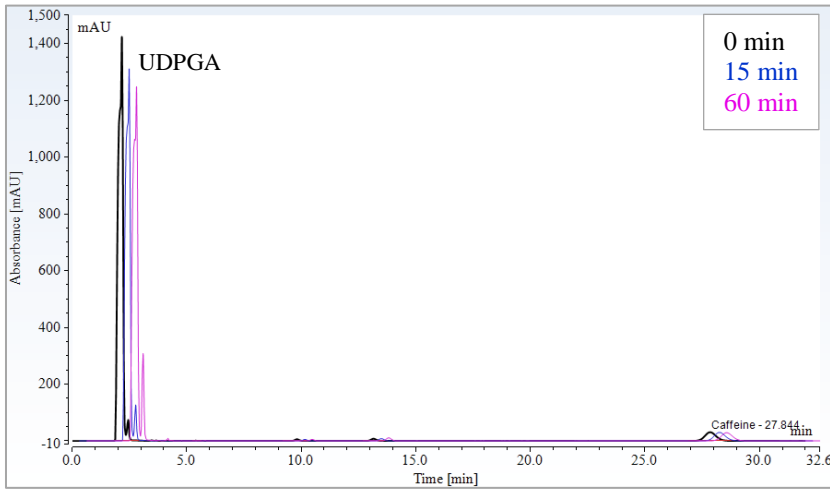
(b)



Replicate	Time Point (min)	Hydroxytyrosol Peak Area <sup>a</sup> (mAU•min)	Caffeine Peak Area <sup>a</sup> (mAU•min)	Ln(PAR)	Conc. from Standard Curve (μM)
<b>A</b>	0	8.26	15.56	-0.6326	119.17
	15	6.89	14.50	-0.7433	106.61
	60	7.85	15.35	-0.6702	114.74
<b>B</b>	0	8.03	15.86	-0.6805	113.55
	15	4.44	15.88	-1.2744	62.38
	60	8.09	15.52	-0.6509	116.99
<b>C</b>	0	8.27	16.39	-0.6846	113.10
	15	7.61	15.46	-0.7082	110.44
	60	8.43	15.50	-0.6097	121.94



(c)



## 2. Rooperol *In Vitro* Data

### Figure 13A: Rooperol Purity

The purity of rooperol was calculated to be about 93% by HPLC by dividing the peak area for the main rooperol peak by the combined area for the peak and the small shoulder. The mobile phase was 35% acetonitrile at 1 mL/min on a 4.6 x 250 mm column monitoring at 260 nm. (Rooperol peak area = 30.21, impurity peak area = 2.33)

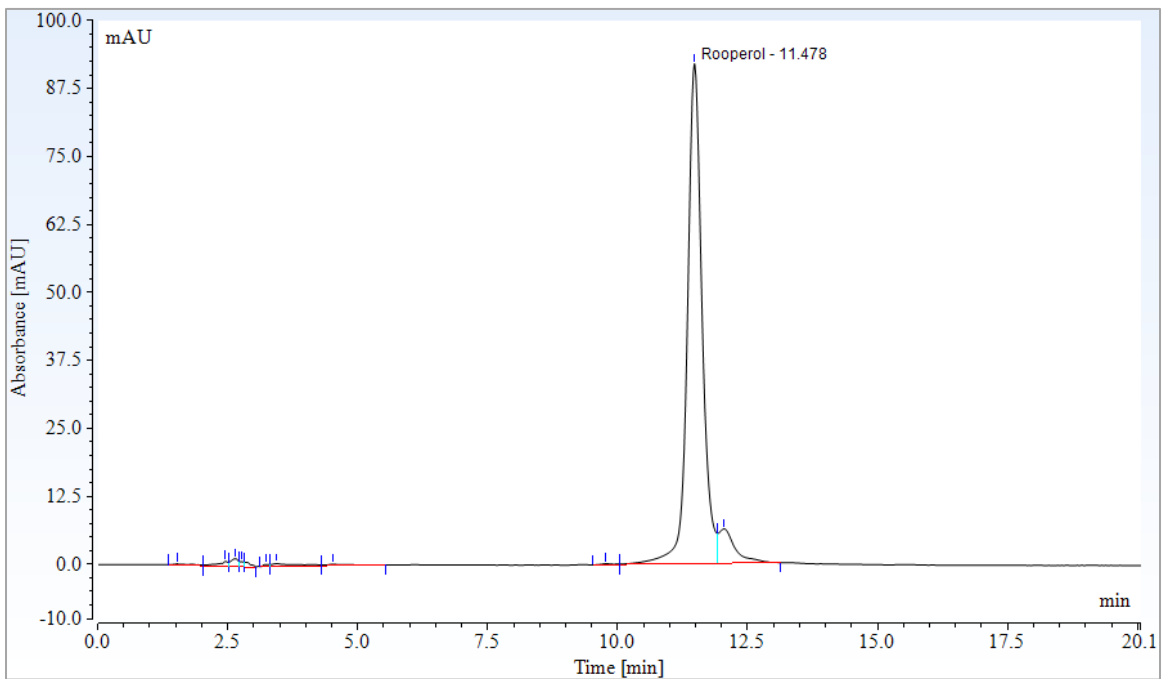
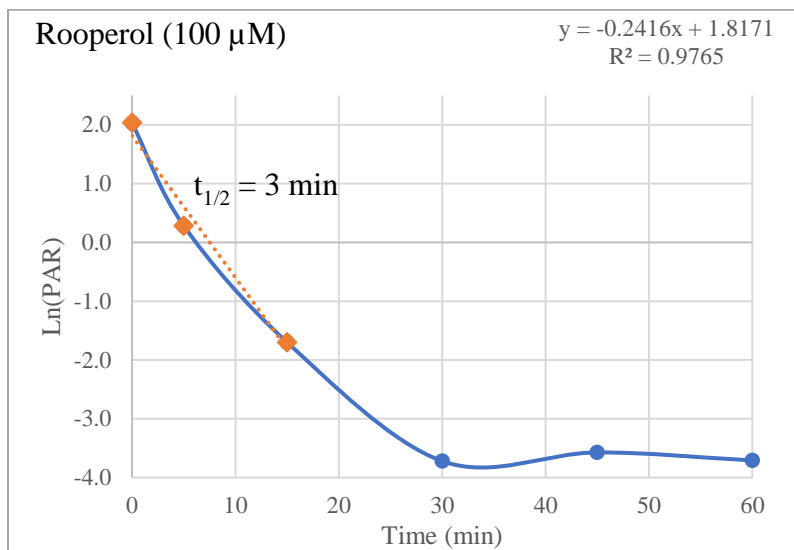


**Figure 14A: Preliminary Rooperol *In Vitro* Assay**

(a) Data table and (b) log plot for the *in vitro* assay with rooperol (100  $\mu\text{M}$ ) with time points taken over 60 minutes.

(a)



(b)

Time Point (min)	Rooperol Peak Area <sup>a</sup> (mAU•min)	Caffeine Peak Area <sup>a</sup> (mAU•min)	Ln(PAR)	Conc. from Standard Curve ( $\mu\text{M}$ )
0	195.3413	25.57	4.0557	221.50
5	15.5766	11.72	0.2846	37.45
15	5.4224	29.65	-1.6990	4.02
30	0.5347	22.05	-3.7196	-0.60
45	0.6342	22.57	-3.5721	-0.49
60	0.5023	20.46	-3.7068	-0.59

$t_{1/2} = 3 \text{ min}$   
 $CL'_{\text{int}} = 0.1^b$

<sup>a</sup> Monitored at 260 nm

<sup>b</sup> Intrinsic clearance units are  $\text{mL}\cdot\text{mg}^{-1}\cdot\text{min}^{-1}$

**Figure 15A: Rooperol (100  $\mu$ M) *In Vitro* Assay**

(a) Data tables and (b) corresponding plots for the *in vitro* assay with rooperol in triplicate.

(a)

Replicate	Time Point (min)	Rooperol Peak Area (mAU•min)	Caffeine Peak Area (mAU•min)	Ln(PAR)	Conc. from Standard Curve ( $\mu$ M)	
<b>A</b>	0	170.85	31.18	5.4790	198.10	$t_{1/2} = 3 \text{ min}$ $CL'_{\text{int}} = 0.1^{\text{b}}$
	2	124.73	23.12	5.3957	195.06	
	4	62.27	17.46	3.5666	128.38	
	6	50.47	30.52	1.6539	58.66	
	8	29.84	35.61	0.8379	28.91	
	10	16.56	31.47	0.5261	17.54	
<b>B</b>	0	163.42	31.38	5.2077	188.21	$t_{1/2} = 2 \text{ min}$ $CL'_{\text{int}} = 0.1^{\text{b}}$
	2	123.76	*	*	*	
	4	58.51	34.66	1.6883	59.91	
	6	47.28	*	*	*	
	8	15.08	31.21	0.4833	15.98	
	10	6.67	31.72	0.2103	6.03	
<b>C</b>	0	131.56	31.38	4.1920	151.18	$t_{1/2} = 3 \text{ min}$ $CL'_{\text{int}} = 0.1^{\text{b}}$
	2	94.87	34.27	2.7683	99.28	
	4	71.52	32.27	2.2165	79.17	
	6	37.88	31.78	1.1918	41.81	
	8	20.38	27.31	0.7462	25.56	
	10	18.45	30.69	0.6012	20.28	
					$t_{1/2} = 3 \pm 0.5 \text{ min}$ $CL'_{\text{int}} = 0.1 \pm 2 \times 10^{-2\text{b}}$	

<sup>a</sup> Monitored at 260 nm

<sup>b</sup> Intrinsic clearance units are  $\text{mL} \cdot \text{mg}^{-1} \cdot \text{min}^{-1}$

\*The time points at 2 and 4 minutes in replicate B did not have caffeine signals and are excluded from the plot.

(b)

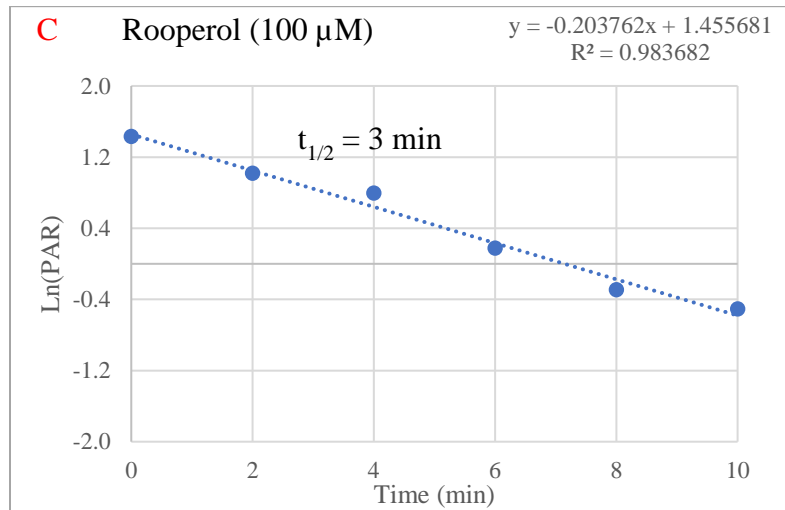
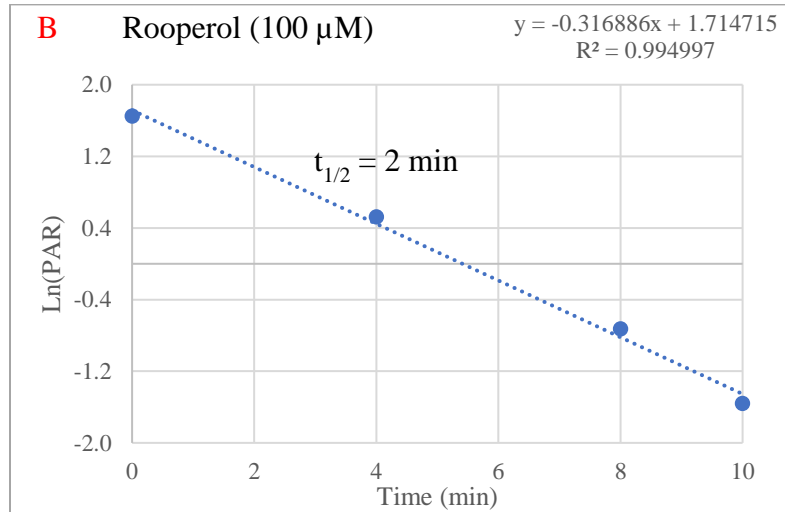
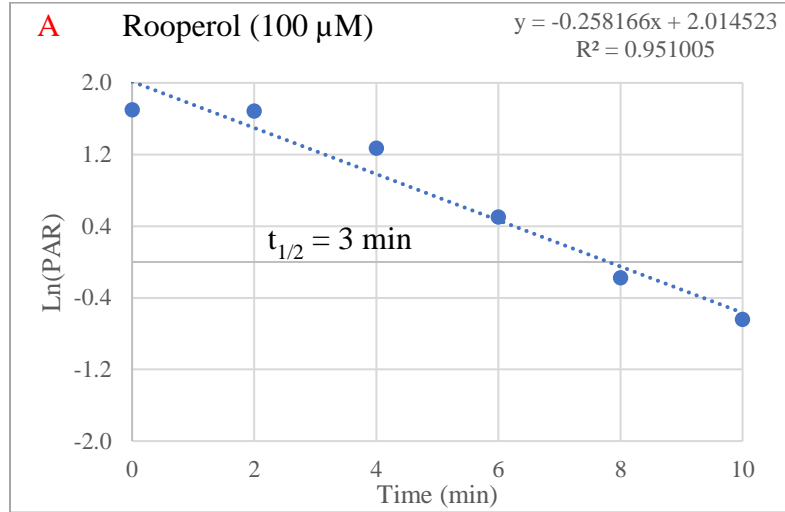


**Figure 16A: Rooperol (100  $\mu$ M) *In Vitro* Assay on a Separate Day**

(a) Data tables and (b) corresponding plots for the *in vitro* assay with rooperol in triplicate on a different day than the figure above.

(a)

Replicate	Time Point (min)	Rooperol Peak Area <sup>a</sup> (mAU•min)	Caffeine Peak Area <sup>a</sup> (mAU•min)	Ln(PAR)	Conc. from Standard Curve ( $\mu$ M)	
<b>A</b>	0	166.08	32.65	1.6267	183.81	$t_{1/2} = 4 \text{ min}$ $CL'_{\text{int}} = 0.07^b$
	2	140.47	31.79	1.4859	159.45	
	4	105.60	33.02	1.1627	114.96	
	6	57.57	27.98	0.7216	73.37	
	8	50.83	31.28	0.4856	57.61	
	10	35.60	33.81	0.0517	36.75	
<b>B</b>	0	162.79	32.98	1.5964	178.28	$t_{1/2} = 3 \text{ min}$ $CL'_{\text{int}} = 0.09^b$
	2	125.90	32.29	1.3608	140.52	
	4	91.15	33.81	0.9916	96.63	
	6	56.71	32.86	0.5457	61.28	
	8	36.61	33.44	0.0906	38.27	
	10	19.35	30.37	0.6373	21.59	
<b>C</b>	0	108.10	28.64	1.3283	135.97	$t_{1/2} = 4 \text{ min}$ $CL'_{\text{int}} = 0.08^b$
	2	93.94	32.67	1.0562	103.19	
	4	72.54	33.43	0.7746	77.46	
	6	51.59	21.03	0.8971	87.77	
	8	26.82	25.89	0.0354	36.13	
	10	20.68	33.83	-0.4921	20.65	
					$t_{1/2} = 4 \pm 0.5 \text{ min}$ $CL'_{\text{int}} = 0.08 \pm 1 \times 10^{-2b}$	

<sup>a</sup> Monitored at 260 nm

<sup>b</sup> Intrinsic clearance units are  $\text{mL} \cdot \text{mg}^{-1} \cdot \text{min}^{-1}$

(b)

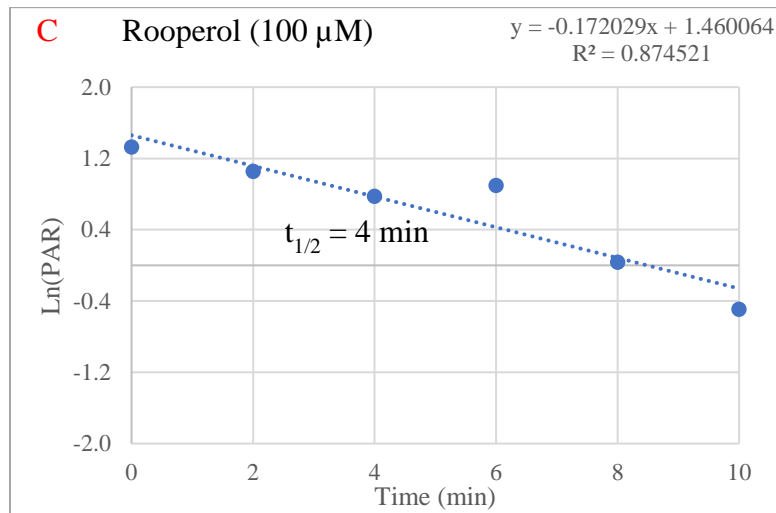
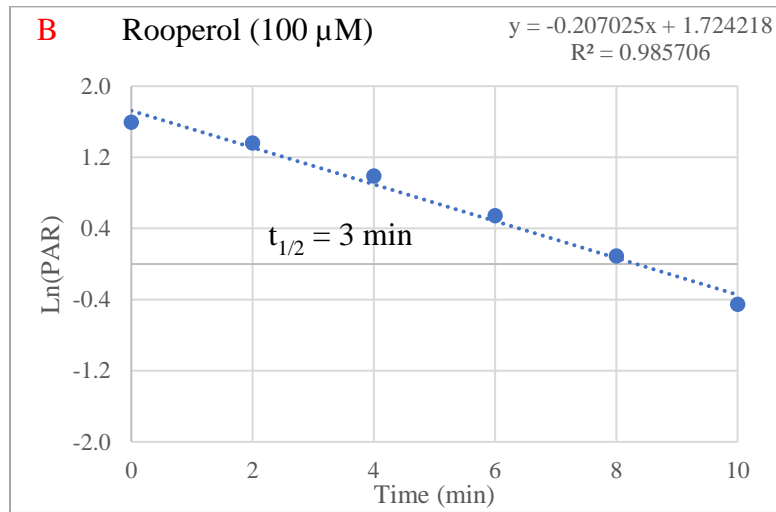
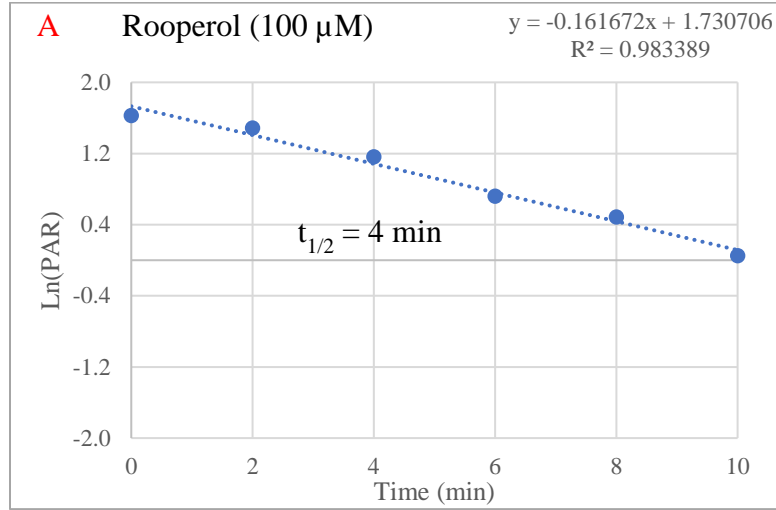


### Figure 17A: The Percent of Rooperol Remaining Over Time

The percent of rooperol was calculated for each replicate (3) from two different days for an n=6. The average of the percent of rooperol remaining for each time point was plotted versus reaction time.

Time Point (min)	Average % Rooperol Remaining	Std. Dev. ( $\pm$ )
0	100.00	0.00
2	81.12	12.29
4	53.79	11.77
6	39.22	14.93
8	19.90	8.31
10	12.13	5.71

### Figure 18A: Rooperol (10 $\mu$ M) *In Vitro* Assay

(a) Data tables and (b) corresponding plots for the *in vitro* metabolis assay with a lower concentration of rooperol in triplicate.

(a)

Replicate	Time Point (min)	Rooperol Peak Area <sup>a</sup> (mAU•min)	Caffeine Peak Area <sup>a</sup> (mAU•min)	Ln(PAR)	Conc. from Standard Curve ( $\mu$ M)	
<b>A</b>	0	1.4341	31.2375	-2.7498	0.04	$t_{1/2} = 4 \text{ min}$ I.C. = 0.08 <sup>b</sup>
	2	0.5948	30.9908	-3.8110	-0.94	
	4	0.3199	29.5184	-4.4083	-1.24	
	6	0.2539	31.2695	-5.0682	-1.34	
	8	0.2250	29.6325	-4.9237	-1.36	
	10	0.2056	30.9278	-4.9725	-1.40	
<b>B</b>	0	1.0652	30.35	-3.3495	-0.36	$t_{1/2} = 4 \text{ min}$ I.C. = 0.08 <sup>b</sup>
	2	0.5248	31.33	-4.0894	-1.03	
	4	0.2439	18.53	-4.1943	-1.16	
	6	0.2140	32.32	-5.3509	-1.40	
	8	0.2109	31.53	-5.6544	-1.39	
	10	0.1652	31.30	0.0035	-1.45	
<b>C</b>	0	1.0677	30.23	-3.3270	-0.35	$t_{1/2} = 3 \text{ min}$ I.C. = 0.1 <sup>b</sup>
	2	0.5375	31.03	-4.0800	-1.01	
	4	0.1762	31.04	-5.1737	-1.43	
	6	0.1338	30.85	-5.1080	-1.48	
	8	0.1116	30.93	-5.7174	-1.51	
	10	0.1162	30.88	-5.7651	-1.50	

<sup>a</sup> Monitored at 260 nm

<sup>b</sup> Intrinsic clearance units are  $\text{mL}\cdot\text{mg}^{-1}\cdot\text{min}^{-1}$

Note: Concentrations are negative because they are under the lower limit of the standard curve (e.g.  $< 1 \mu\text{M}$ )

**$t_{1/2} = 4 \pm 0.5 \text{ min}$**   
**I.C. =  $0.09 \pm 1 \times 10^{-2b}$**

(b)

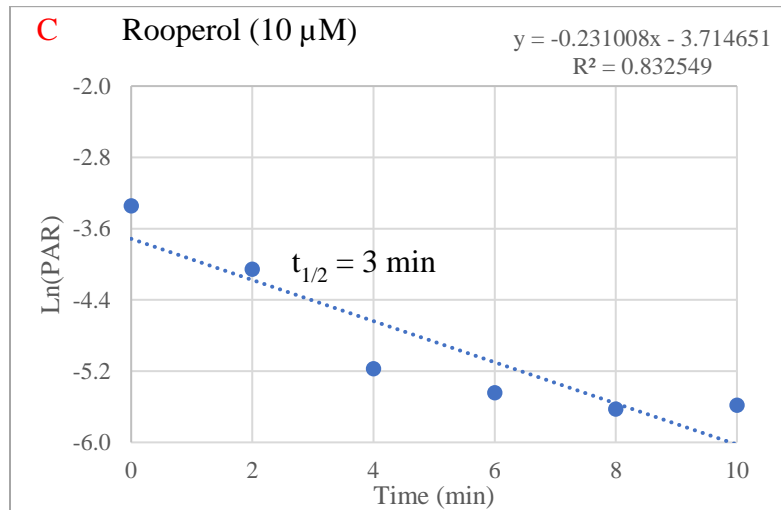
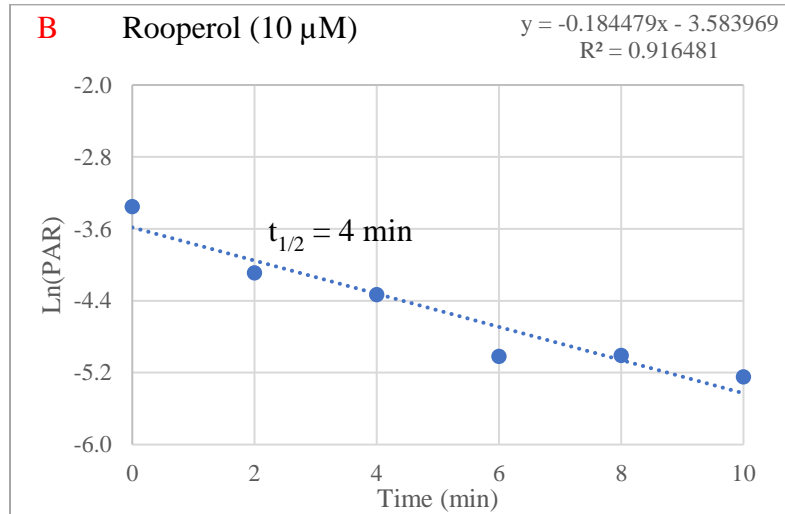
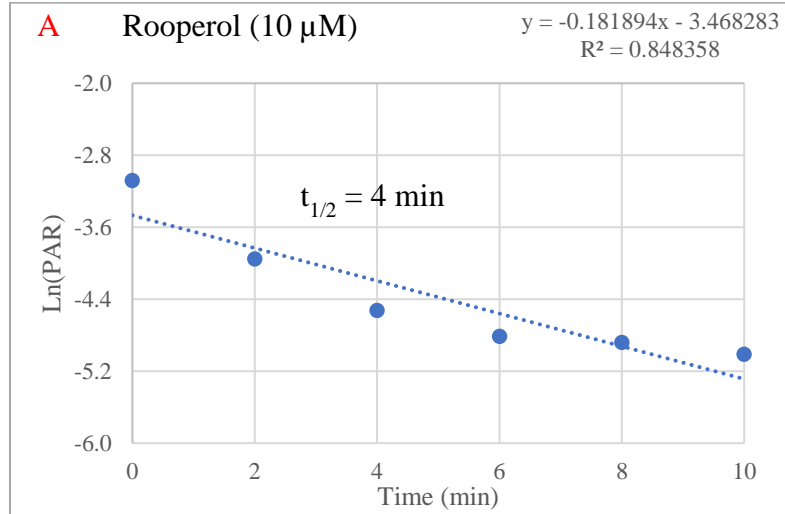
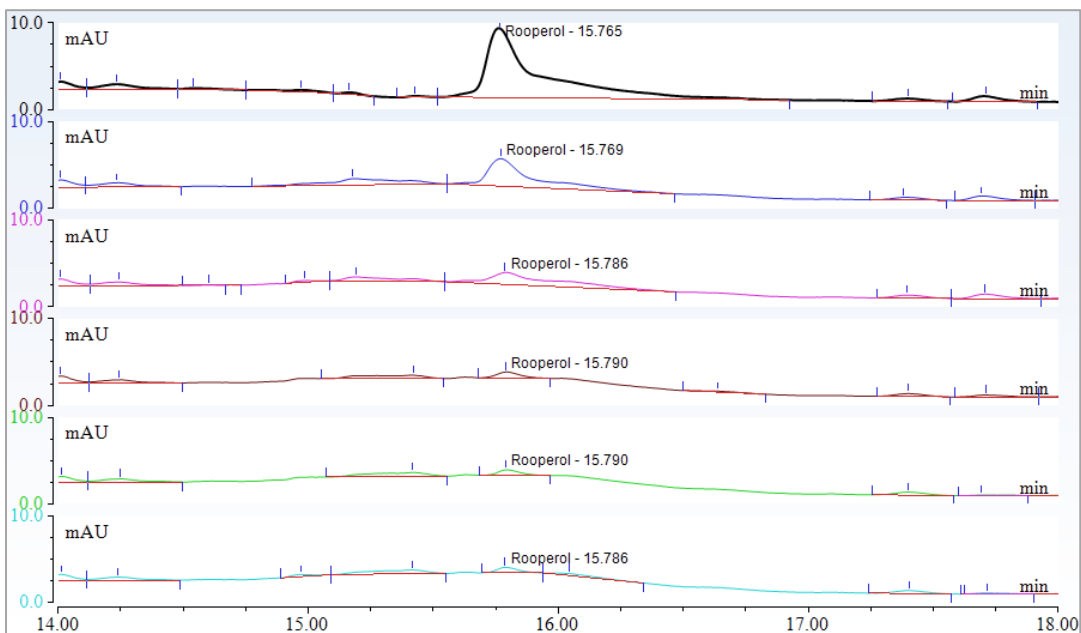


**Figure 19A: Auto-Integration vs. Manual Integration of Rooperol Peaks.**

Comparison of (a) auto-integration of the peaks by the HPLC software versus (b) manual peak integration for the peaks at RT  $\approx$  15.8 minutes for replicate A with 10  $\mu$ M rooperol. The positions of the baselines (red) were decreased vertically in the last three chromatograms to more closely resemble the preceding peak shapes. The peak delimiters (blue) were adjusted horizontally to be uniform across all chromatograms.

(a)



(b)

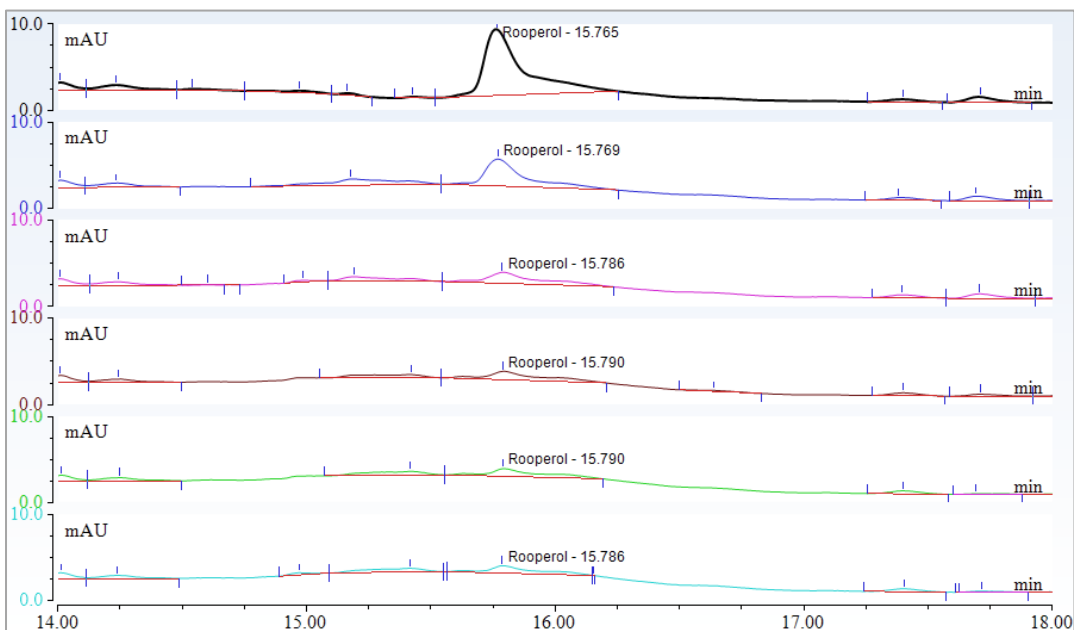
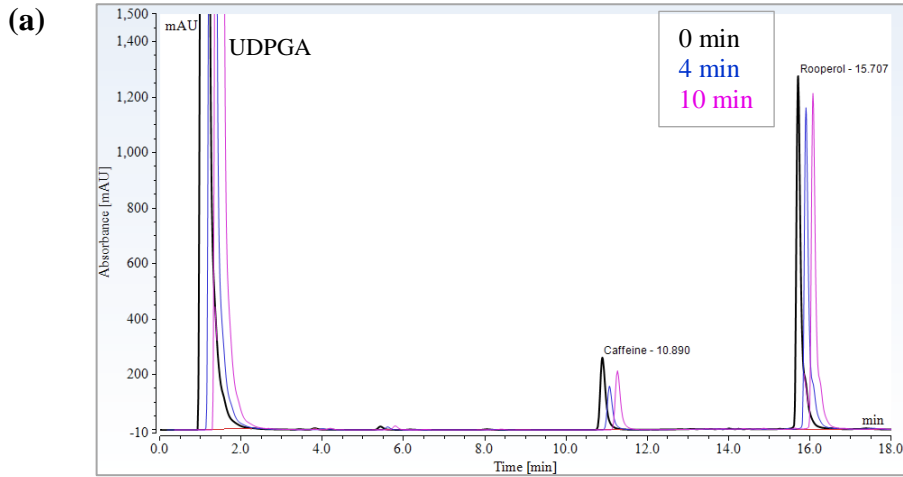


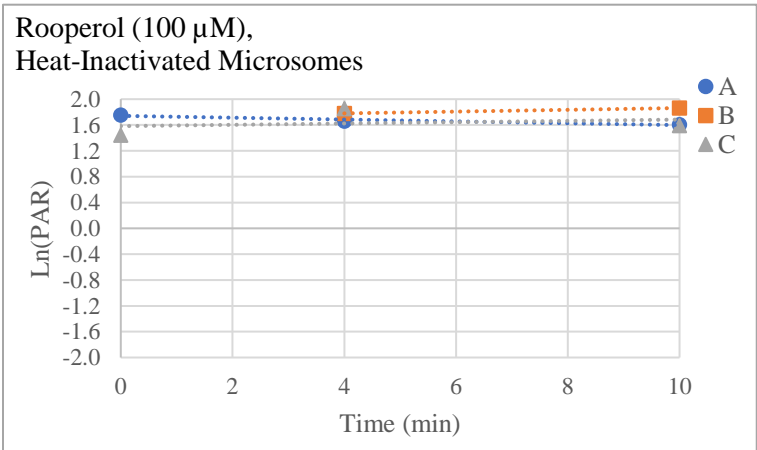
**Figure 20A: Negative Controls for the *In Vitro* Assay with Rooperol.** An HPLC chromatogram overlay (one replicate) and the data table and log plot for the triplicate reactions with (a) heat-inactivated microsomes and (b) no UDPGA. (c) The HPLC chromatogram overlay (one replicate) for the vehicle. The HPLC mobile phase was a gradient from 5-35% ACN in 5mM ammonium acetate.



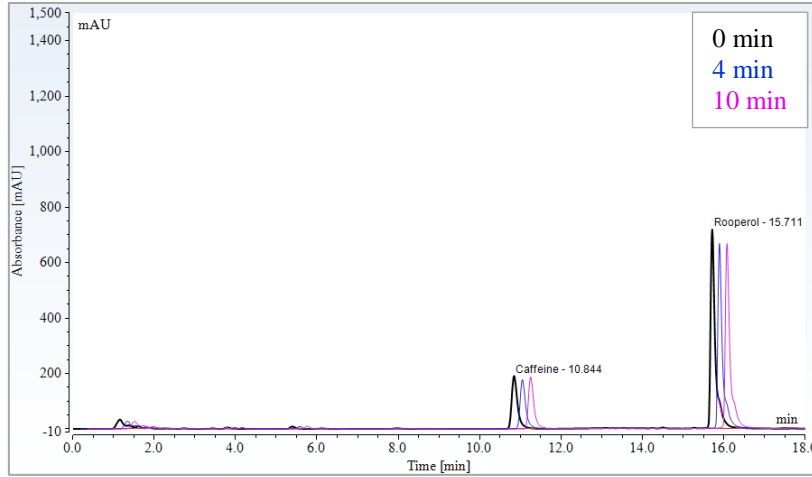
Replicate	Time Point (min)	Rooperol Peak Area <sup>a</sup> (mAU•min)	Caffeine Peak Area <sup>a</sup> (mAU•min)	Ln(PAR)	Conc. from Standard Curve (μM)
<b>A</b>	0	168.33	29.08	1.7559	209.39
	15	178.10	33.80	1.6619	190.45
	60	125.14	25.08	1.6074	180.26
<b>B</b>	0	169.9962	*	*	*
	15	201.4603	33.98	1.7799	214.51
	60	190.3270	29.55	1.8627	233.17
<b>C</b>	0	176.75	41.66	1.4452	153.04
	15	157.61	24.72	1.8526	230.80
	60	166.28	33.83	1.5924	177.56

<sup>a</sup>Monitored at 260 nm

\*Caffeine signal was missing in Replicate B and was excluded from the log plot

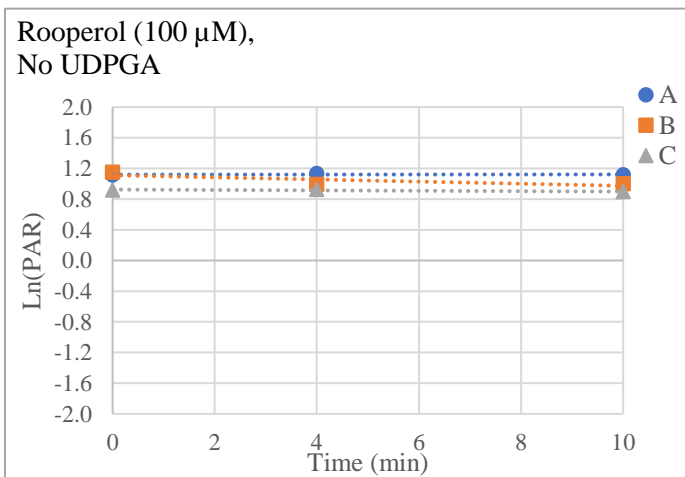


(b)

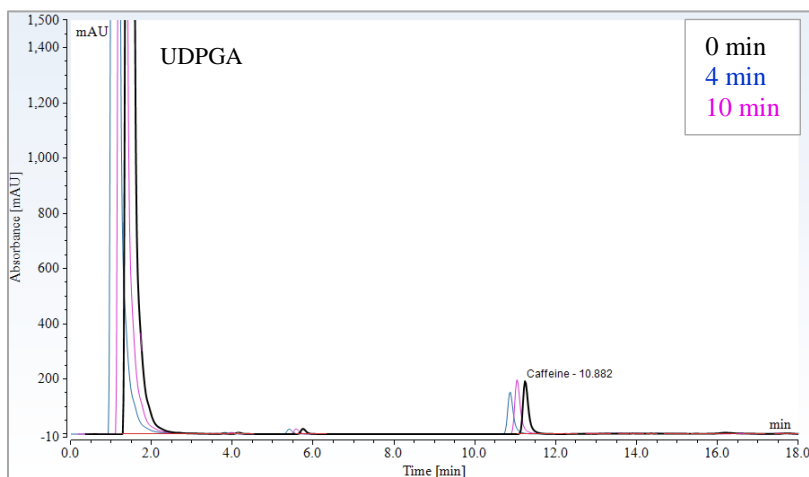


Replicate	Time Point (min)	Rooperol Peak Area <sup>a</sup> (mAU•min)	Caffeine Peak Area <sup>a</sup> (mAU•min)	Ln(PAR)	Conc. from Standard Curve (μM)
<b>A</b>	0	97.79	32.21	1.1105	109.03
	15	90.31	29.04	1.1347	111.75
	60	92.07	30.15	1.1163	109.68
<b>B</b>	0	105.66	33.50	1.1488	113.36
	15	84.93	31.48	0.9927	96.73
	60	76.57	28.21	0.9985	97.31
<b>C</b>	0	83.85	33.47	0.9182	89.68
	15	87.18	34.59	0.9245	90.25
	60	79.03	32.32	0.8942	87.51

<sup>a</sup>Monitored at 260 nm



(c)

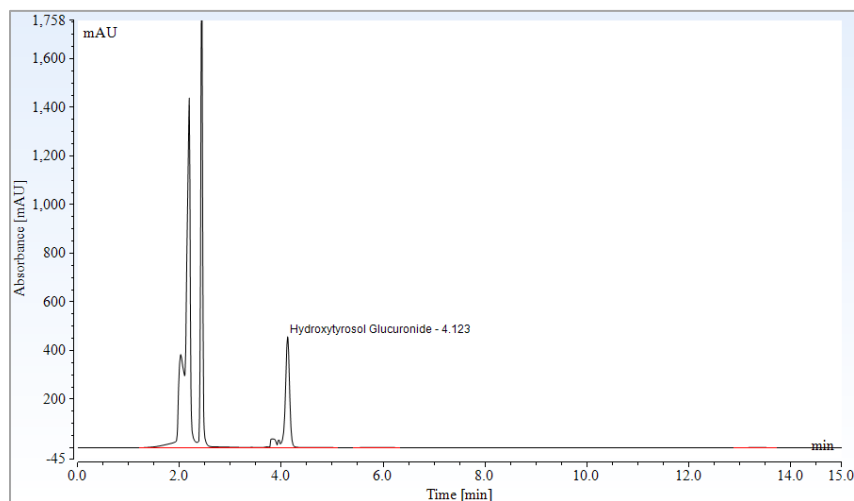


#### 4. HPLC/MS Data

##### Figure 21A: HPLC/MS of Hydroxytyrosol Metabolites

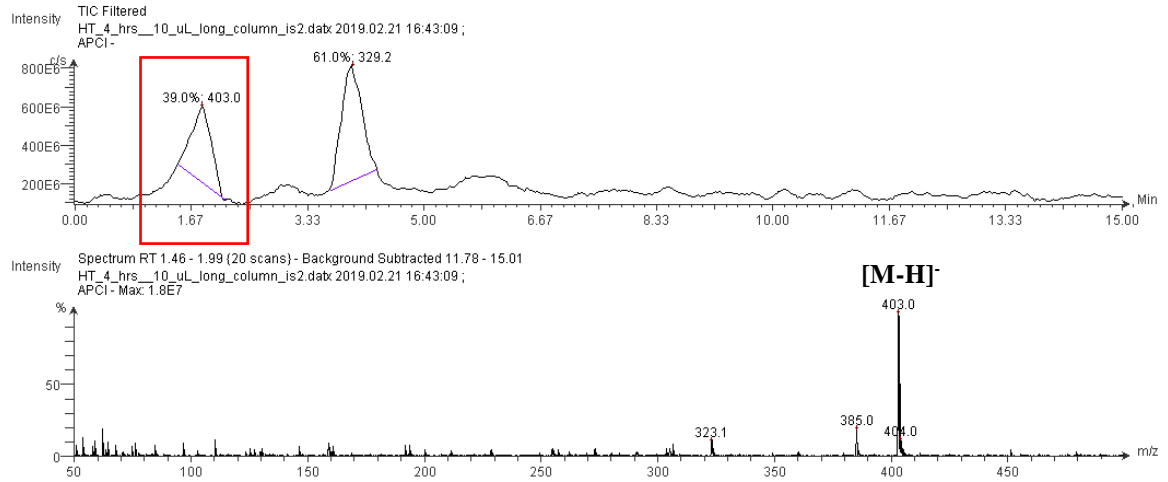
(a) HPLC chromatogram for the *in vitro* assay after a reaction time of 4 hours. Analysis was carried out with a 4.6 x 250 mm column, isocratically at 5% acetonitrile at 1 mL/min and monitored at 280 nm. (b) The MS spectrum acquired for the UDPGA/UDP peak. Note: a signal for UDPGA is not present because the molecular weight is outside of the masses scanned for this spectrum. (c) The MS spectrum obtained for the hydroxytyrosol glucuronide peak (RT = 4.12). The molecular structure shown is an example of one possible position of the glucuronide moiety on hydroxytyrosol.

(a)



(b)

UDP, MW = 404.16



(c)

Hydroxytyrosol Glucuronide, MW = 330.29

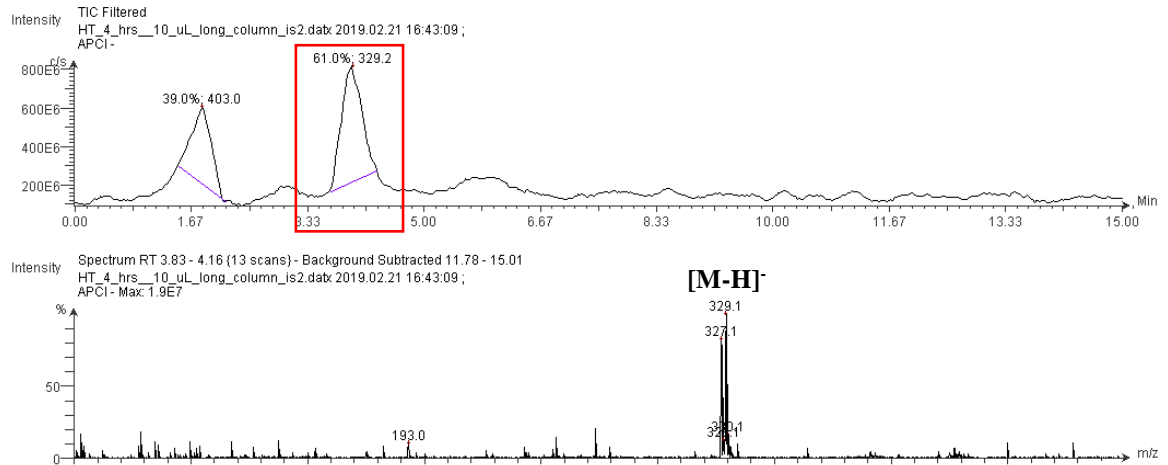
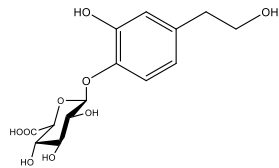
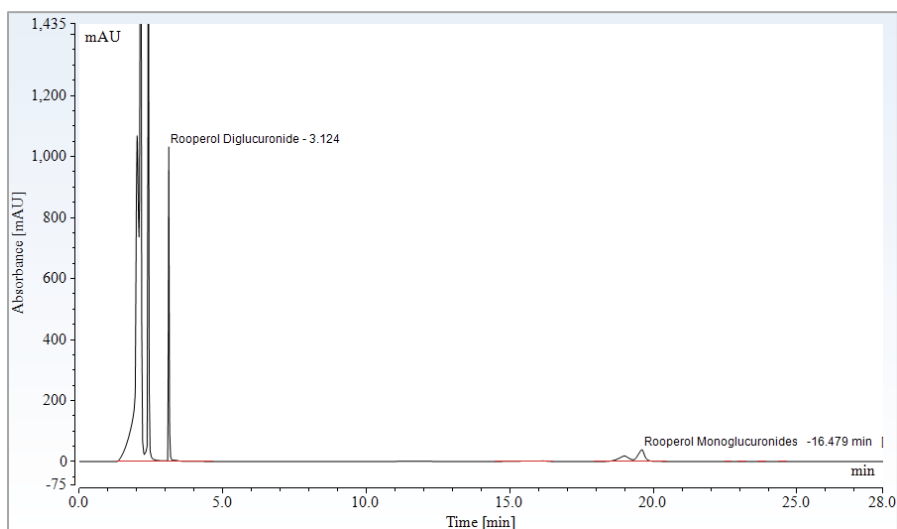


### Figure 22A: HPLC/MS of Rooperol Metabolites

(a) HPLC chromatogram from a sample taken after a reaction time of 60 minutes. MS spectrums were acquired for peaks corresponding to (b) UDPGA/UDP, (c) the monoglucuronide of rooperol, and (d) the diglucuronide rooperol. Note: The molecular structure shown is an example of one possible position of the glucuronide moiety on rooperol.

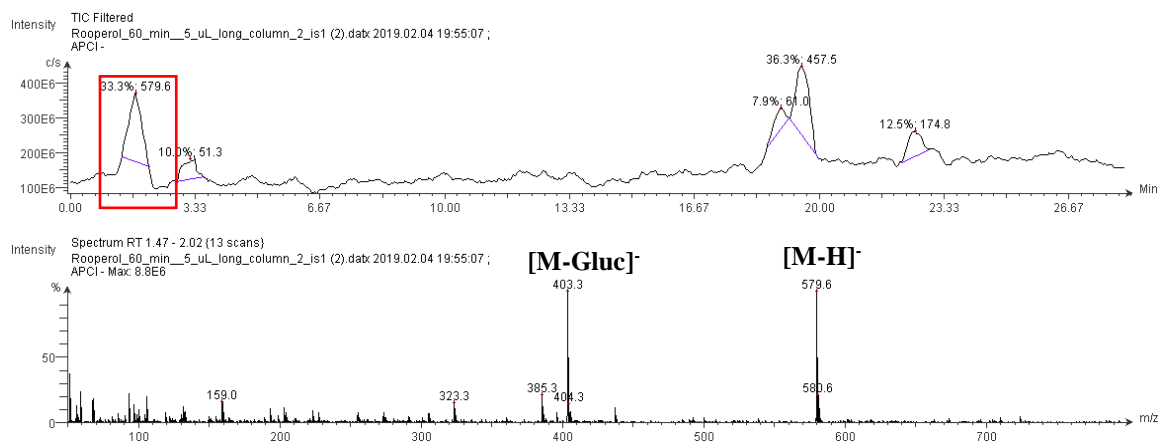
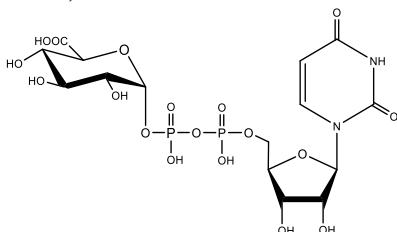
(a)



(b)

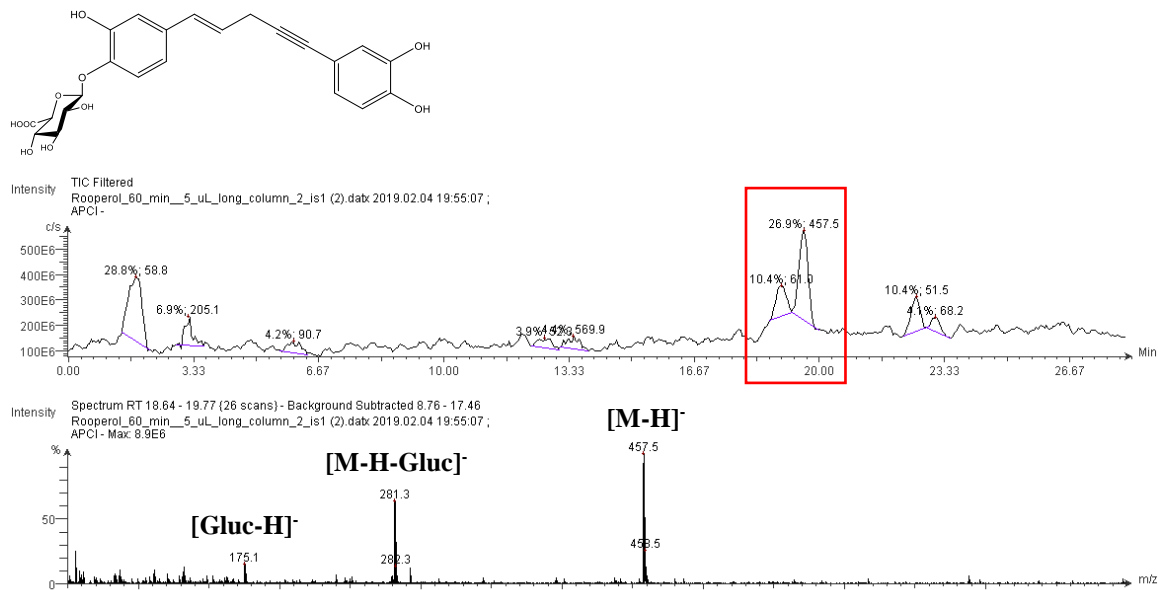
UDPGA, MW = 580.29

UDP, MW = 404.16



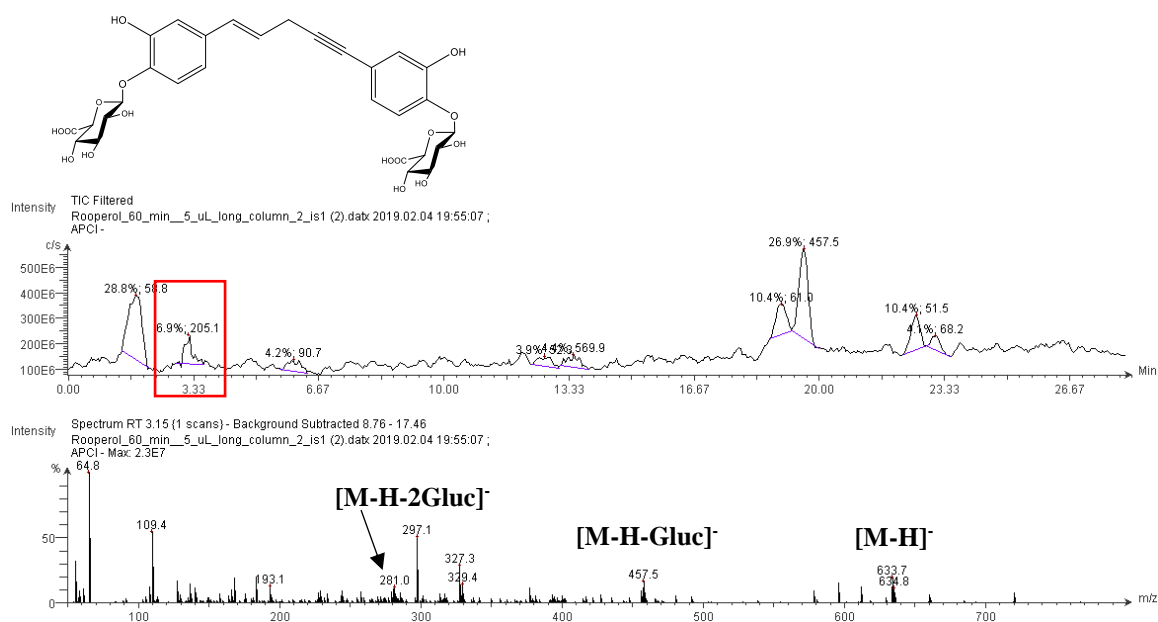
(c)

### Rooperol Monoglucuronide, MW = 458.42



(d)

### Rooperol Diglucuronide, MW = 634.54



## LITERATURE CITED

1. Balunas, M. J.; Kinghorn, A. D., Drug discovery from medicinal plants. *Life Sci* 2005, 78 (5), 431-441.
2. Wink, M., Introduction: Biochemistry, Physiology and Ecological Functions of Secondary Metabolites. In *Biochemistry of Plant Secondary Metabolism*, Annual Plant Reviews: 2010; Vol. 40, pp 1-19.
3. Seca, A. M. L.; Pinto, D. C. G. A., Plant Secondary Metabolites as Anticancer Agents: Successes in Clinical Trials and Therapeutic Application. *Int. J. Mol. Sci* 2017, 19 (1), 263.
4. Loike, J. D.; Horwitz, S. B., Effect of podophyllotoxin and VP-16 on microtubule assembly in vitro and nucleoside transport in HeLa cells. *Biochemistry* 1976, 15 (25), 5435-5442.
5. Johnson, I. S.; Armstrong, J. G.; Gorman, M.; Burnett, J. P., Jr., The Vinca Alkaloids: A New Class of Oncolytic Agents. *Cancer Res* 1963, 23, 1390-427.
6. Owellen, R. J.; Hartke, C. A.; Dickerson, R. M.; Hains, F. O., Inhibition of tubulin-microtubule polymerization by drugs of the Vinca alkaloid class. *Cancer Res* 1976, 36 (4), 1499-502.
7. Long, B. H.; Fairchild, C. R., Paclitaxel Inhibits Progression of Mitotic Cells to G1 Phase by Interference with Spindle Formation without Affecting Other Microtubule Functions during Anaphase and Telephase. *Cancer Research* 1994, 54 (16), 4355-4361.
8. Ncube, B.; Ndhlala, A. R.; Okem, A.; Van Staden, J., Hypoxis (Hypoxidaceae) in African traditional medicine. *J Ethnopharmacol* 2013, 150 (3), 818-27.
9. Drewes, S. E.; Elliot, E.; Khan, F.; Dhlamini, J. T. B.; Gcumisa, M. S. S., Hypoxis hemerocallidea-Not merely a cure for benign prostate hyperplasia. *J Ethnopharmacol* 2008, 119 (3), 593-598.
10. Ojewole, J. A., Antinociceptive, anti-inflammatory and antidiabetic properties of Hypoxis hemerocallidea Fisch. & C.A. Mey. (Hypoxidaceae) corm ['African Potato'] aqueous extract in mice and rats. *J Ethnopharmacol* 2006, 103 (1), 126-34.
11. Nicoletti, M.; Galeffi, C.; Messana, I.; Marini-Bettolo, G. B., Hypoxidaceae. Medicinal uses and the norlignan constituents. *J Ethnopharmacol* 1992, 36 (2), 95-101.
12. Bettolo, G. B. M.; Patamia, M.; Nicoletti, M.; Galeffi, C.; Messana, I., Research on African Medicinal-Plants: Hypoxoside, a New Glycoside of Uncommon Structure from Hypoxis-Obtusa Busch. *Tetrahedron* 1982, 38 (11), 1683-1687.

13. Drewes, S. E.; Hall, A. J.; Learmonth, R. A.; Upfold, U. J., Isolation of hypoxoside from hypoxis rooperi and synthesis of (E)-1,5-bis(3',4'-dimethoxyphenyl)pent-4-en-1-yne. *Phytochemistry* 1984, 23 (6), 1313-1316.
14. Drewes, S.; Liebenberg, R. W., Rooperol and its derivatives. Google Patents: 1985.
15. Owira, P. M.; Ojewole, J. A., 'African Potato' (Hypoxis hemerocallideacorm): A Plant-Medicine for Modern and 21st Century Diseases of Mankind? – A Review. *Phytother. Res.* 2009, 23 (147-152).
16. Potgieter, M.; Wenteler, G. L.; Drewes, S. E., Synthesis of rooperol [1,5-bis(3',4'-dihydroxyphenyl)pent-1-en-4-yne]. *Phytochemistry* 1988, 27 (4), 1101-1104.
17. Boukes, G. J.; van de Venter, M., Rooperol as an antioxidant and its role in the innate immune system: An in vitro study. *J Ethnopharmacol* 2012, 144 (3), 692-699.
18. Albrecht, C. F.; Theron, E. J.; Kruger, P. B., Morphological characterisation of the cell-growth inhibitory activity of rooperol and pharmacokinetic aspects of hypoxoside as an oral prodrug for cancer therapy. *S Afr Med J* 1995, 85 (9), 853-60.
19. Theron, E. J.; Albrecht, C. F.; Kruger, P. B.; Jenkins, K.; van der Merwe, M. J., beta-Glucosidase activity in fetal bovine serum renders the plant glucoside, hypoxoside, cytotoxic toward B16-F10-BL-6 mouse melanoma cells. *In Vitro Cell Dev Biol Anim* 1994, 30A (2), 115-9.
20. Boukes, G. J., Daniels, B.B., Van de Venter, M., Albrecht, C.F., Cell survival or apoptosis: Rooperol's role as anticancer agent. *Oncology Research* 2010, 18 (8), 365-376.
21. Azouaou, S. A.; Emhemmed, F.; Idris-Khodja, N.; Lobstein, A.; Schini-Kerth, V.; Muller, C. D.; Fuhrmann, G., Selective ROS-dependent p53-associated anticancer effects of the hypoxoside derivative rooperol on human teratocarcinoma cancer stem-like cells. *Invest New Drug* 2015, 33 (1), 64-74.
22. Sell, S., Stem cell origin of cancer and differentiation therapy. *Crit Rev Oncol Hematol* 2004, 51 (1), 1-28.
23. Li, J.; Kaoud, T. S.; LeVieux, J.; Gilbreath, B.; Moharana, S.; Dalby, K. N.; Kerwin, S. M., Recruitment Site Binders: Identification of Rooperol as a Novel p38 $\alpha$  Kinase Inhibitor. *Chembiochem* 2013, 14 (1), 66-71.
24. Johnson, G. L.; Lapadat, R., Mitogen-activated protein kinase pathways mediated by ERK, JNK, and p38 protein kinases. *Science* 2002, 298 (5600), 1911-2.

25. Smit, B. J.; Albrecht, C. F.; Liebenberg, R. W.; Kruger, P. B.; Freestone, M.; Gouws, L.; Theron, E.; Bouic, P. J. D.; Etsebeth, S.; van Jaarsveld, P. P., A phase I trial of hypoxoside as an oral prodrug for cancer therapy - absence of toxicity. *S Afr Med J* 1995, 85 (9), 865-868.
26. Albrecht, C. F.; Kruger, P. B.; Smit, B. J.; Freestone, M.; Gouws, L.; Miller, R.; Vanjaarsveld, P. P., The Pharmacokinetic Behavior of Hypoxoside Taken Orally by Patients with Lung-Cancer in a Phase-I Trial. *South African Medical Journal* 1995, 85 (9), 861-865.
27. Krugera, P. B.; Albrecht, C. F. d. V.; Liebenberg, R. W.; Jaarsveld, P. P. v., Studies on hypoxoside and rooperol analogues from *Hypoxis rooperi* and *Hypoxis latifolia* and their biotransformation in man by using high-performance liquid chromatography with in-line sorption enrichment and diode-array detection. *Journal of Chromatography B* 1994, 662, 71-78.
28. de Graaf, M.; Boven, E.; Scheeren, H. W.; Haisma, H. J.; Pinedo, H. M., Beta-glucuronidase-mediated drug release. *Curr Pharm Des* 2002, 8 (15), 1391-403.
29. *Bioisosteres in Medicinal Chemistry*. John Wiley & Sons, Inc.: 2012.
30. Wermuth, C. G., Similarity in drugs: reflections on analogue design. *Drug Discov Today* 2006, 11 (7-8), 348-54.
31. Guo, Z., The modification of natural products for medical use. *Acta Pharmaceutica Sinica B* 2016, 7 (2), 119-136.
32. Drewes, S. E.; Khan, F., The African potato (*Hypoxis hemerocallidea*): a chemical-historical perspective. *South African Journal of Science* 2004, 100, 425-430.
33. Cho, S. Y.; Kim, M. K.; Mok, H.; Choo, H.; Chong, Y., Separation of Quercetin's Biological Activity from Its Oxidative Property through Bioisosteric Replacement of the Catecholic Hydroxyl Groups with Fluorine Atoms. *J. Agric. Food Chem.* 2012, 60 (26), 6499-6506.
34. Sean M. Kerwin, J. C., A concise synthesis of rooperol and related 1,5-diarylpent-1-en-4-yne. *Tetrahedron Letters* 2013, 55, 137-141.
35. Ionescu, C.; Caira, M. R., Drug Metabolism in Context. In *Drug Metabolism: Current Concepts*, Springer, Dordrecht: 2005; pp 1-40.
36. Ionescu, C.; Caira, M. R., Pathways of Biotransformation - Phase I Reactions. In *Drug Metabolism: Current Concepts*, Springer: 2005.

37. Herd, F. J. D. C., Human Cytochrome P450 Enzymes: A Status Report Summarizing Their Reactions, Substrates, Inducers and Inhibitors. *Drug Metab Rev* 1997, 29 (1&2), 413-580.
38. Chillistone, S.; Hardman, J. G., Modes of drug elimination and bioactive metabolites. *Anaest Intens Care M* 2017, 18 (9), 458-461.
39. Jancova, P.; Anzenbacher, P.; Anzenbacherova, E., Phase II drug metabolizing enzymes. *Biomed Pap Med Fac Univ Palacky Olomouc Czech Repub* 2010, 154 (2), 103-16.
40. Burchell, B., Transformation Reactions: Glucuronidation. In *Handbook of Drug Metabolism*, Woolf, T. F., Ed. CRC Press.: 1999.
41. Wells, P. G.; Mackenzie, P. I.; Chowdhury, J. R.; Guillemette, C.; Gregory, P. A.; Ishii, Y.; Hansen, A. J.; Kessler, F. K.; Kim, P. M.; Chowdhury, N. R.; Ritter, J. K., Glucuronidation and the UDP-glucuronosyltransferases in health and disease. *Drug Metab Dispos* 2004, 32 (3), 281-90.
42. Rowland, A.; Miners, J. O.; Mackenzie, P. I., The UDP-glucuronosyltransferases: Their role in drug metabolism and detoxification. *Int J Biochem Cell B* 2013, 45 (6), 1121-1132.
43. Magdalou, J.; Fournel-Gigleux, S.; Ouzzine, M., Insights on membrane topology and structure/function of UDP-glucuronosyltransferases. *Drug Metab Rev* 2010, 42 (1), 159-66.
44. Radomska-Pandya, A.; Czernik, P. J.; Little, J. M.; Battaglia, E.; Mackenzie, P. I., Structural and functional studies of UDP-glucuronosyltransferases. *Drug Metab Rev* 1999, 31 (4), 817-899.
45. Zamek-Gliszczynski, M. J.; Hoffmaster, K. A.; Nezasa, K.-i.; Tallman, M.; Brouwer, K. L. R., Integration of hepatic drug transporters and phase II metabolizing enzymes: Mechanisms of hepatic excretion of sulfate, glucuronide, and glutathione metabolites. *Eur. J. Pharm. Scie* 2006, 27 (5), 447-486.
46. Meech, R.; Mackenzie, P. I., Structure and Function of Uridine Disphosphate Glucuronosyltransferases. *Clin. Exp. Pharmacol. Physiol.* 1997, 27, 907-915.
47. Battaglia, E.; Pritchard, M.; Ouzzine, M.; Fournel-Gigleux, S.; Radomska, A.; Siest, G.; Magdalou, J., Chemical modification of human UDP-glucuronosyltransferase UGT1\*6 by diethyl pyrocarbonate: possible involvement of a histidine residue in the catalytic process. *Arch Biochem Biophys* 1994, 309 (2), 266-72.

48. Li, D.; Fournel-Gigleux, S.; Barre, L.; Mulliert, G.; Netter, P.; Magdalou, J.; Ouzzine, M., Identification of aspartic acid and histidine residues mediating the reaction mechanism and the substrate specificity of the human UDP-glucuronosyltransferases 1A. *J Biol Chem* 2007, 282 (50), 36514-24.
49. Owens, I. S.; Basu, N. K.; Banerjee, R., UDP-glucuronosyltransferases: gene structures of UGT1 and UGT2 families. *Methods Enzymol* 2005, 400, 1-22.
50. Sugatani, J., Function, genetic polymorphism, and transcriptional regulation of human UDP-glucuronosyltransferase (UGT) 1A1. *Drug Metab Pharmacokinet* 2013, 28 (2), 83-92.
51. Shiratani, H.; Katoh, M.; Nakajima, M.; Yokoi, T., Species differences in UDP-glucuronosyltransferase activities in mice and rats. *Drug Metab Dispos* 2008, 36 (9), 1745-52.
52. Court, M. H.; Duan, S. X.; von Moltke, L. L.; Greenblatt, D. J.; Patten, C. J.; Miners, J. O.; Mackenzie, P. I., Interindividual variability in acetaminophen glucuronidation by human liver microsomes: identification of relevant acetaminophen UDP-glucuronosyltransferase isoforms. *J Pharmacol Exp Ther* 2001, 299 (3), 998-1006.
53. Court, M. H., Feline drug metabolism and disposition: pharmacokinetic evidence for species differences and molecular mechanisms. *Vet Clin North Am Small Anim Pract* 2013, 43 (5), 1039-54.
54. Jia, L.; Liu, X., The conduct of drug metabolism studies considered good practice (II): in vitro experiments. *Curr Drug Metab* 2007, 8 (8), 822-9.
55. Obach, R. S.; Baxter, J. B.; Liston, T. E.; Silber, B. M.; Jones, B. C.; Macintyre, F.; Rance, D. J.; Wastall, P., The Prediction of Human Pharmacokinetic Parameters from Preclinical and *In Vitro* Metabolism Data. *J Pharmacol. Exp. Ther.* 1997, 283, 46-58.
56. Liu, Y.; Coughtrie, M. W. H., Revisiting the Latency of Uridine Diphosphate-Glucuronosyltransferases (UGTs)-How Does the Endoplasmic Reticulum Membrane Influence Their Function? *Pharmaceutics* 2017, 9 (3).
57. Fisher, M. B.; Campanale, K.; Ackermann, B. L.; Vandenbranden, M.; Wrighton, S. A., *In vitro* Glucuronidation Using Human Liver Microsomes and the Pore-Forming Peptide Alamethicin. *Drug Metab Dispos* 2000, 28 (5), 560-566.
58. Little, J. M., Lehman, P.A., Nowell, S., Samokyszyn, V., Radomska, A., Activation of Rat Liver Microsomal UDP-Glucuronosyltransferase Activity by Alamethicin. *Drug Metab Dispos* 1997, 25 (1), 5-11.

59. Shin-ichi Ikushiro, Y. E., Takashi Iyanagi, Activation of Glucuronidation through Reduction of a Disulfide Bond in Rat UDP-glucuronosyltransferase 1A6. *Biochemistry* 2002, *41*, 12813-12820.
60. Khymenets, O.; Joglar, J.; Clapes, P.; Parella, T.; Covas, M.-I.; Torre, R. d. l., Biocatalyzed Synthesis and Structural Characterization of Monoglucuronides of Hydroxytyrosol, Tyrosol, Homovanillic Alcohol, and 3-(4'-Hydroxyphenyl)propanol. *Adv. Synth. Catal.* 2006, *348*, 2155-2162.
61. Ethell, B. T.; Anderson, G. D.; Beaumont, K.; Rance, D. J.; Burchell, B., A universal radiochemical high-performance liquid chromatographic assay for the determination of UDP-glucuronosyltransferase activity. *Anal Biochem* 1998, *255* (1), 142-7.
62. Walsky, R. L.; Bauman, J. N.; Bourcier, K.; Giddens, G.; Lapham, K.; Negahban, A.; Ryder, T. F.; Obach, R. S.; Hyland, R.; Goosen, T. C., Optimized Assays for Human UDP-Glucuronosyltransferase (UGT) Activities: Altered Alamethicin Concentration and Utility to Screen for UGT Inhibitors. *Drug Metab Dispos* 2012, *40* (5), 1051-1065.
63. Obach, R. S., Prediction of Human Clearance of Twenty-Nine Drugs from Hepatic Microsomal Intrinsic Clearance Data: An Examination of In Vitro Half-Life Approach and Nonspecific Binding to Microsomes. *Drug Metab Dispos* 1999, *27* (11).
64. Angie Seo, J. L. J., Jolene V Schuster, Didem Vardar-Ulu, Using UV-absorbance of intrinsic dithiothreitol (DTT) during RPHPLC as a measure of experimental redox potential in vitro. *Anal Bioanal Chem.* 2013, *405* (19), 6379-6384.
65. Soars, M. G.; Burchell, B.; Riley, R. J., In vitro analysis of human drug glucuronidation and prediction of in vivo metabolic clearance. *J Pharmacol Exp Ther* 2002, *301* (1), 382-390.
66. Higashi, E.; Ando, A.; Iwano, S.; Murayama, N.; Yamazaki, H.; Miyamoto, Y., Hepatic microsomal UDP-glucuronosyltransferase (UGT) activities in the microminipig. *Biopharm Drug Dispos* 2014, *35* (6), 313-20.
67. Liang, S. C.; Ge, G. B.; Liu, H. X.; Shang, H. T.; Wei, H.; Fang, Z. Z.; Zhu, L. L.; Mao, Y. X.; Yang, L., Determination of propofol UDP-glucuronosyltransferase (UGT) activities in hepatic microsomes from different species by UFLC-ESI-MS. *J Pharm Biomed Anal* 2011, *54* (1), 236-41.
68. Ghosheh, O.; Hawes, E. M., Microsomal N-glucuronidation of nicotine and cotinine: human hepatic interindividual, human intertissue, and interspecies hepatic variation. *Drug Metab Dispos* 2002, *30* (12), 1478-83.

69. Jae Hong Kim, L. J., Bruno Goud, Claude Antony, Clifford A. Lingwood, Richard Daneman, Sergio Grinstein, Noninvasive Measurement of the pH of the Endoplasmic Reticulum at Rest and during Calcium Release. *PNAS* 1998, 95 (6), 2997-3002.
70. C. Berg, A. R., R. Lester, J. Gollan Membrane Translocation and Regulation of Uridine Diphosphate-Glucuronic Acid Uptake in Rat Liver Microsomal Vesicles. *Gastroenterology* 1995, 108, 183-192.
71. Lee Jia1, X. L., The Conduct of Drug Metabolism Studies Considered Good Practice (II): In Vitro Experiments. *Curr Drug Metab.* 2007, 8 (8), 822-829.
72. Judy Easterbrook, C. L., Yumiko Sakai, Albert P. Li, Effects of Organic Solvents on the Activities of Cytochrome P450 Isoforms, UDP-Dependent Glucuronyl Transferase, and Phenol Sulfotransferase in Human Hepatocytes. *Drug Metab Dispos* 2001, 29 (2), 141-144.
73. Liu, X., Testa, B., Fahr, A., Lipophilicity and Its Relationship with Passive Drug Permeation. *Pharm Res* 2011, 28, 962-977.
74. Tetko, I. V. G., J.; Todeschini, R.; Mauri, A.; Livingstone, D.; Ertl, P.; Palyulin, V. A.; Radchenko, E. V.; Zefirov, N. S.; Makarenko, A. S.; Tanchuk, V. Y.; Prokopenko, V. V. , Virtual computational chemistry laboratory - design and description. *J. Comput. Aid. Mol. Des.* 2005, 19, 453-463.